CONNECTING POINTS IN TIME: FROM THE EVOLUTION OF CLOUDS IN SUBSTELLAR ATMOSPHERES TO STUDENTS' PERCEPTIONS OF EARTH'S PLACE IN THE UNIVERSE

by

Laci Shea Brock

A Dissertation Submitted to the Faculty of the

DEPARTMENT OF PLANETARY SCIENCES

In Partial Fulfillment of the Requirements
For the Degree of

DOCTOR OF PHILOSOPHY

In the Graduate College

THE UNIVERSITY OF ARIZONA

2021

THE UNIVERSITY OF ARIZONA
GRADUATE COLLEGE

As members of the Dissertation Committee, we certify that we have read the dissertation prepared by Laci Shea Brock, titled: Connecting Points in Time: From the Evolution of Clouds in Substellar Atmospheres to Students' Perceptions of Earth's Place in the Universe and recommend that it be accepted as fulfilling the dissertation requirement for the Degree of Doctor of Philosophy.

Professor Travis Barman — Date: November 8, 2021

Professor Edward Prather — Date: November 8, 2021

Professor Christopher Impey — Date: November 8, 2021

Professor Amy Mainzer — Date: November 8, 2021

Professor Timothy Swindle — Date: November 8, 2021

Final approval and acceptance of this dissertation is contingent upon the candidate's submission of the final copies of the dissertation to the Graduate College.

We hereby certify that we have read this dissertation prepared under our direction and recommend that it be accepted as fulfilling the dissertation requirement.

Professor Travis Barman
Dissertation Committee Co-Chair — Date: November 8, 2021

Professor Edward Prather
Dissertation Committee Co-Chair — Date: November 8, 2021

ACKNOWLEDGEMENTS

I want to express my upmost gratitude to my advisor, Travis Barman, for taking a chance on a transfer student. Thank you for your patience, guidance, and understanding. To my co-advisor, Ed Prather, thank you for your honesty and helping me find my path. Chris Impey, for insightful discussions about education and letting me be a part of your research group. And of course, thanks to the rest of my committee, Tim Swindle and Amy Mainzer, for embarking on this journey and all that you have taught me.

Thank you to Steve Kortenkamp and Sanlyn Buxner for helping me secure funding and opportunities in science education upon my arrival at the University of Arizona. Although they are unfortunately not here to read it, I especially want to thank my undergraduate advisor Jay Melosh and my master's advisor Nadine Barlow for believing in me against all odds. Thank you to all the administrative staff at LPL, especially Amy, Mary, Vicki, Bert, Tara, Eneida, Maria, and many others.

Thank you to all my friends at LPL for the fun times. In particular, thanks to my bff Kyle Pearson for teaching me how to be pythonic. Molly Simon for being an awesome roommate and getting me out of a bad situation. I also want to thank Adam Sutherland, Sarah Peacock, Tracy Esman, and Rachel Fernandes. Thanks to my fellow TAPS members and The Art of Planetary Science for reminding me of my love of painting. Finally, thanks to all my friends I didn't name directly and all the internet strangers following me on social media supporting this journey. I appreciate you all, especially DN who wishes to remain anonymous.

The untimely nature of the pandemic brought with it isolation and several friends moving away around the same time. I'd like to thank all of my gaming friends across the world for their virtual support and providing me with strength the last year and a half. Shout out to Lulu, Tanner, and Devi's Twitch communities, and my friends in the 5'5 mod squad. To the Diamond Dinguses, thanks for tolerating my excessive decoys.

Thanks to my dad who fostered my love of science from a young age, and my grandma for supporting my dreams. Finally, an important thank you to the love of my life, Cody, for all your help completing this journey and to the cutest shiba inu ever, Tachikoma.

DEDICATION

To Cody, for telling me which Zelda is best and never leaving my side.

TABLE OF CONTENTS

TABLE OF CONTENTS – *Continued*

TABLE OF CONTENTS – *Continued*

LIST OF FIGURES

LIST OF FIGURES – *Continued*

LIST OF TABLES

ABSTRACT

Equally as important as growing the body of human knowledge through scientific discoveries and analysis is relaying this information to the general public in a digestible manner to establish a scientifically literate society. This dissertation approaches the multifaceted issue by combining an in-depth study of brown dwarf binary atmospheres with an astronomy education component. Thus, the goal of this work is twofold: to improve our current understanding of clouds in brown dwarf atmospheres and to identify preconceptions non-science undergraduate students posses about Earth's place in time and space in the Universe.

The first portion of the dissertation seeks to constrain atmospheric and cloud properties in a sample of well-known brown dwarf binaries. I answer this question using spatially-resolved optical and near-infrared photometry from the Hubble Space Telescope (HST) and the W. M. Keck Telescopes to explore cloud properties in detail across a broad range of effective temperatures and surface gravities. New grids of synthetic spectra were created using the PHOENIX atmosphere model code, extending clouds to deeper pressures and smaller mean grain sizes. I report bulk atmospheric properties with trends in cloud location and mean grain size for mid-L through mid-T type brown dwarfs (Chapter 2). The results of this study led to a detailed analysis in Chapter 3 of an individual triple system, HD 130948, containing a solar analogue star and two brown dwarfs of similar mass, luminosity, and spectral type. Moderate-resolution spectroscopy from the OSIRIS instrument on Keck was

fit to synthetic spectra to determine the best-fitting atmosphere parameters of HD 130948B and HD 130948C for solar and stellar metallicity. I measure the C/O ratio of each binary and confirm it is consistent with the host star.

In the second component (Chapter 4), I investigate students' conceptions of time in astronomy as it relates to Earth's formation and location in the Universe. A set of open-ended questions were developed and issued to a sample of students in an astronomy course. Thematic analysis of the responses suggested students struggle with fundamental topics in astronomy related to the origin and formation of the Universe, planet formation, the age of the Universe and Earth, and the composition and structure of the Universe. Incorporating explicit discussion and instruction regarding time in astronomy can be a useful tool toward improving non-science students' grasp of difficult, abstract concepts in introductory astronomy courses.

CHAPTER 1

Introduction

This dissertation contains two distinct fields of research: planetary science and astronomy education. The chapters within reflect the author's desire to pursue a doctorate with a hybrid format, gaining experience in research practices associated with scientific study and supplementing this knowledge with an understanding of educational theory. Chapters 2 and 3 are the planetary science portion of this dissertation and focus on constraining bulk properties of benchmark brown dwarf binary systems, encompassing an in-depth study on clouds. Chapter 4 is the educational component, which explores undergraduate students' conceptions of cosmological time.

1.1 Brown Dwarfs

Stars form from the gravitational collapse of molecular clouds of gas and dust. Generating thermal energy in their cores from nuclear fusion, stars sustain a majority of their lifetimes on the main sequence in hydrostatic equilibrium. Immense stellar core temperatures (millions of Kelvin) are required to fuse hydrogen into helium. Theoretical interior models suggest masses around $\sim$75 M_{Jup} (depending upon metallicity) are required to reach these high temperatures (Chabrier and Baraffe, 1997, 2000). Kumar (1963) was the first to propose the star-forming process should produce lower-mass objects below the hydrogen-burning limit. Today, we call these

objects brown dwarfs—a class of substellar objects colloquially referred to as 'failed stars'. Brown dwarfs are not massive enough to sustain thermonuclear fusion like their stellar counterparts but are perhaps too massive to be considered planets. Thus, the lower mass limit for brown dwarfs is less defined and often cited as the mass required for deuterium fusion ($\sim$13 M_{Jup}). The existence of brown dwarfs was theoretically predicted nearly 30 years before the first bonafide detection in 1995 (Nakajima et al., 1995; Oppenheimer et al., 1995).

Brown dwarfs remained elusive for so long because a majority of their energy is emitted in the infrared portion of the spectrum making them difficult to detect. They are hottest and brightest a few million years after formation. Unlike stars which retain a constant radius and luminosity for billions of years, brown dwarfs cool and contract as they age. As they evolve to an age of $\geq$ 1 Gyr, the radius of a brown dwarf contracts to $\sim$1 R_{Jup} (Chabrier and Baraffe, 2000). Brown dwarfs span an extensive range of temperatures from the lowest-mass stars to planet-like in nature. The discovery of numerous substellar objects with unique spectral signatures of their own required an extension to the existing stellar classification system. Three new spectral types—L, T, and Y—were added to accommodate brown dwarfs cooler than the latest M-type red dwarf stars (Kirkpatrick, 2005). The earliest spectral types (M7 and later) have the warmest temperatures ($T_{eff} \sim$ 2800 K) and the latest Y types can be as cool as $\leq$ 500 K.

1.2 Detection and Characterization

Large astronomical surveys including the Two Micron All-Sky Survey (2MASS; Skrutskie et al. (2006)), the Sloan Digital Sky Survey (SDSS; York et al. (2000)), and the Deep Near-Infrared Survey of the Southern Sky (DENIS; Epchtein et al. (1997)) have been instrumental in discovering and characterizing brown dwarfs. Photometric observations of thousands of L and T dwarfs have been used to establish near-infrared color trends, providing insight into the atmospheric processes at work (Kirkpatrick et al., 1999; Knapp et al., 2004; Golimowski et al., 2004). Near-infrared

photometric JHK bands establish the color magnitude diagram of cool low-mass objects. L dwarfs become progressively redder than M dwarfs, and T dwarfs become significantly bluer (Burrows et al., 2006; Marley et al., 2002). Figure 1.1 shows the location of different brown dwarf spectral types across the color-magnitude diagram.

Low-to-moderate resolution optical and infrared spectroscopy (∼0.6-14.5 μm) and the establishment of large repositories of brown dwarf spectra—such as the SpeX Prism Library (Burgasser, 2014)—has been essential in characterizing the evolution of prominent atomic and molecular absorption features and defining subtypes of brown dwarfs (i.e., L0, L1, L2, etc.) as a function of temperature (Stephens et al., 2009; Cushing et al., 2008; Luhman et al., 2009; Kirkpatrick, 2005; Kirkpatrick et al., 2008). Additional classification schemes from Martín et al. (1999) and Allers and Liu (2013) built upon this foundation to characterize features of brown dwarfs into categories based upon low, intermediate, and high surface gravities. Continuing efforts focused on untangling the influence of gravity with other secondary effects from age, metallicity, and clouds. For example, Mclean et al. (2007) used high-resolution spectra (R ∼ 20,000) of late-M, L, and T dwarfs to identify weak spectral features in the J-band to constrain chemical processes for various spectral types and search for signs of pressure broadening as a consequence of gravity.

The L dwarfs ($T_{\rm eff}$ ∼ 2200-1300 K) encompass both the lowest mass stars at the edge of the main sequence and brown dwarfs. Dupuy and Liu (2017) determined a model-independent substellar boundary at ∼L4 in spectral type (∼70 M_{Jup}). The spectral energy distribution of brown dwarfs deviates significantly from a black-body function, lacking the optical bands of TiO and VO characteristic of M dwarfs (Jones and Tsuji, 1997) and show features of pressure-broadened alkali lines and deep molecular absorption bands.

T dwarfs ($500 \leq T_{\rm eff} \leq 1300$), in addition to their bluer colors, are distinct from L dwarfs due to the appearance of strong CH_4 features in the H and K bands, show little to no photospheric dust, and have pressure-broadened H_2 absorption features in near-infrared spectra (Burrows et al., 2001; Borysow et al., 1997). The rapid infrared color evolution that occurs during the transition from L to T spectral types

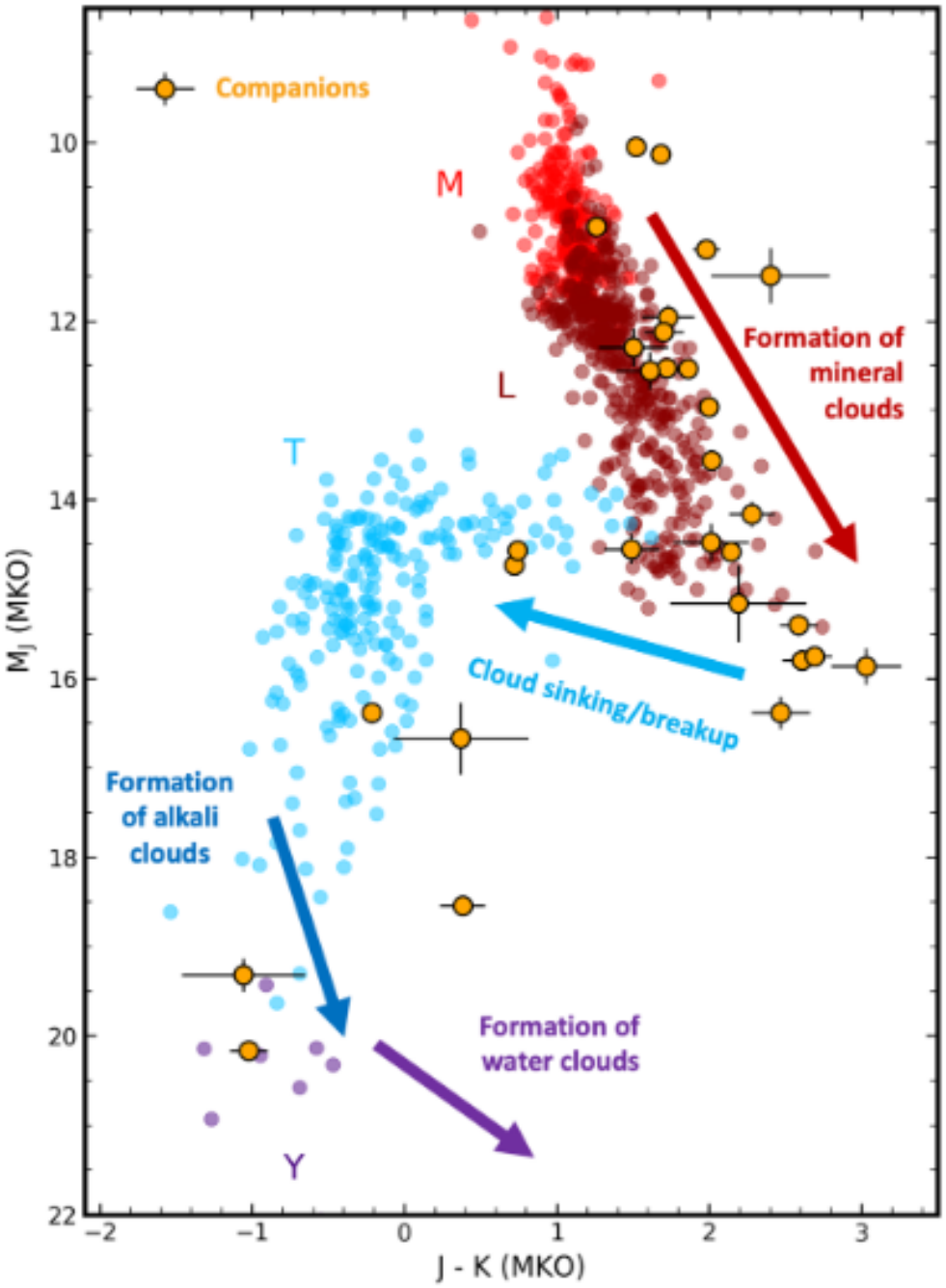

Figure 1.1: Color-magnitude diagram of field brown dwarfs (MKO photometry) color coded by spectral types with current understanding of cloud types. M dwarfs are in red, L dwarfs in dark red, T dwarfs in blue, and Y dwarfs in purple. Directly imaged planets are shown in orange. Figure originally published in Gao et al. (2021). Data are from Best et al. (2020b), Best et al. (2017), Dupuy and Liu (2012), Dupuy and Kraus (2013), Liu et al. (2016).

is an outstanding problem in substellar atmospheres (discussed in 1.4.1). Evidence suggests clouds are to blame, including the emergence of holes in the clouds (Burgasser et al., 2003), a sudden collapse of the cloud deck (Tsuji and Nakajima, 2003), or an increase in the sedimentation efficiency of the clouds (Knapp et al., 2004). Influences from surface gravity and metallicity are also believed to play an important role in the width of the L and T dwarf regions on color magnitude diagrams (Burrows et al., 2003; Knapp et al., 2004).

Y dwarfs are the most recent spectral class of brown dwarfs added and are essentially an extension of the T dwarfs to even cooler temperatures ($250 \leq T_{eff} \leq 500$) (Cushing et al., 2011; Kirkpatrick et al., 2012, 2019, 2021). The Wide-Field Infrared Survey Explorer (WISE; Wright et al. (2010)) extended photometric sky surveys to longer wavelengths resulting in the detection of fainter and cooler brown dwarfs. Y dwarfs are characterized by their strong water and methane absorption features and, although there is not a clear spectral feature that defines the T/Y transition, the width of the J band is often used to separate a Y dwarf from a late-T dwarf (Cushing et al., 2011). Figure 1.2 shows the evolution of spectral features for M through Y type brown dwarfs.

1.2.1 Benchmark Systems

Brown dwarfs differ fundamentally from stars due to their cooler temperatures, partially degenerate interiors, and dominant molecular opacities; yet, they have similar physical and chemical properties observed in giant planet atmospheres (Chabrier and Baraffe, 2000). Decades of work show brown dwarfs are rather plentiful in the local galactic neighborhood and typically brighter than directly imaged exoplanets (Kirkpatrick, 2005), making them excellent candidates to study the physical properties that govern cool atmospheres and provide insight into the planetary-stellar connection. Because multiple parameters affect the spectral energy distribution of substellar objects, it is challenging to disentangle the influence from bulk properties, atmospheric chemistry, and clouds.

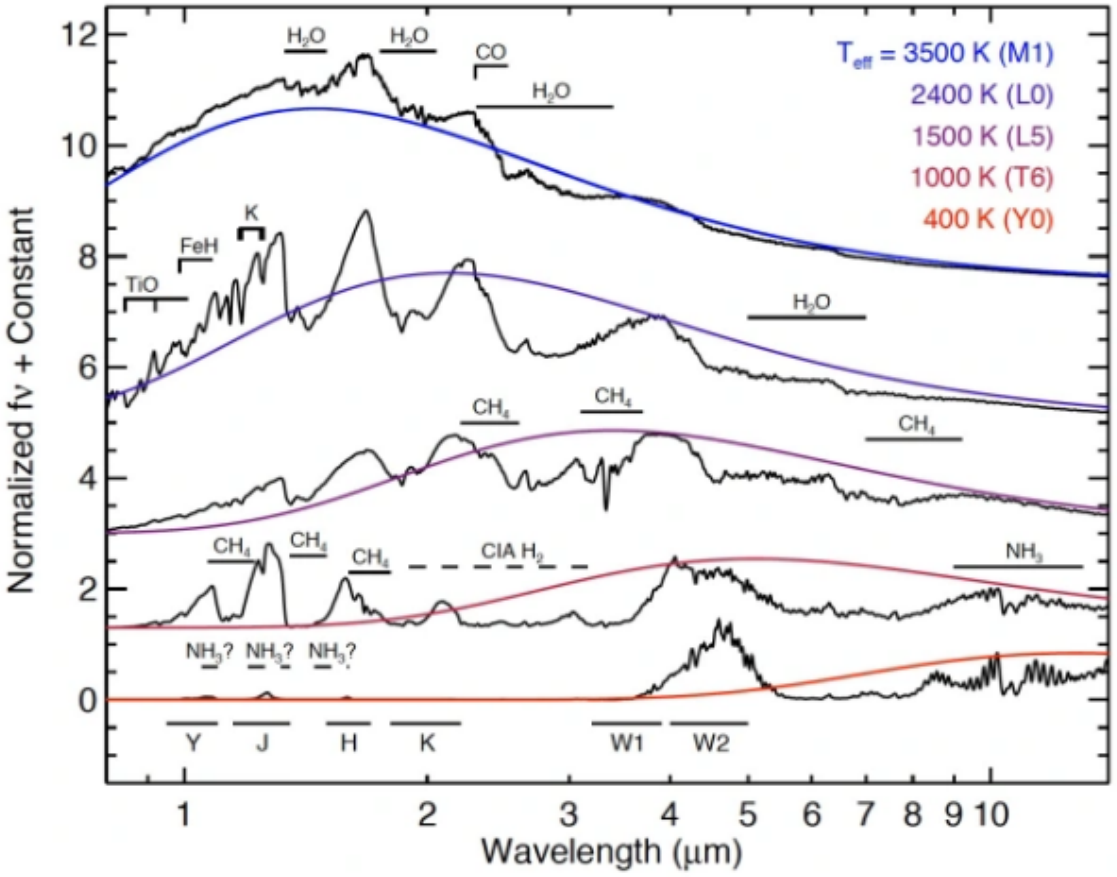

Figure 1.2: Evolution of spectral features for the warmest to coolest brown dwarfs. CH_4 begins to dominate over CO as objects progress from late-L to T-type. Figure from Michael Cushing (personal communication).

Benchmark systems are brown dwarfs whose properties (e.g., mass, age, distance) can be independently determined and used to constrain models. Precise, individual measurements of distance, mass, luminosity, radius, and age are required to construct a concise picture of brown dwarf evolution. Properties of luminosity and temperature are degenerate for mass and age such that a young, low-mass brown dwarf could have similar observational properties as an older, higher-mass object. One approach to tackling brown dwarf degeneracies is by studying binary systems to reduce the number of unknown variables. Photometric observations can be combined with distance measurements derived from parallax to provide better estimates of the effective temperature and luminosity (Dupuy and Kraus, 2013).

Constraints on dynamical mass are perhaps one of the most important parameters for studying substellar objects because the initial mass at formation determines how the object will evolve throughout its lifetime. An individual system with known mass and age can greatly reduce the predicted range of temperature, gravity, and luminosity. Furthermore, binary systems are assumed to be coeval, sharing the same age and composition. Each object in a binary forms from the same molecular cloud, thus they should have the same (or very similar) metallicity.

High angular resolution imaging surveys with the Hubble Space Telescope and ground-based adaptive optics on the W. M. Keck Telescopes over the last decade have been instrumental in studying visual binaries with spectral types of M7 and later (e.g., Lane et al., 2002; Liu et al., 2008; Bouy et al., 2004; Konopacky et al., 2010; Dupuy et al., 2009a; Burgasser et al., 2007). Through sufficient astrometric monitoring, the orbital parameters can be obtained and used to derive the total system mass and, in some cases, the individual masses. This process is time consuming due to the lengthy orbital periods of many systems, often ranging between 10-30 years. To date, approximately two dozen ultracool dwarfs have fully determined orbits and constraints on individual masses spanning 30-115 M_{Jup} (Konopacky et al., 2010; Dupuy and Liu, 2017). Binary systems with host star companions can be particularly helpful by providing an additional constraint on the age of the system via magnetic activity, elemental depletion, or gyrochronology (Dupuy et al., 2014).

Absolute astrometry from *Hipparcos* and *Gaia* continue to provide mass constraints for the coolest brown dwarfs (Brandt et al., 2020) and directly imaged exoplanets (Brandt et al., 2021).

Mass and age can be determined by comparing observed physical properties to those from evolutionary models; however, these comparisons rely on the accuracy of atmosphere models. Benchmark brown dwarfs—objects with independently determined masses, luminosities, and ages—are extremely powerful and provide the most robust tests of theoretical substellar atmosphere and evolution models. Early work hinted at a luminosity problem where comparisons between dynamical masses and masses predicted by evolutionary models differed significantly (Dupuy et al., 2009a; Konopacky et al., 2010; Dupuy et al., 2014). The consistency between predicted and measured masses has improved with continued astrometric monitoring (Dupuy and Liu, 2017) and models that consider cloud clearing (Saumon and Marley, 2008; Allers and Liu, 2013). A related problem exists for benchmark brown dwarfs when comparing the effective temperatures and gravities predicted by evolution models to those obtained by comparing model spectra to observed photometry or spectra. Differences in temperature as large as several hundred Kelvin and differences in gravity of an order of magnitude are not uncommon across the L/T transition (Cushing et al., 2008). Including clouds can alleviate some of the discrepancy between evolutionary and atmosphere model comparisons but does not eliminate the problem completely (Wood et al., 2019). Some of the issues may be improved with very broad wavelength coverage (Briesemeister et al., 2019). In addition to refined cloud parameters, metallicity (Wood et al., 2019; Crepp et al., 2018), non-equilibrium chemistry (Barman et al., 2011a; Zhang et al., 2020), or other missing physics in the models (Charnay et al., 2018) (e.g., cloud microphysics) may be remaining sources of tension.

Benchmark systems are rare compared to the total number of known brown dwarfs ($\sim 10^3$; Smart et al. (2017)) and prior studies identified discrepancies between benchmark systems and models, resulting in over/under predicted luminosities and temperatures (Dupuy et al., 2009b; Konopacky et al., 2010; Dupuy et al., 2014). The

lower temperatures of T dwarfs are expected to yield relatively low masses (∼30-50 M_{Jup}) with ages of other field dwarfs (1-5 Gyr) Liu et al. (2008). Recently, several T dwarfs have measured dynamical masses that are larger than expected and possibly at odds with evolutionary model predictions. This includes the T5.5 dwarf WISE J0720-0846B with a mass of 66 ± 4 M_{Jup} (Dupuy et al., 2019), the T1.5 and T6 components of ϵ Indi BC with masses of 68-75 and 53-70 M_{Jup} (Kasper et al., 2009; King et al., 2010; Dieterich et al., 2018), and a late T dwarf HD 4113C with a mass of 66^{+5}_{-4} M_{Jup} (Cheetham et al., 2018).

The inconsistencies that arise are a multifaceted problem stemming from uncertainties in observable quantities (e.g., distance and therefore mass) and sources of tension in atmosphere and evolution models (e.g., incomplete molecular opacities at low temperatures). Some discrepancies have been resolved with additional coverage at longer wavelengths (Briesemeister et al., 2019), improving the treatment of clouds (Wood et al., 2019), including non-equilibrium chemistry (Barman et al., 2011a; Zhang et al., 2020), or considering non-solar metallicity (Crepp et al., 2018). Hybrid evolutionary models that consider the break-up or apparent disappearance of clouds across the L/T transition have also improved comparisons (Saumon and Marley, 2008). It will be important to compare benchmark systems to the next generation of atmosphere and evolution models that expand the diversity of parameters, such as the new Sonora Bobcat substellar models that include cooler temperatures and a greater range of C/O abundances (Marley et al., 2021).

1.3 Theoretical Modelling

Interpreting photometric and spectroscopic observations of brown dwarfs requires the use of substellar atmosphere and evolution models. The goal of these models is to solve the radiative transfer equation and determine how energy is transported from deep in the interior to the outer layers. Historically, studying atmospheres of brown dwarfs has relied on self-consistent, one-dimensional models. Below, I briefly describe the development and history of the first substellar models.

1.3.1 Atmosphere and Evolutionary Models

The development of substellar atmosphere models capable of accurately describing the spectral energy distribution of objects below the minimum mass for hydrogen burning was a long and complex process. Characteristics of the first brown dwarfs detected showed spectral features inconsistent with existing stellar atmosphere models for the coolest stars (Oppenheimer et al., 1998). The earliest interior and evolution models were unable to reproduce observations at the bottom of the main sequence nor able to accurately determine properties of mass, age, effective temperature, or luminosity (Lunine et al., 1986; VandenBerg et al., 1983; Dorman et al., 1989; Burrows et al., 1989). Early modelling efforts were challenged by how convection was handled and incomplete molecular opacity databases (Allard et al., 1997). The first models for cool M dwarfs (T_{eff} = 4750-3000 K) were developed by (Mould, 1975, 1976) and included opacities for TiO, H_2O, and a mixing-length treatment of convection (Tsuji et al., 1996; Auman, 1967).

Molecular absorption features of TiO and VO suddenly reduced in strength in objects with spectral types later than M6 (Jones and Tsuji, 1997) and led Kirkpatrick et al. (1999) to designate the L spectral type. Early L dwarfs have similar photospheric compositions to M dwarfs with alkali lines (K, Na), metal hydrides (FeH, CrH), oxides (TiO, VO), and water. Grids of synthetic spectra became possible below temperatures $<$ 3000 K when opacities of hydrides (CaH, MgH, SiH, OH, CH), VO, and CO were incorporated (Allard, 1990). Decreasing temperatures combined with complex atmospheric reactions suggested models would need to include the onset of photospheric dust and (eventually) clouds to match the strong absorption features present in brown dwarf spectra (Allard et al., 1998). Chemical equilibrium models predicted the most important dust species were those of iron (Fe), enstatite ($MgSiO_3$), and corundum (Al_2O_3) (Tsuji et al., 1996). Models that began to incorporate this dust were indeed better fits to the spectrum of the earliest L dwarfs detected, such as Gliese 165B (Tinney, 1993). Several atmosphere models were developed that provided a better match to the redder colors across late-M and

L dwarfs including the NEXTGEN-DUSTY (Allard et al., 1998), DUSTY (Chabrier and Baraffe, 2000), and AMES-DUSTY (Allard et al., 2001) models.

Self-consistent models could be used to create large grids of atmosphere models that span across a range of predicted temperatures and gravities, typically for solar metallicity. Fitting observations to synthetic spectra produced from grid models, bulk atmospheric properties could be predicted for a range of brown dwarfs. The DUSTY models matched spectra well in the temperature range of ∼2000-2500 K (Allard et al., 1998; Chabrier and Baraffe, 2000; Allard et al., 2001). It soon became clear that models appropriate for the warmer late-M and L dwarfs were not appropriate for cooler T dwarfs. Gliese 229B was one of the first discovered brown dwarfs with a much cooler temperature (T_{eff} ∼1000 K) (Nakajima et al., 1995; Oppenheimer et al., 1995) and helped to define the spectral class of T type brown dwarfs (Kirkpatrick et al., 1999). Near-infrared CO bands strengthen for mid-L dwarfs, but these bands weaken as methane begins to dominate in cooler T dwarfs. Work from Allard et al. (2001) explored the opposite case of the DUSTY models where dust disappears from the atmosphere by efficient gravitational settling. These COND, or "cloud-free" models, were a much better match to substellar objects with $T_{eff} \leq$ 1000 K.

The development of models to describe brown dwarf evolution required appropriate input from atmosphere models. Without steady hydrogen fusion in their core, brown dwarfs cool throughout time causing a mass-luminosity-age degeneracy. Brown dwarfs lose energy, dim in luminosity, and their radius shrinks. Improvements to interior physics aided in the development of the first substellar evolutionary models. Chabrier and Baraffe (1997) determined improved equations of state, treatment of thermonucelar reactions, and appropriate treatment of boundary conditions. In cooler atmospheres, the convection zone can reach the outermost photospheric layers and evolutionary models depend critically on how this boundary is handled (Allard et al., 1997). The first successful evolutionary models were developed by two groups who coupled interior models with the new generation of atmosphere models and are commonly referred to as the Lyon and Tucson evolutionary tracks (Baraffe and

Chabrier, 1995; Chabrier and Baraffe, 1996; Allard and Hauschildt, 1995; Saumon et al., 2012). Later evolutionary models were developed in order to improve the treatment of clouds, such as the hybrid evolutionary models from Saumon and Marley (2008), and to provide an evolutionary sequence at cooler temperatures (Marley et al., 2021).

1.4 Clouds in Brown Dwarf Atmospheres

One of the greatest challenges and uncertainties in the field of substellar astrophysics is to model the clouds that form in ultracool atmospheres ($T_{eff} < 3000$ K). Molecules and condensate species present in the atmospheres of brown dwarfs vary strongly with wavelength and cause spectra to deviate significantly from blackbody values (Marley and Robinson, 2015; Kirkpatrick et al., 1999). Clouds redden near-infrared emission spectra and reduce the depth of molecular absorption features. They further impact the atmospheric structure and radiative balance in the upper atmosphere via scattering and absorption of radiation. The formation of clouds deplete the atmosphere of refractory elements as condensation and rainout occurs. Thus, the temperature-pressure profile is highly dependent upon the structure and location of clouds, making it a challenge to fit spectral energy distributions to global stellar atmosphere models (e.g., DUSTY, COND).

Improvements to molecular opacity databases (Freedman et al., 2008; Sharp and Burrows, 2007; Tennyson and Yurchenko, 2012), line broadening (Burrows et al., 2001; Allard et al., 2001), and the chemistry of gas and condensates at cool temperatures (Lodders and Fegley, 2002) in addition to incorporating parameterized clouds into atmosphere models (Ackerman and Marley, 2001; Marley et al., 2002) have significantly improved the interpretation of observational data. Developing models that reduce uncertainties and accurately represent how atmospheric processes change at spectral type transition regions—condensate cloud formation for M-to-L types, cloud breakup/sinking across the L/T transition, and the appearance of ammonia for T/Y dwarfs—is a key requirement going forward (Konopacky et al.,

2010). In the following section, I discuss the region of cloud formation most relevant to work in this dissertation—the L/T transition—in more detail. The work in this dissertation is motivated by this problem and seeks to investigate if refining cloud properties for well-studied benchmark brown dwarf binary systems can alleviate some of the previous tension between observations and theoretical models. Furthermore, one of the goals of this work is to see if best-fitting atmosphere model parameters can yield properties in line with evolutionary model derived properties.

1.4.1 L/T Transition

A region referred to as the L/T transition marks the rapid near-infrared color change (see 1.1) in brown dwarfs from red to blue across a narrow range of effective temperatures (∼200-300 K) near ∼1400 K and spectral types (L8-T3) (Fegley Jr. and Lodders, 1996; Golimowski et al., 2004). The phase transition from CO to CH_4 and the onset of methane absorption (1-2.5 μm) that occurs in mid-to-late L dwarfs, resulting in suppressed H- and K-band fluxes, is partly responsible for the color change (Allard et al., 1997; Chabrier and Baraffe, 2000; Helling and Casewell, 2014). Other evidence that marks the existence of the L/T transition includes brightening in the J band, which is believed to be an intrinsic feature of brown dwarf evolution and not caused by gravity or age differences (Burgasser et al., 2000; Leggett et al., 2000; Burgasser et al., 2006).

Results from photometric and spectroscopic monitoring coupled with atmosphere models have put forth several physical explanations for the mechanism(s) responsible for the rapid color changes across the L/T transition. This includes a sudden collapse of the cloud deck (Tsuji and Nakajima, 2003), changes in cloud thickness (Tsuji, 2005), patchy clouds or holes in the cloud deck (Burrows et al., 2003; Ackerman and Marley, 2001; Marley et al., 2010; Saumon and Marley, 2008; Burgasser et al., 2002), increase in sedimentation efficiency (Knapp et al., 2004), or thermochemical instabilities (Tremblin et al., 2016).

In addition to cloud property changes, gravity, metallicity, and the presence of

unresolved binaries contribute to the observed spread of brown dwarfs across the cooling sequence (Saumon and Marley, 2008). After removing binaries, Best et al. (2020a) identified a significant 0.5 mag wide gap in J - K (MKO) colors in the L/T transition suggesting rapid atmospheric evolution in contrast to the pile up identified for the same colors from Saumon and Marley (2008). Similar work implies there is a phase of rapid atmospheric evolution in brown dwarfs near 1300 K (Dupuy and Liu, 2017). The implications are that brown dwarfs in the L/T transition are rare (Best et al., 2020a).

A single, self-consistent model has not yet been able to describe the evolution of brown dwarfs and match observations across the full color space of the L/T transition (Burrows et al., 2006; Marley et al., 2010). Both atmosphere and evolutionary models have difficulty reproducing observed effective temperatures and luminosities for L/T transition objects with known masses and/or ages (Leggett et al., 2008; Dupuy et al., 2015; Barman et al., 2011a; Bowler et al., 2010). Currently, the Saumon and Marley (2008) hybrid evolutionary models are the only models that agree with the mass-luminosity relationship of transition brown dwarfs (Dupuy et al., 2015; Dupuy and Liu, 2017). These models assume cloudy atmospheres for $T_{eff} > 1400$, clear atmospheres for objects with $T_{eff} < 1200$, and an interpolation of the two conditions for the L/T transition. Part of the reason mapping out brown dwarf evolution across the L/T transition has moved rather slowly is due to the limited availability of accurate, parallax-based luminosities for these spectral types (Best et al., 2017).

1.4.2 Atmospheric Variability and Dynamics

One-dimensional models that incorporate clouds are essential to capture the average properties across spectral trends using simplified modelling assumptions, but they do not capture the atmospheric dynamics such as the effects of winds or horizontal advection (Showman et al., 2018; Zhang and Showman, 2014; Tan and Showman, 2019). Atmospheric dynamics and global circulation likely plays a significant role

in the formation of clouds in brown dwarf atmospheres. There is strong evidence of variability on timescales much shorter than evolutionary timescales. Saumon et al. (2006) predicted the chemical composition in brown dwarfs can deviate from abundances expected from equilibirum chemistry, which suggests the dynamical mixing timescale is shorter than the chemical reaction timescales. Brown dwarfs exhibit temporal variability in broadband spectra as they rotate indicative of non-uniform layers of heterogeneous clouds or variations in thickness (Radigan, 2014; Apai et al., 2013; Manjavacas et al., 2017, 2019). Photometric variability is common for L3-T8 dwarfs (Metchev et al., 2015) and evidence has suggested brown dwarfs are variable in the L/T transition at higher amplitudes and with greater frequency than field dwarfs of other spectral types (Radigan, 2014; Buenzli et al., 2014; Lew et al., 2020). For example, Vos et al. (2020) found Spitzer IRAC observations of young, low-gravity brown dwarfs have increased variability amplitudes for late L dwarfs at 4.5 μm.

Brown dwarfs tend to rotate over periods of a few to tens of hours (Metchev et al., 2015) and cloud structures are likely dominated by bands, jets, spots, and storms similar to giant planets in our Solar System (Ackerman and Marley, 2001). Temperature fluctuations alone are not able to account for observed color and spectral variations of brown dwarfs, particularly near the L/T transition (Radigan, 2014; Apai et al., 2013). Time series spectroscopy has been used to probe different atmospheric depths and constrain heterogeneous cloud structures (Lew et al., 2016, 2020). Futhermore, two and three-dimensional simulations suggest large-scale horizontal winds and jets are possible in brown dwarf atmospheres, and gravity-wave induced mixing can prevent dust grains from settling (Showman and Kaspi, 2013; Showman et al., 2018; Freytag et al., 2010). Continued and future variability studies, such as with the James Webb Space Telescope, will be increasingly important in order to properly constrain assumptions for multidimensional atmosphere models.

1.5 Types of Cloud Models

Several one-dimensional models have been developed to describe the bulk properties of clouds in L and T-type brown dwarf atmospheres. The models can be broadly grouped into three categories: dusty, cloudy, cloud free. Estimates of condensate cloud opacities are described by assumptions of the physical and chemical processes in substellar atmospheres, including properties such as the vertical extent of the cloud and particle size distributions. A major assumption of these models is that the atmosphere is assumed to be in thermochemical equilibrium, where material is removed from the gas phase as condensation occurs (Marley and Robinson, 2015).

The extreme limits of clouds are described by the DUSTY (Allard et al., 1998; Chabrier and Baraffe, 2000) and COND (Burrows et al., 1997; Allard et al., 2001) PHOENIX models. DUSTY models are governed by the assumption that condensates (dust) remain dispersed throughout the atmospheric gas in chemical equilibrium and gravitational settling is negligible. The COND, or cloud-free models, on the other hand assume the opposite—all condensates are removed from the photosphere as they form via gravitational settling. These models explain early L and late-T dwarfs well but are not able to reproduce observed properties of all brown dwarfs, particularly for objects near the L/T transition (Faherty et al., 2012; Dupuy and Liu, 2012; Leggett et al., 2002; Kirkpatrick, 2005). Newer PHOENIX models that include an intermediate approach to clouds are discussed in the following section.

Models that simulate clouds in-between the aforementioned limiting cases are capable of describing a more accurate picture of spectra, colors, and chemical compositions of late-L and early-T dwarfs. Because the size of cloud particles can vary strongly with effective temperature, surface gravity, and atmospheric height, these models represent a more detailed example of condensate cloud formation. In the well-known Ackerman and Marley (2001) cloud model, dust formation is parameterized by f_{sed}, where a greater value results in an optically thinner cloud with a larger mean particle size. Tsuji and Nakajima (2003) use a critical temperature, T_{cr}, to

parameterize dust formation. Burrows et al. (2006) developed models for L/T transition objects that use homogeneous forsterite grains at larger grain sizes (e.g., 3, 10, 30, 100 μm). Work from the Helling group incorporate a more complex treatment of grain nucleation, growth, and evaporation by investigating the role of turbulence in the process of dust formation (Helling and Woitke, 2006; Helling et al., 2008a,c,b). Their work focuses on size-dependent heterogeneous dust particles. Models from Charnay et al. (2018) were able to reproduce the spread of near-IR colors across the L/T transition and those observed in reddened low-gravity objects by computing cloud particle radii estimated from simple microphysics.

1.5.1 PHOENIX

In this dissertation, I use the PHOENIX 1-D atmosphere model for interpreting observed photometric and spectroscopic properties of brown dwarf atmospheres. PHOENIX is a well-tested and diverse atmosphere code capable of modeling a range of phenomena including supernovae (Hauschildt and Starrfield, 1995), protoplanetary disks (Hauschildt et al., 1997), brown dwarfs (Allard et al., 2001), and planetary atmospheres (Barman et al., 2001; Barman, 2007). The radiative transfer equation can be solved in PHOENIX using plane-parallel or spherically symmetric geometry. Input parameters are provided, such as effective temperature and surface gravity. The initial atmospheric structure and composition is then calculated under the assumptions of hydrostatic and chemical equilibrium. In order to ensure flux is conserved in the atmosphere, the model calculations are repeated by iteratively adjusting the temperature structure until radiative-convective equilibrium is reached. Some of the first model atmospheres for cool dwarfs were developed in PHOENIX (Allard and Hauschildt, 1995; Hauschildt et al., 1999). The benefits of PHOENIX are that the opacity information is computed directly line-by-line for each run and use a large opacity database including molecular lines from over 130 different species (Fontenla et al., 2015) (e.g., H, H_2, C, N, O, Na, Mg, Al, Si, S, etc.).

The basic structure of clouds in PHOENIX rely on the microphysical timescale

arguments of Rossow (1978) and assume condensate cloud grains form in local thermal equilibrium. The downward transport of cloud particles by sedimentation efficiency is balanced with the upward mixing of condensates, defining the cloud location and particle size. Convection timescales dominate over other growth timescales. The cloud properties are governed by two free parameters—the cloud pressure (P_c) and grain size (a_0)—that jointly function similarly to the f_{sed} parameter in the Ackerman and Marley (2001) with more flexibility. We are able to increase or decrease the thickness of the cloud independent of grain size, but the grain size distribution remains constant with cloud height and follows a log-normal particle size distribution. The base of the cloud is defined by the intersection between the condensation curve with the temperature-pressure profile similar to other models, such as those from Burrows et al. (2006).

1.5.2 Atmospheric Retrieval

Retrieval techniques are another way to interpret observations and characterize cool atmospheres. Some of the earliest examples of retrievals were used to study Earth's atmosphere (Kaplan, 1959). The general framework of atmospheric retrievals is to combine a forward atmosphere model with a statistical method (e.g., Monte Carlo) to test different model parameters. The forward model is often based on simplied assumptions, such as a plane-parallel atmosphere, and a synthetic spectrum is generated. The benefits of the forward model are that they do not have to be self-consistent, in other words, the model does not have to be in chemical or radiative equilibrium like a majority of the models I previously discussed. Several variables can be constrained from retrieval methods including the molecular abundances of various molecules, effective temperature, surface gravity, thermal structure, radius, and optical depth of clouds. Retrieval techniques have been used for several brown dwarfs including L dwarfs (Burningham et al., 2017, 2021), T dwarfs (Line et al., 2017), and Y dwarfs (Zalesky et al., 2019).

1.6 Cosmological Time in Astronomy Education

The study presented in Chapter 4 shifts gears to the educational component. This portion of the dissertation is part of an initiative to identify undergraduate students' perceptions of Earth's place in the Universe through an exploration of how students construct their knowledge of causality and chronology from a cosmic evolutionary perspective. In order for learners to develop scientifically accurate explanations of astronomical phenomena, students are required to imagine events from different perspectives and time frames, such as before Earth existed (e.g., Wilhelm, 2003; Kikas, 2006; Black, 2005; Heyer et al., 2013; Slater, 2015). It has been shown there is a key link in the conceptual understanding of time through its relationship with spatial thinking (Chrysikou and Ramey, 2006; Friedman, 1989; Matlock et al., 2005).

Topics in astronomy education have become more diverse in the past several decades and expanded beyond traditional concepts (e.g., lunar cycles, Earth-Sun-Moon system, cosmology). Fundamental changes in students' pre-instructional knowledge may be occurring to incorporate topics that have become more commonplace in and out of the classroom such as the study of exoplanets and astrobiology. It is important to understand how students are constructing their new understanding of Earth's place in time and space in the Universe in order to develop effective curricula and instruction.

Research regarding how learners approach the concept of time is stretched across science education, cognitive science, and psychology. The majority of work relevant to this dissertation is within the geosciences literature. Studies on students' understanding of geological time is closely related and has been conducted on students at the elementary (Ault, 1982; Schoon, 1992), high school (Marques and Thompson, 1997; Schoon, 1992), and college levels (Delaughter and Stein, 1998; Libarkin and Anderson, 2005). The age of the Earth has been a strong focus of many studies and has unfortunately shown that learners of various ages are unable to quote the correct order of magnitude estimate for the Earth's age (Marques and Thompson, 1997; Libarkin et al., 2005, 2007).

Although there are educational parallels between timescales in geology and astronomy, research on the concept of time in astronomy has not been investigated as thoroughly. Only a few of the geology papers described above included an astronomical event, such as the Big Bang (Trend, 2001b; Delgado, 2013). Furthermore, the formation of the Solar System and cosmology are two topics that were reported to be lacking in the literature in terms of both student understanding and means of assessment (Slater, 2015). Conceptualizing vast timescales in astronomy is essential in order to understand the scientific concepts involved; yet, such magnitudes of time lack a certain relatable human experience, leaving learners faced with challenges when trying to grasp how long ago an astronomical event occurred (e.g., the Big Bang), the duration of individual events (e.g., formation of the Solar System or other planetary systems), and the amount of time between major events. Our work was motivated by this gap in literature explicitly addressing students' knowledge of timescales in astronomy.

We investigated non-science undergraduate students' pre-instructional views by asking open-ended response questions that place the time of (and events prior to) Earth's formation within the larger context of the formation of the Universe. We examined how students approached these "big idea" concepts within astronomy and how students incorporated new information (e.g., exoplanets) into their pre-existing knowledge. We thematically coded student-supplied responses for common themes, ideas, and misconceptions. Additionally, we conducted an extensive literature review across multiple disciplines to create a comprehensive source of information regarding students' understanding of time as it relates to astronomy education. This work significantly expands upon existing time-related research and provides insight into students' pre-instructional ideas important for developing learner-centered curricula and assessment instruments in the future.

1.7 Summary of Dissertation

This dissertation seeks to add to the current understanding of two fields of research—planetary science and astronomy education—described in the previous sections. Chapter 2 is an in-depth study of the atmospheric properties of 12 brown dwarf binary objects spanning from mid-L to mid-T in spectral type ($T_{eff} \approx$ 1900-1000 K). Chapter 3 branches off from this study to focus on an individual benchmark system HD 130948B+C, a pair of L4+L4 brown dwarfs orbiting a solar-type primary star, HD 130948A. Chapter 4 presents the education component where I focus on analysis of four open-ended questions answered by undergraduate students. The work in Chapter 4 was selected and published in a special astronomy education issue of Physical Review Physics Education Research (PRPER) with an accompanying invited talk to the 2019 American Astronomical Association (AAS) conference in Seattle, Washington. Since publication, Chapter 4 has been updated and improved upon for the sake of this dissertation. Chapter 5 wraps up the work presented here with a summary of key findings and looks ahead to future work.

CHAPTER 2

Cloud Properties of Brown Dwarf Binaries Across the L/T Transition

The contents of this chapter were published in Brock et al. (2021)

2.1 Abstract

We present a new suite of atmosphere models with flexible cloud parameters to investigate the effects of clouds on brown dwarfs across the L/T transition. We fit these models to a sample of 13 objects with well-known masses, distances, and spectral types spanning L3-T5. Our modelling is guided by spatially-resolved photometry from the Hubble Space Telescope and the W. M. Keck Telescopes covering visible to near-infrared wavelengths. We find that, with appropriate cloud parameters, the data can be fit well by atmospheric models with temperature and surface gravity in agreement with the predictions of evolutionary models. We see a clear trend in the cloud parameters with spectral type, with earlier-type objects exhibiting higher-altitude clouds with smaller grains (0.25-0.50 μm) and later-type objects being better fit with deeper clouds and larger grains ($\geq$1 μm). Our results confirm previous work that suggests L dwarfs are dominated by submicron particles, whereas T dwarfs have larger particle sizes.

2.2 Introduction

As important opacity sources, clouds play a major role in determining the atmospheric structures, emergent spectra, and evolution of brown dwarfs. Clouds fundamentally impact the observational properties of color, magnitude, and spectra with compositions that span a diverse mix of condensates dependent upon a wide range of effective temperatures, gravities, metallicities, and pressures (Helling and Casewell, 2014; Marley and Robinson, 2015). The transition from L to T spectral types is perhaps the most well-known impact of changes in cloud opacity with observations of over 1000 field dwarfs highlighting the drastic shift in near-infrared colors from red to blue that occurs around a narrow range of effective temperatures (≈1400 K) (Faherty et al., 2012; Dupuy and Liu, 2012; Leggett et al., 2002; Kirkpatrick, 2005).

Atmospheres of L dwarfs are dominated by refractory materials condensing and forming optically thick cloud layers (e.g., Tsuji et al., 1996; Allard et al., 2001; Cushing et al., 2008; Marley et al., 2002). The common species include iron (Fe), corundum (Al_2O_3), enstatite ($MgSiO_3$), and forsterite (Mg_2SiO_4). T dwarfs mark the disappearance of thick iron and silicate clouds from the photosphere and the appearance of methane absorption (Kirkpatrick, 2005; Marley et al., 2010; Burgasser et al., 2003). Matching observed colors and spectra of L dwarfs requires some type of cloud layer in atmosphere models (Burrows et al., 2006). Mid-T dwarfs and cooler types are often best approximated using cloud-free atmosphere models (Kirkpatrick, 2005); however, in some cases models with optically thin or inhomogeneous clouds composed of low temperature condensates (Na_2S, KCl, ZnS, MnS, Cr) can match T-dwarf photometry (Morley et al., 2012; Charnay et al., 2018).

Self-consistent, one-dimensional atmosphere models have been the most widely used to study brown dwarfs. While they do not capture the atmospheric dynamics (e.g., Showman et al., 2018; Zhang and Showman, 2014; Tan and Showman, 2019, 2021; Charnay et al., 2018) they do an excellent job of capturing the average properties and allow one to study the spectral trends across the brown dwarf population with a homogeneous set of modelling assumptions. The most recent model

spectra have reached a high degree of realism through the development of molecular opacity databases (Freedman et al., 2008; Sharp and Burrows, 2007; Tennyson and Yurchenko, 2012), the chemistry of gas and condensate species (Lodders and Fegley, 2002), and resonance line broadening (Burrows et al., 2001; Allard et al., 2001). Incorporating parameterized clouds into atmosphere models better facilitates the interpretation of observational data, and these approaches have shown that L dwarfs and early T dwarfs are better represented by cloudy models rather than previous cloud-free models (Marley et al., 2002; Ackerman and Marley, 2001; Allard et al., 2001; Tsuji et al., 1996). In general, if appropriate input is provided, synthetic photometry, spectra, and colors generated by models are able to reproduce observational data quite well (Saumon and Marley, 2008).

Cloudy and cloud-free limits provide useful insight into the photometric and spectroscopic trends across brown dwarf spectral types, but these limiting cases do not accurately predict the scatter of colors within the L spectral type (Marley et al., 2010) and often fail to match individual brown dwarfs (Burrows et al., 2006). Liu et al. (2016) confirmed that low-gravity objects occupy a distinct region of the color-magnitude diagram separate from field brown dwarfs of the same spectral type. The complexities pose additional challenges in understanding how brown dwarfs evolve through time, especially across the L/T transition($\approx$ L8-T4), where major changes in atmospheric chemistry and dynamics occur. L dwarfs with red near-infrared colors are associated with signs of youth (Kirkpatrick et al., 2008; Cruz et al., 2009), low gravity, and/or high metallicity (McLean et al., 2003; Looper et al., 2008b; Stephens et al., 2009); whereas bluer L dwarfs are typically associated with an older age, higher gravity, and/or low metallicity (Schmidt et al., 2010; Burgasser et al., 2010; Cushing et al., 2010). Secondary influences from clouds can cause additional color dispersion, ranging from the thickness of the clouds to larger grain sizes (Knapp et al., 2004; Burgasser et al., 2008b). Although models can reproduce spectra of red L dwarfs with thick condensate clouds, there has been disagreement in effective temperatures across models (Gizis et al., 2012). The challenge is developing comprehensive atmosphere models while disentangling the effects of local cloud

properties (e.g., thickness, grain size) within an atmosphere from global parameters (e.g., surface gravity, metallicity). Recent advancements use rotational modulation coupled with heterogeneous cloud models that include disequilibrium CO/CH_4 chemistry to isolate differences between cloud-induced and gravity-induced features (Lew et al., 2016, 2020).

Another approach to this problem is to investigate the properties of clouds in a sample of well-studied brown dwarf binary systems with precisely measured properties. Resolved photometry and spectroscopy for field age binaries of known distance and mass provide the clearest picture of the L-T spectral sequence as coevality can be assumed for such systems. The two components often have similar compositions, surface gravities, relatively constant radii for their age ($\geq$ 0.5 Gyr), and tend to have nearly equal masses (Dupuy and Liu, 2012). Furthermore, individually resolved brown dwarf binaires provide the most robust tests for atmospheric and evolutionary models to-date through precisely measured dynamical masses. Mass is one of the most fundamental parameters of brown dwarfs that can aid in unravelling atmospheric complexities through its influence on surface gravity and evolution; however, mass is often difficult to measure and observations are complicated by the largely unknown span of ages for field objects due to degeneracies between mass and age (Konopacky et al., 2010; Dupuy and Liu, 2017).

Testing and constraining substellar evolutionary models requires benchmark brown dwarfs–objects with independently determined masses, luminosities, and ages. Early work hinted at a luminosity problem where comparisons between dynamical masses and masses predicted by evolutionary models differed significantly (Dupuy et al., 2009a; Konopacky et al., 2010; Dupuy et al., 2014). The consistency between predicted and measured masses has improved with continued astrometric monitoring (Dupuy and Liu, 2017) and models that consider cloud clearing (Saumon and Marley, 2008; Allers and Liu, 2013). A related problem exists for benchmark brown dwarfs when comparing the effective temperatures and gravities predicted by evolution models to those obtained by comparing model spectra to observed photometry or spectra. Differences in temperature as large as several hundred Kelvin

and differences in gravity of an order of magnitude are not uncommon across the L/T transition (Cushing et al., 2008). Clouds can alleviate some of the discrepancy between evolutionary and atmosphere model comparisons but does not eliminate the problem completely (Wood et al., 2019). Some of the issues may be improved with very broad wavelength coverage (Briesemeister et al., 2019). In addition to refined cloud parameters, metallicity (Wood et al., 2019; Crepp et al., 2018), non-equilibrium chemistry (Barman et al., 2011a; Zhang et al., 2020), or other missing physics in the models (Charnay et al., 2018) (e.g., cloud microphysics) may be remaining sources of tension.

The importance of clouds shaping observed properties across the L/T transition motivates our work to investigate cloud properties of individual brown dwarf binaries. An increase in the number of binary systems with known distance and mass across a broad range of temperatures allows us to explore the validity of previous discrepancies between predictions of atmosphere and evolutionary models.

In this paper, we test whether cloudy atmosphere models can be produced that match multi-band photometric observations to a reasonable degree. We focus on a sample of seven brown dwarf binary systems that span mid-L to mid-T in spectral type. By using a small sample size and a range of spectral types on either side of the L/T transition, we are able to explore cloud properties in finer detail across a broad range of temperature and gravity. In addition to studying the cloud properties, we determine the effective temperatures for each binary component in the sample, independent of spectral type. Near-infrared photometry can be used to estimate $T_{\rm eff}$; however, because $T_{\rm eff}$ is a bolometric quantity, broad coverage of the spectral energy distribution (SED), especially on both sides of $\lambda_{\rm max}$, is highly desirable. We are able to determine a robust value of $T_{\rm eff}$ for these binaries for the first time using optical, spatially-resolved photometry provided by HST.

2.3 Brown Dwarf Binary Sample

2.3.1 Sample Selection

Approximately 68 visual, ultracool binaries (spectral type M7 or later) in the solar neighborhood have been identified in the last decade using high angular resolution imaging surveys conducted with the Hubble Space Telescope (HST) and ground-based adaptive optics systems (e.g., Lane et al., 2002; Liu et al., 2008; Burgasser et al., 2007). Over half of these binaries have been well-studied, undergoing extensive astrometric monitoring to determine precisely measured total and individual masses (30-115 $M_{\rm Jup}$) and robust orbits have been determined for 23 systems (Konopacky et al., 2010; Dupuy and Liu, 2017). For a discussion on the larger initial sample selection, see Burgasser et al. (2007) and for more information regarding astrometric monitoring see Konopacky et al. (2010) and Dupuy and Liu (2017).

We selected seven binary systems from the set reported in Konopacky et al. (2010). These systems include 13 objects spanning spectral types from ≈L4-T5 and one late-M dwarf. Since the work published Konopacky et al. (2010), distance and mass values have been updated for many objects in our sample. A summary of properties from the literature and updated masses are provided in Table 2.1. Distance uncertainties have been improved for all objects in our sample. Table 2.2 shows previously used parallaxes with updated distance calculations based on work from Dupuy and Liu (2017) and the recent GAIA DR2 release (Brown et al., 2018).

2.3.2 Photometry Measurements

The years of astrometric monitoring of the brown dwarf binary components in our sample resulted in precise, spatially resolved J, H, and K broad-band flux measurements. The majority of these near-infrared photometric measurements were obtained at the Keck Observatory using the NIRC2 instrument behind adaptive optics. Details on the observing and reduction procedure can be found in Konopacky et al. (2010).

Table 2.1: Properties of Binary Sample

	Primary Component				Secondary Component					
System	$M_{\rm Jup}$	$\log(L_{\rm bol}/L_\odot)$	SpT	$T_{\rm eff}$ (K)	$M_{\rm Jup}$	$\log(L_{\rm bol}/L_\odot)$	SpT	$T_{\rm eff}$ (K)	Age (Gyr)	Ref.
HD 130948BC	$59.8^{+2.0}_{-2.1}$	-3.85 ± 0.06	L4 ± 1	1920^{+70}_{-60}	$55.6^{+2.0}_{-1.9}$	-3.96 ± 0.06	L4 ± 1	1800^{+50}_{-70}	0.4-0.8	1,2,3
2MASS J0920+3517AB	71 ± 5	-4.270 ± 0.030	L5.5 ± 1	1621^{+32}_{-30}	116^{+6}_{-8}	-4.340 ± 0.030	L9 ± 1.5	1320 ± 250	$3.1^{+1.5}_{-1.7}$	1
2MASS J1728+3948AB	73 ± 7	$-4.29^{+0.04}_{-0.05}$	L5 ± 1	1600 ± 40	67 ± 5	-4.49 ± 0.04	L7 ± 1	1440 ± 40	$3.4^{+2.8}_{-2.1}$	1
2MASS J0850+1057AB[a]	54 ± 8	-4.22 ± 0.18	L6.5 ± 1	1590 ± 290	54 ± 8	-4.47 ± 0.18	L8.5 ± 1.0	1380 ± 250	0.25-1.5	4
LHS2397aAB	93 ± 4	-3.34 ± 0.04	M8± 0.5	2560 ± 50	66 ± 4	-4.48 ± 0.04	L7.5 ± 1	1440 ± 40	$2.6^{+0.6}_{-1.0}$	1
SDSS 1021-0304AB[b]	52^{+6}_{-7}	···	T0 ± 1	1332 ± 100	52^{+6}_{-7}	···	T5 ± 0.5	1103 ± 100	···	1,5
2MASS J1534-2952AB	51 ± 5	-4.91 ± 0.07	T4.5 ± 0.5	1150^{+40}_{-50}	48 ± 5	-4.99 ± 0.07	T5 ± 0.5	1097 ± 50	$3.0^{+0.4}_{-0.5}$	1,2

References [1] Dupuy and Liu (2017), [2] Konopacky et al. (2010), [3] Dupuy et al. (2014), [4] Burgasser et al. (2010), [5] Stephens et al. (2009)

[a] Total mass and temperature from Dupuy and Liu (2017). Luminosity reported from Konopacky et al. (2010).

[b] Total mass from Dupuy and Liu (2017), and temperatures calculated from Stephens et al. (2009) spectral type-temperature relationship.

Table 2.2: Distances of Sample

Target	Distance [pc]	Parallax [mas]	Updated Distance [pc]	Δ
HD 130948BC	18.18 ± 0.08	55.73 ± 0.80	17.94 ± 0.25	1%
2MASS 0920+35AB	24.3 ± 5.0	32.3 ± 0.6	31.0 ± 0.60	28%
2MASS 1728+39AB	24.1 ± 2.1	36.4 ± 0.6	27.5 ± 0.47	14%
2MASS 0850+10AB	38.1 ± 7.3	31.4 ± 0.6	31.8 ± 0.55	17%
LHS 2397aAB	14.3 ± 0.4	69.4903 ± 0.1760	14.3905 ± 0.0364	1%
SDSS 1021-03AB	···	33.7 ± 1.2	29.7 ± 1.05	···
2MASS 1534-29AB	13.59 ± 0.22	63.0 ± 1.1	15.9 ± 0.3	15%

We provide updated distances using the most recent parallax values from Brown et al. (2018) and Dupuy and Liu (2017). A percent difference is calculated in column five to show improvement in precision. Note, SDSS 1021-03AB was not included in Konopacky et al. (2010).

To obtain photometry and astrometry, we used the package StarFinder from Diolaiti et al. (2000) (see Konopacky et al. 2010 for more details on the application for this dataset). For photometry, StarFinder provides the ratio of the fluxes of the binary components. We then use that ratio and the combined light magnitudes from 2MASS (Cutri et al., 2003) to derive individual apparent magnitude values for each component. Uncertainties are calculated by computing the RMS of the photometry from all individual images, and then propagating those uncertainties with those provided in the 2MASS catalog.

Additional photometric measurements were obtained from the Mikulski Archive for Space Telescopes (MAST). Most of the archival data are from programs 10559/PI:Bouy and 9451/PI:Brandner using Advanced Camera for Surveys (ACS) and filters F625W, F775W, F850LP. The archived data were supplemented with more recent observations using the Wide Field Camera 3 (WFC3/UVIS), 11605/PI:Barman. The filters (F625W, F775W, and F850LP) were chosen to provide Sloan-equivalent r, i, and z-band photometric measurements.

Data were collected in 2010 for Program 11605. We observed each target four times per filter. Both raw and calibrated data frames were retrieved post observation from MAST. Data are processed through the standard calibration pipeline for WFC3, as described in the WFC3 Data Handbook (Gennaro et al., 2019), including correction for geometric distortion.

Photometric measurements were obtained in two ways. First, we used the StarFinder algorithm to derive positions and fluxes of the components. We ran this algorithm on the distortion-corrected images. Since StarFinder requires a PSF estimate in the case of an uncrowded image like that of a binary star, we used TinyTim to generate synthetic PSFs at the proper wavelengths. Based on this PSF, StarFinder detected the components of the binary and returned a centroid and estimated flux. Based on those fluxes, we used the WFC3/UVIS zeropoints to compute the magnitudes of each source.

We also used the code written specifically for Hubble observations for photometry and astrometry, *img2xym* (Anderson and King, 2006), modified for WFC3/UVIS. It is designed to be used with the "FLT" images, on which distortion has not been applied. It outputs the positions and fluxes of stars that it identifies based on an isolation index which describes the allowed separation between sources. Running this code on our frames provided positions and fluxes, which were converted to magnitudes using the proper zeropoints.

Uncertainties in the WFC3/UVIS fluxes were determined as they were for NIRC2 data, by fitting all data frames individually and then looking at the RMS variation. We found that StarFinder and *img2xym* returned consistent fluxes, and hence magnitudes, for most cases. However, since a number of the binaries were very closely separated in the epoch of observation (e.g., 2MASS 0920+35AB was separated by $<$1.5 pixels), we opted to present here the results from the StarFinder analysis, as the *img2xym* code warns about unreliable results for stars separated by $<$2 pixels.

A complete list of photometry for our sample is provided in Tables 2.3 and 2.4. In cases where the photometry was previously published, we have adopted those values here.

2.4 Spectral Type Classification

We derive spectral types for the nine objects in our sample using template fits to the SEDs composed of resolved photometry for each object. We then compare our

Table 2.3: HST Photometric Observations

Target	F625W	F625W	F775W	F775W	F814W	F850LP	F850LP	F1042W
Instrument	[ACS]	[WFC3]	[ACS]	[WFC3]	[WFPC2]	[ACS]	[WFC3]	[WFPC2]
2MASS 0920+35A	···	21.14 ± 0.25	···	18.35 ± 0.12	17.37 ± 0.18	···	15.75 ± 0.18	···
2MASS 0920+35B	···	22.28 ± 0.71	···	19.36 ± 0.36	18.25 ± 0.21	···	16.07 ± 0.15	···
2MASS 1728+39A	···	···	···	···	18.06 ± 0.07	···	···	15.60 ± 0.10
2MASS 1728+39B	···	···	···	···	18.71 ± 0.07	···	···	15.35 ± 0.12
LHS 2397aA	···	17.66 ± 0.04	···	15.75 ± 0.05	14.27 ± 0.04	···	12.63 ± 0.05	···
LHS 2397aB	···	22.50 ± 0.33	···	20.60 ± 0.34	18.69 ± 0.17	···	16.78 ± 0.09	···
2MASS 0850+10A	21.32 ± 0.28	···	18.80 ± 0.24	···	17.78 ± 0.15	16.56 ± 0.24	···	···
2MASS 0850+10B	22.62 ± 0.39	···	19.96 ± 0.28	···	19.25 ± 0.18	17.42 ± 0.26	···	···
SDSS 1021-03A	···	···	···	20.87 ± 0.63	···	···	17.01 ± 0.62	···
SDSS 1021-03B	···	···	···	22.03 ± 0.64	···	···	17.42 ± 0.62	···
2MASS 1534-29A	···	···	···	21.11 ± 0.14	19.22 ± 0.05	···	16.64 ± 0.36	15.39 ± 0.12
2MASS 1534-29B	···	···	···	21.61 ± 0.20	19.52 ± 0.06	···	17.04 ± 0.15	15.59 ± 0.24

Table 2.4: Near-IR Photometric Observations

Target	J	H	K_s
HD 130948B	12.53 ± 0.07	11.76 ± 0.10	10.98 ± 0.04
HD 130948C	12.84 ± 0.08	12.05 ± 0.11	11.18 ± 0.04
2MASS 0920+35A	13.89 ± 0.17	12.92 ± 0.07	12.12 ± 0.08
2MASS 0920+35B	13.94 ± 0.33	13.01 ± 0.09	12.44 ± 0.10
2MASS 1728+39A	14.27 ± 0.09	13.11 ± 0.08	12.20 ± 0.06
2MASS 1728+39B	14.58 ± 0.09	13.56 ± 0.08	12.80 ± 0.06
LHS 2397aA	11.18 ± 0.02	10.50 ± 0.03	10.02 ± 0.02
LHS 2397aB	14.65 ± 0.08	13.61 ± 0.08	12.79 ± 0.04
2MASS 0850+10A	14.24 ± 0.07	13.27 ± 0.11	12.56 ± 0.10
2MASS 0850+10B	14.70 ± 0.14	13.70 ± 0.14	12.91 ± 0.16
SDSS 1021-03A	14.22 ± 0.09	13.48 ± 0.09	13.27 ± 0.08
SDSS 1021-03B	14.33 ± 0.09	14.27 ± 0.11	14.25 ± 0.08
2MASS 1534-29A	14.57 ± 0.08	14.48 ± 0.07	14.46 ± 0.13
2MASS 1534-29B	14.73 ± 0.12	14.83 ± 0.10	14.73 ± 0.15

inferred spectral types to spectral types determined using spatially unresolved data and reported in the literature (Dupuy and Liu, 2012, 2017).

We compiled a set of brown dwarf template spectra listed in Table 2.5 spanning spectral types M7 to T9 to compare to the objects in our sample. Both optical and near-IR spectral templates were used when available. Template spectra come from the Spex Prism Library collected by and maintained by Burgasser (2014). Each spectral template was absolute flux calibrated using 2MASS J-band photometry, and an absolute magnitude was determined for each brown dwarf template for seven of our band-pass filters for which there is complete spectral template coverage from 0.8-2.5 μm.

$$M = -2.5\ log \frac{\int f_\lambda\ S(\lambda)\ d\lambda}{\int f_{\rm Vega}\ S(\lambda)\ d\lambda}, \tag{2.1}$$

where f_λ and $f_{\rm Vega}$ are the photon flux densities of the template spectrum and Vega, respectively, at 10 parsecs. $S(\lambda)$ is the filter response function.

We used a χ^2 approach to find the best match

$$\chi^2 = \sum_i^n \frac{(M_{\rm obs,i} - M_{\rm Spex,i} + \delta M_{\rm avg})^2}{\sigma^2_{\rm obs,i}}, \tag{2.2}$$

where n is the number of photometric measurements available for a given object,

Table 2.5: Spex Spectral Standards

SpT	Template (NIR)	Template (OPT)	References
M7	VB 8	···	[1]
M8	VB 10	···	[2]
M9	LHS 2924	···	[3]
L0	2MASS J0345+2540	···	[3]
L1	2MASSW J2130-0845	2MASSW J1439+1929	[2,4]
L2	2MASSI J04082-1450	···	[12]
L3	2MASSW J1506+1321	2MASSW J1146+2230	[5,6]
L4	2MASS J21580457-1550098	···	[4]
L5	SDSS J083506.16+195304.4	DENIS-P J1228.2-1547	[5,7]
L6	2MASSI J1010-0406	2MASSs J0850+1057	[5,8]
L7	2MASSI J0103+1935	DENIS-P J0205.4-1159	[5,9]
L8	2MASSW J1632+1904	···	[6]
L9	DENIS-P J0255-4700	···	[10]
T0	SDSS J120747.17+024424.8	···	[11]
T1	SDSS J015141.69+124429.6	···	[2]
T2	SDSSp J125453.90-012247.4	···	[2]
T3	2MASS J1209-1004	···	[2]
T4	2MASSI J2254188+312349	···	[2]
T5	2MASS J15031961+2525196	···	[2]
T6	SDSSp J162414.37+002915.6	···	[10]
T7	2MASSI J0727+1710	···	[10]
T8	2MASSI J0415-0935	···	[2]
T9	UGPS J072227.51-054031.2	···	[2]

A list of all brown dwarf templates used for spectral type determination obtained from the Spex Library. All templates had complete coverage from 0.8-2.5 μm. Additional optical spectral standards were included for a few L-types due to their availability in the library.

References: [1] Burgasser et al. (2008a), [2] Burgasser et al. (2004), [3] Burgasser and McElwain (2006), [4] Kirkpatrick et al. (2010), [5] Burgasser et al. (2010), [6] Burgasser et al. (2007), [7] Chiu et al. (2006), [8] Reid et al. (2006), [9] Cruz et al. (2004), [10] Burgasser et al. (2006), [11] Looper et al. (2008b), [12] Cruz et al. (2017)

Table 2.6: Spectral Type Fitting

Target	SpT Lit.	Fit SpT	Fit Name	χ^2
HD 130948B	L4±1	L3±1	2MASSW J1146345+223053	3.3
HD 130948C	L4±1	L5±1	SDSS J083506.16+195304.4	5.3
2MASS 0920+35A	L5.5±1	L3±3	SDSS J083506.16+195304.4	4.5
2MASS 0920+35B	L9 ±1.5	L4±3	DENIS-P J0205.4-1159	0.2
2MASS 1728+39A	L5 ±1	L7±1	2MASS J0103320+193536	5.4
2MASS 1728+39B	L7 ±1	L9±1	DENIS-P J0255-4700	5.4
LHS 2397aA	M8±1	M8±1	VB 10	5.60
LHS 2397aB	L7.5±1	L8±1	2MASSW J1632291+190441	2.1
2MASS 0850+10A	L6.5±1	L5±2	SDSS J083506.16+195304.4	0.5
2MASS 0850+10B	L8.5±1	L6±2	2MASSs J0850359+105716	3.1
SDSS 1021-03A	T0 ±1	T2±1	SDSSp J125453.90-012247.4	5.2
SDSS 1021-03B	T5 ±1	T8±1	2MASSI J0415195-093506	1.6
2MASS 1534-29A	T4.5±1	T5±1	2MASS J15031961+2525196	5.4
2MASS 1534-29B	T5±1	T6±1	SDSSp J162414.37+002915.6	6.6

Previously determined spectral types for objects in our sample are listed in column two (Dupuy and Liu, 2017). Columns 3-4 provide the best-fitting brown dwarf template from Table 2.5. HD 130948B and 2MASS 0850+10B were both fit to optical templates for L3 and L6, respectively.

M_{obs} are our observations, M_{Spex} are the Spex absolute magnitudes for each spectral template, δM_{avg} is the average offset between the observations and Spex magnitudes, and σ_{obs} are the uncertainties for our observations. The results of our fitting and resulting component spectral types are provided in Table 2.6.

A lack of brown dwarf spectral templates with broad coverage across optical and near-infrared wavelengths limited our ability to use all of our HST data. However, the majority of spectral types we determined from our template fitting were consistent with previously reported types from the literature. Table 2.6 shows a summary of our results. In a few cases for the coolest objects in our sample, we found a slightly later classification by 1-2 spectral types than Dupuy and Liu (2017).

The 2MASS 0920+35AB system warrants further discussion. 2MASS 0920+35A was fit to an earlier L3 ± 3 but was consistent with literature (L5.5 ± 1). 2MASS 0920+35B was fit to L4 ± 3 discrepant from the literature value by 0.5 (L9 ± 1.5). It was difficult to determine a type for both components in this system due to similar χ^2 values for L3, L4, L5, L7 types. Dupuy and Liu (2017) suggest 2MASS 0920+35B may be an unresolved binary partially due to a large individual mass of 116^{+7}_{-8} M_{Jup}.

The trends in spectral type and local minima further strengthen the possibility that 2MASS 0920+35B is indeed composed of more than one object.

The consistency of our fitted spectral types to the types reported in the literature gives us confidence that our data, taken over multiple epochs and using multiple instruments, is sound. Given the large errors on some of our fitted spectral types; however, we will defer to the more precise types reported by Dupuy and Liu (2017) whenever a spectral type is necessary.

2.5 Model Atmospheres

To investigate the properties of the brown dwarfs in our sample further, we use the model atmosphere code PHOENIX to produce grids of synthetic spectra and photometry to compare to our data. We use the one-dimensional version of PHOENIX which self-consistently calculates the atmospheric structure and emergent spectrum under the assumptions of hydrostatic, chemical, and radiative-convective equilibrium (Hauschildt et al., 1998). PHOENIX solves the radiative transfer line-by-line and maintains a frequently updated database of molecular opacities (Tennyson and Yurchenko, 2012). The atmosphere models were calculated with a sampling of 1 Å between 0.9 and 5 μm. For the remaining wavelength ranges, the sampling varies from 2 to 5 Å. For clarity, the model spectra have been convolved with a Gaussian of FWHM $\approx$ 70 Å unless otherwise specified.

Solid and liquid particles suspended in an atmosphere (clouds) are arguably the most complex process to include in brown dwarf and giant planet atmosphere models. Atmospheres of substellar-mass objects span a large range of temperatures and pressures that allow the formation of a complex mixture of condensate species. Early works tackling the issues of cloud formation often focused on bracketing the extreme limits of condensate opacities by exploring cloud-free and complete chemical equilibrium clouds. Examples include the COND and DUSTY models of Allard et al. (2001) and comparable models from Burrows et al. (2001). These early works explained well the broad range of near-IR colors of brown dwarfs but were not

intended to reproduce the observed properties of all objects, especially not those in or near the L/T transition.

A number of cloud models with higher degrees of parameterization were developed to expand the applicability of atmosphere models for a greater variety of brown dwarfs suspected of containing clouds. Such models have included a range of tunable parameters for solid particle growth, mixing, and sedimentation timescales as well as mean grain size, particle size distributions, and explicit limits on position and vertical extent of the cloud (see Marley et al. (2002) or Helling et al. (2008a) for a comprehensive review). For this work we are interested in quantifying the simplest set of cloud parameters capable of reproducing the SEDs of brown dwarfs across the L/T transition. New atmosphere grids were developed specifically for this study informed by previous exoplanet atmosphere grids (Barman et al., 2011a, 2015; Stone et al., 2020; Miles et al., 2020) and after extensive testing of various cloud properties.

To that end we use the parameterized cloud model described in Barman et al. (2011a). The model includes one cloud composed of multiple condensates, each contributing to the total opacity based on their absorption and scattering cross-sections and relative number densities. A multiplicative weighting function is applied to the chemical equilibrium number densities where the value of the function is one for $P_{gas} > P_c$ and decreases exponentially for $P_{gas} \leq P_c$ (only a single P_c value is used for each atmosphere model). This weighting function is similar to the family of models described in Burrows et al. (2006); however, here the base of the cloud is always set by the deepest model layer where the chemical equilibrium condensate number density is non-zero. Figure 2.1 illustrates the basic structure for a model where P_c is larger than P_{gas} at the cloud base. In such a situation, the condensate number densities across the cloud layers are multiplied only by the exponentially decaying part of the weighting function and, thus, are less than the chemical equilibrium values across all cloud layers. For models where P_c is smaller than P_{gas} at the cloud base, the condensate number densities will be equal to their chemical equilibrium values for layers between P_c and the cloud base, then dropping

off for $P_{gas} < P_c$. With this simple model, we can adjust the cloud's vertical extent and particle number density with a single parameter.

The cloud opacity is included self-consistently in the overall model calculation. Each model starts from a previous model calculation that is the closest to the new model across the various parameters. After each iteration, the gas and condensate chemistry and associated opacities are recalculated based on a revised temperature structure. The process is repeated as the model converges toward radiative-convective equilibrium. Figure 2.2 illustrates how cloud pressure influences the spectrum and temperature-pressure profile.

For simplicity, grain size is assumed to be independent of height and governed by an additional free parameter of mean particle size, a_0. A log-normal distribution of grain sizes is included based on work from Marley et al. (1999). The range of mean particle sizes in our models span 0.25-10 μm. Model grains include those in the PHOENIX database that are thermodynamically permissible and included in the total cloud opacity (Ferguson et al., 2005). Figure 2.3 illustrates how grain size influences the spectrum when P_c is held constant at 20 bars. At 1500 K adjustments to grain size have little impact at the J band near 1.3 μm. However, as objects approach the L/T transition and the temperature is decreased to 1300 K, changes in J-band flux are more apparent and large differences in spectral shape can be seen between the H and K bands when comparing cloudy versus cloud-free models.

2.6 Results

2.6.1 Grid Fitting

We fit resolved photometry to model grids to better understand the nature of clouds in substellar atmospheres spanning the L/T transition. Table 2.7 summarizes the grid properties and includes the new grids created specifically for this work, extending cloud properties across a broader range of pressures and incorporating models with smaller mean grain sizes. All models in the grid are solar metallicity with effec-

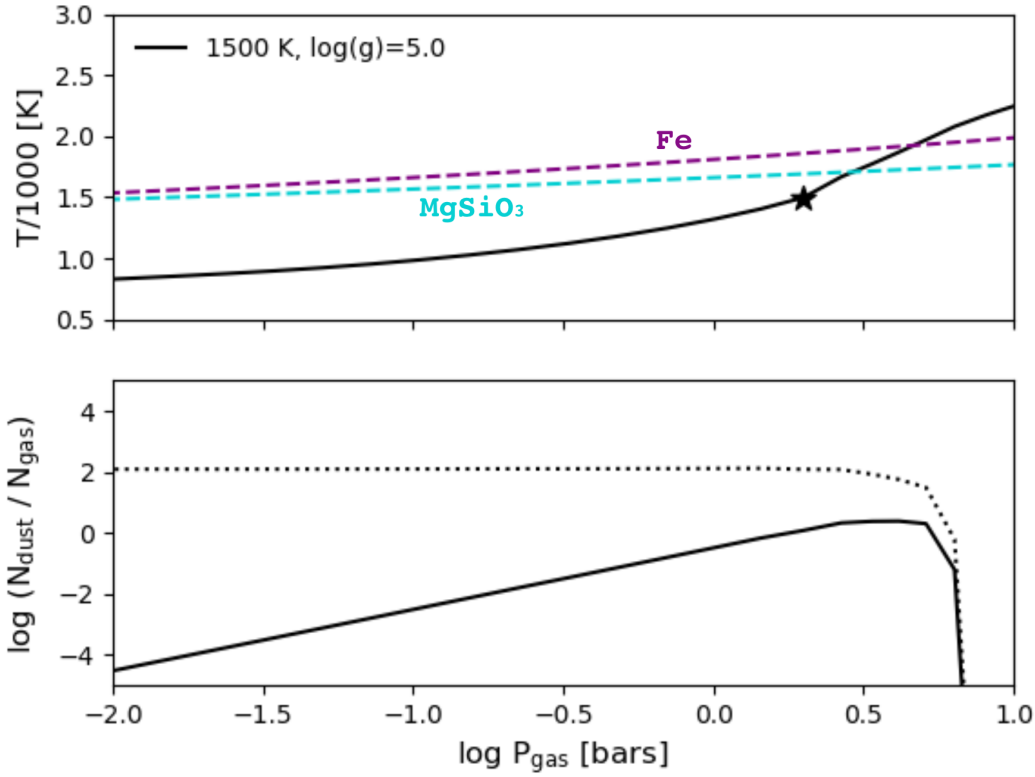

Figure 2.1: *Top panel:* Temperature-Pressure profile for cloudy atmosphere model with P_c=20 bars and a_0=0.25 μm. Condensation curves for iron and enstatite are shown. The star represents the location of the photosphere. *Bottom panel:* Dust-to-gas ratio for pure equilibrium clouds (dotted line) and intermediate cloudy model (solid line).

tive temperatures ranging from 800-2000 K and surface gravities of log(g)=3.0-5.5. The conservative range of our models is suitable for objects from early L through early T dwarfs (Kirkpatrick, 2005).

We calculate synthetic photometry for all models using HST and 2MASS filter transmission curves mentioned in Section 2.3. A best-fitting model is determined for each object using a χ^2 fitting approach. We take the scale factor as

$$s = (R/D)^2, \tag{2.3}$$

where R is the radius of the object to be fit, and D is 10 parsecs for absolute magnitude.

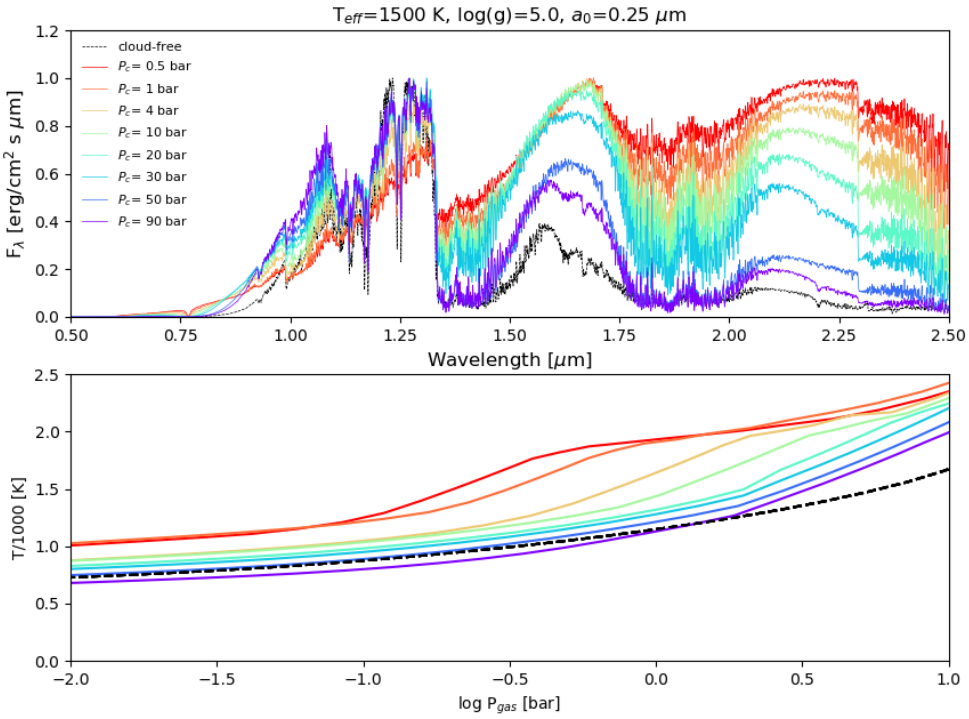

Figure 2.2: Comparison between model spectra and T-P profiles when cloud pressure, P_c, is varied. A cloud-free model is provided in black. Spectra were normalized and convolved with a Gaussian of FWHM≈12 Å for clarity. All parameters are held constant except for cloud pressure.

Table 2.7: Model Parameter Ranges

T_{eff}	log(g) [cm s^{-2}]	P_c [bar]	a_0 [μm]	IncrementsK>K
800-2000	3.5-5.5	0.5, 1, 4	1	100 K; 0.5 in log(g)
800-2000	4.75, 5.0, 5.5	10, 20, 30	0.25, 0.5, 1	100 K
1700-2000	4.5-5.5	0.1, 0.5	0.25	100 K; 0.5 in log(g)

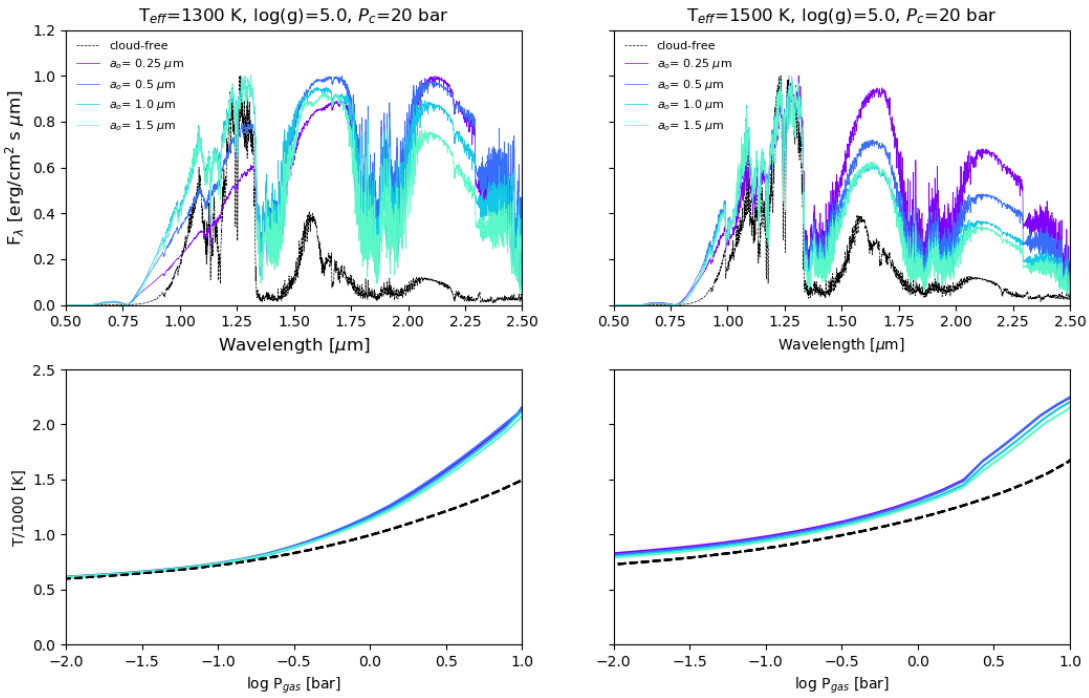

Figure 2.3: Comparison between model spectra and T-P profiles when mean grain size is varied. A cloud-free model is provided in black. Normalized spectra are shown for two effective temperatures. Spectra are convolved with a Gaussian of FWHM≈12 Å for clarity. All parameters held constant except for grain size in each panel.

Table 2.8 shows the results of our model fitting. Models are allowed at the 68% confidence level by taking χ^2 distributed with five degrees of freedom (the four atmosphere model parameters in Table 2.7 and the object's radius, which is simultaneously fit). This includes all models with $\Delta\chi^2 < 11.3$. Listed first is the overall best-fitting model from the cloudy atmosphere grids. We then calculate the weighted mean parameters by

$$\bar{m} = \frac{\Sigma_i W_i m_i}{\Sigma_i W_i}, \tag{2.4}$$

where the weight W_i for each model m_i is given by

$$W_i = H_i e^{-0.5\chi^2}, \tag{2.5}$$

where H_i is a scaling factor that accounts for the uneven spacing of some atmospheric parameters on the grid, down weighting regions of dense sampling and up weighting regions of coarse sampling in proportion to the amount of parameter space covered.

We used the same approach as Stone et al. (2016) to calculate uncertainties using sided variance estimates with

$$\sigma_m = \frac{\Sigma_i W_i (m_i - \bar{m})^2}{\Sigma_i W_i}, \tag{2.6}$$

where the sum is calculated using parameters above (+) or below (-) the mean values. In cases where the edge of the grid boundary was approached, we report an upper/lower limit for our uncertainty.

The results of our analysis are shown in Figures 2.4 through 2.9 for our sample of objects. We plot the best-fit and weighted mean grid models for each object from Table 2.8. These fits highlight the role clouds play in the uncertainties of effective temperature, gravity, and radius when fitting cloudy model grids to photometric observations. Three objects, 2MASS 1728+39AB and LHS 2397aB, were fit well by the grid and had properties consistent with evolutionary models shown in Figures 2.6 and 2.7.

Our fit of five parameters to HD 130948BC is not adequately constrained by the three photometric points used here. To help guide our fitting in subsequent sections and approach a unique solution for these objects, we applied a prior on

Table 2.8: Model Atmosphere Fits

	Best Fit					Weighted Mean				
Name	T_{eff}	log(g)	R_{Jup}	P_c	a_0	T_{eff}	log(g)	R_{Jup}	P_c	a_0
HD 130948B	1400	3.5	1.68	4	1.0	1903^{+97}_{-4}	$4.5^{+0.50}_{-1.0}$	$1.04^{+0.27}_{-0.29}$	$0.22^{+0.28}_{-0.12}$	≤ 1.0
HD 130948C	1400	4.0	1.76	4	1.0	1808^{+92}_{-8}	$4.5^{+0.59}_{-1.0}$	$1.03^{+0.16}_{-0.34}$	$0.47^{+0.03}_{-0.67}$	≤ 1.0
2MASS 0920+35A	1300	4.75	1.50	4	1.0	1517^{+331}_{-194}	$4.88^{+0.47}_{-0.72}$	$1.41^{+0.34}_{-0.47}$	$2.9^{+2.9}_{-2.6}$	$0.70^{+0.30}_{-0.43}$
2MASS 1728+39A	1500	5.5	0.95	30	0.25	1487^{+29}_{-131}	$5.17^{+0.33}_{-0.32}$	$0.97^{+0.13}_{-0.05}$	20^{+10}_{-9}	$0.26^{+0.68}_{-0.01}$
2MASS 1728+39B	1400	4.75	0.83	20	1.0	1420^{+100}_{-22}	$4.99^{+0.43}_{-0.83}$	$0.89^{+0.06}_{-0.09}$	8^{+10}_{-5}	$0.93^{+0.07}_{-0.44}$
LHS2397aB	1300	4.75	0.95	30	1.0	1413^{+93}_{-102}	$4.84^{+0.23}_{-0.09}$	$0.81^{+0.12}_{-0.11}$	23^{+7}_{-3}	$0.54^{+0.46}_{-0.27}$
2MASS 0850+10A	1800	5.5	0.56	10	0.25	1717^{+91}_{-207}	$5.08^{+0.42}_{-0.63}$	$0.65^{+0.22}_{-0.10}$	$7.2^{+4.2}_{-6.1}$	$0.36^{+0.55}_{-0.11}$
2MASS 0850+10B	1500	5.5	0.74	20	0.25	1423^{+80}_{-277}	$5.3^{+0.20}_{-0.69}$	$0.93^{+0.80}_{-0.18}$	14^{+10}_{-7}	$0.37^{+0.63}_{-0.12}$
SDSS 1021-03A	1700	5.0	0.50	30	0.25	1668^{+37}_{-97}	$4.92^{+0.09}_{-0.17}$	$0.52^{+0.09}_{-0.03}$	28^{+20}_{-8}	$0.36^{+0.57}_{-0.11}$
SDSS 1021-03B	1700	4.75	0.36	30	1.0	1698^{+2}_{-98}	≤ 5.5	$0.36^{+0.06}_{-0.02}$	≥ 0.1	$0.96^{+0.04}_{-0.57}$
2MASS 1534-29A	1700	5.5	0.38	30	0.25	1699^{+1}_{-99}	≥ 3.5	$0.38^{+0.02}_{-0.01}$	24^{+7}_{-4}	≤ 1.0
2MASS 1534-29B	1700	5.5	0.32	20	0.25	1699^{+1}_{-99}	≥ 3.5	0.33 ± 0.01	21^{+9}_{-3}	≤ 1.0

Best-fitting grid models and weighted means with 2-σ uncertainties are provided. Weighted mean fits for HD 130948BC use a fixed range for radius 0.8-1.2 R_{Jup} constrained by Saumon and Marley (2008) evolutionary models. Fits in the table for 2MASS 1728+39B exclude the F814W photometric point and are discussed further in Section 2.7.3.

radius (0.8-1.2 R_{Jup}) from evolutionary models for the weighted mean fits in Table 2.8. The unconstrained best-fit model and weighted fit are provided in Figure 2.4. This shows how two atmosphere models with very different effective temperatures, gravities, and cloud properties can match JHK photometric observations well. The best fits plotted in purple are much cooler than expected for early L-type objects and approach non-physical radii ($\geq$ 1.5 R_{Jup}).

We note a few other objects where the grid fits present tension: 2MASS 0850+10AB, 2MASS 0920+35A, SDSS 1021-03AB, 2MASS 1534-29AB. Without incorporating evolutionary constraints on radius for the aforementioned systems, models allowed at 2-σ over or under-predict effective temperature expected for a given spectral type (Leggett et al., 2002; Nakajima et al., 2004) and can result in non-physical radii. We believe this may be influenced by an unresolved component for some objects (e.g., 2MASS 0850+10A), and the cloud parameter space used in our grids does not appear to be appropriate for early-to-mid T dwarfs (e.g., 2MASS 1534-29AB). Figures 2.5, 2.8, and 2.9 show the grid fits for 2MASS 0850+10AB, SDSS 1021-03AB, and 2MASS 1534-29AB are warmer ($T_{\rm eff} \geq$ 1700 K) and approach smaller than expected radii ($\leq$ 0.70 R_{Jup}) for objects of field age (Dupuy and Liu, 2017). Conversely, the model fits for 2MASS 0920+35A shown in Figure 2.7 have radii larger than expected ($\geq$ 1.4 R_{Jup}) for mid-L dwarfs (Leggett et al., 2002; Nakajima et al., 2004).

2.7 Evolutionary Model Comparisons

The addition of cloud properties in atmosphere models can lead to further degeneracies in mass and radius resulting in good fits to photometric data but producing non-physical properties given what we know of brown dwarf physics. An effective way to evaluate the quality of atmosphere model fits is by comparing the results to the bulk properties from evolutionary model predictions. We use bolometric luminosity constrained from our grid fits combined with the measured masses (Dupuy and Liu, 2017; Konopacky et al., 2010) to derive evolutionary predictions. We derive

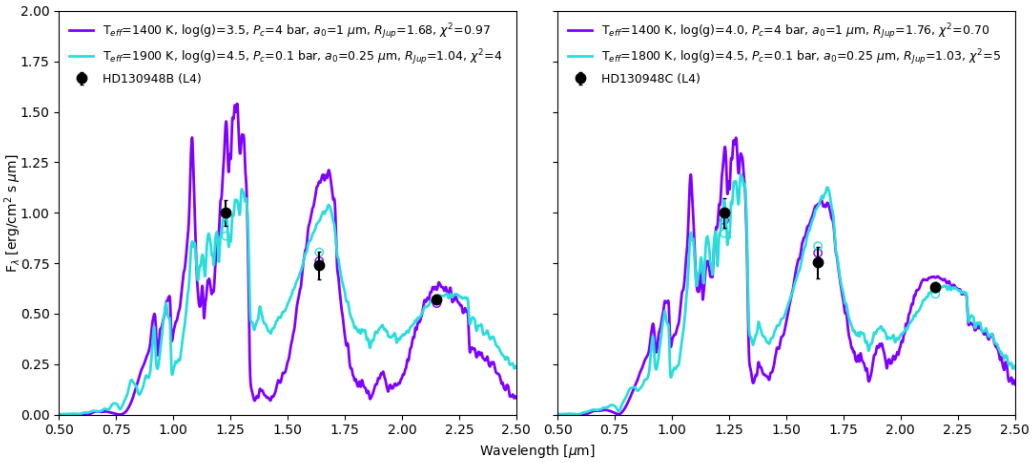

Figure 2.4: Best-fit (purple) and weighted mean (cyan) atmosphere models from Table 2.8 for HD 130948B and C. We chose the closest available model from our grid to the mean parameters. Corresponding synthetic photometry is plotted in same color as model spectra. Surface gravity is in cm s^{-2}. Spectral types included are from Dupuy and Liu (2017)

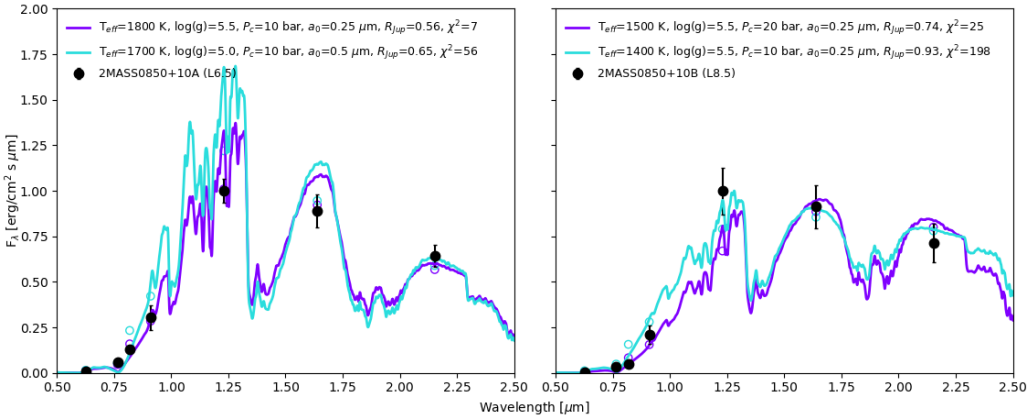

Figure 2.5: Best-fit (purple) and weighted mean (cyan) atmosphere models from Table 2.8 for 2MASS 0850+10A and B. We chose the closest available model from our grid to the mean parameters. Corresponding synthetic photometry is plotted in same color as model spectra. Surface gravity is in cm s^{-2}. Spectral types included are from Dupuy and Liu (2017)

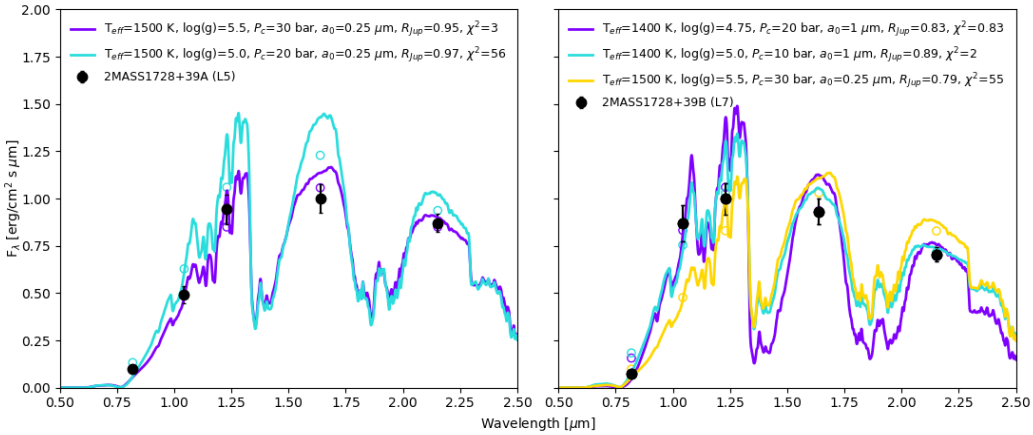

Figure 2.6: Best-fit (purple) and weighted mean (cyan) atmosphere models from Table 2.8 for 2MASS 1728+39A and B. We chose the closest available model from our grid to the mean parameters. Corresponding synthetic photometry is plotted in same color as model spectra. Surface gravity is in cm s^{-2}. Spectral types included are from Dupuy and Liu (2017)

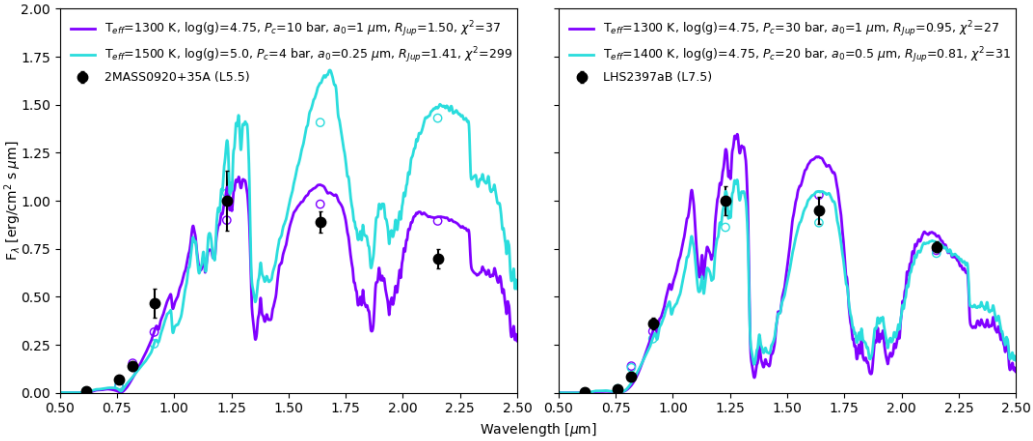

Figure 2.7: Best-fit (purple) and weighted mean (cyan) atmosphere models from Table 2.8 for 2MASS 0920+35A and LHS 2397aB. We chose the closest available model from our grid to the mean parameters. Corresponding synthetic photometry is plotted in same color as model spectra. Surface gravity is in cm s^{-2}. Spectral types included are from Dupuy and Liu (2017)

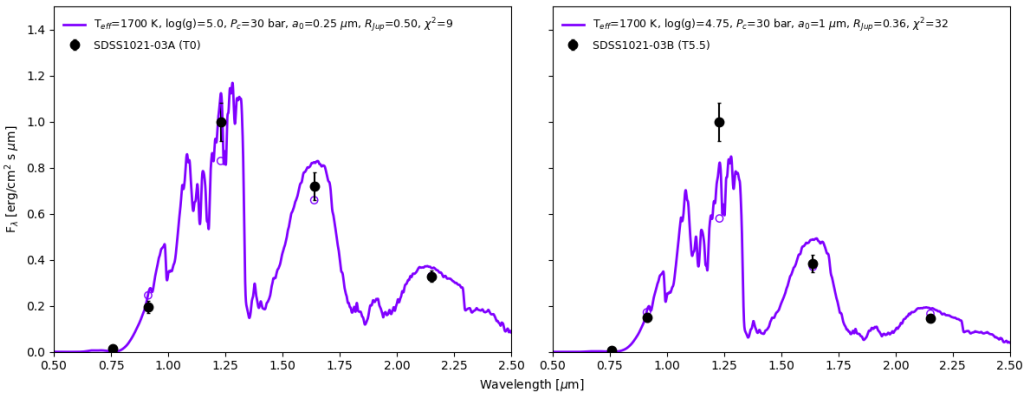

Figure 2.8: Best-fit (purple) atmosphere models for SDSS 1021-03A and B. Weighted mean parameters are not included because they are similar to the best-fit models. Corresponding synthetic photometry is plotted in same color as model spectra. Surface gravity is in cm s^{-2}. Spectral types included are from Dupuy and Liu (2017)

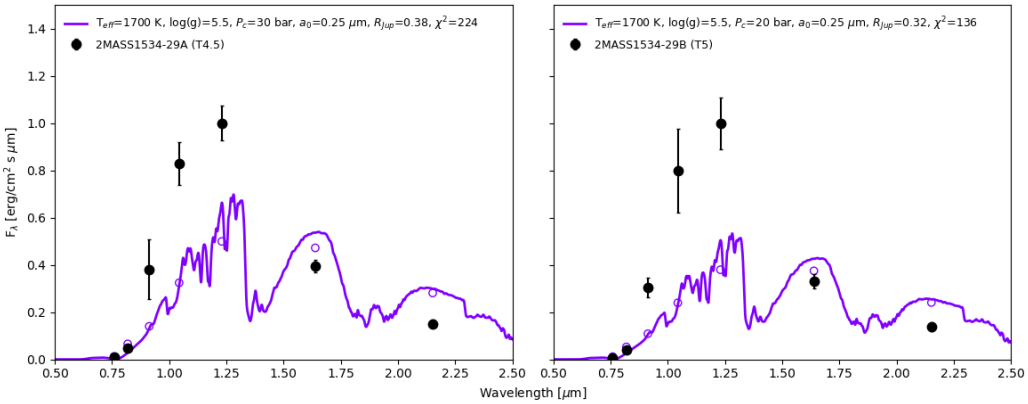

Figure 2.9: Best-fit (purple) atmosphere models for 2MASS 1534-29A and B. Only best-fit models are included because the mean weighted parameters are similar. Corresponding synthetic photometry is plotted in same color as model spectra. Surface gravity is in cm s^{-2}. Spectral types included are from Dupuy and Liu (2017)

evolutionary predictions using Saumon and Marley (2008) hybrid grids for mid-to-late L dwarfs in our sample and use the COND grids from Baraffe et al. (2003) for T dwarfs with $T_{eff} \sim 1300$ K. Evolutionary properties are given in Table 2.9 and individual systems are discussed below.

We take comparisons a step further by running additional atmosphere models using a fixed value for effective temperature, gravity, and radius from evolutionary predictions in Table 2.9. Holding evolutionary properties constant, we ran additional models around the best-fitting cloud properties determined from our grid fits in Section 2.6. The goal was to determine if our cloudy atmosphere models could fit data well and remain consistent with substellar evolutionary model predictions.

Because we know the masses for these binary systems, distinguishing between different atmospheric fits becomes more reliable. We are able to eliminate model fits that may represent the data well yet result in implied masses that deviate from empirical observations. Implied mass is calculated from surface gravity and radius for a given atmosphere model. All model fits for individual systems are discussed below.

2.7.1 HD 130948B+C

The best grid fit for the HD 130948B+C system does not match evolutionary-derived properties. This is not surprising because previous work has shown discrepancies between atmosphere grids and evolutionary properties ($\pm$ 250 K) when only J, H, and K photometry are used (Dupuy et al., 2009a). Barman et al. (2011a) and other groups find similar issues for directly imaged planets. Additionally, limited SED coverage for this system leads to several well-fit models given grid fits are formally under-constrained. However, by fixing effective temperature, gravity, and radius using evolutionary-derived values we can fit for two cloud parameters to arrive at a more reliable solution that is formally allowed.

In Figure 2.10 we show our previous weighted mean grid fit compared to our new evolutionary fit with fixed $T_{\rm eff}$, log(g), and $R_{\rm Jup}$. A good fit to the data can

Table 2.9: Evolutionary Model Predictions

	Primary					Secondary					
System	M_{Jup}	$\log(L_{bol}/L_{\odot})$	T_{eff}	R_{Jup}	log(g)	M_{Jup}	$\log(L_{bol}/L_{\odot})$	T_{eff}	R_{Jup}	log(g)	Age(Gyr)
HD 130948BC	59±1	-3.85 ± 0.09	1916^{+94}_{-90}	1.05 ± 0.02	5.12 ± 0.02	56^{+2}_{-1}	-3.91 ± 0.05	1851^{+46}_{-45}	1.05 ± 0.02	$5.10^{+0.02}_{-0.03}$	$0.42^{+0.06}_{-0.04}$
2MASS 0920+35AB	71^{+3}_{-4}	-4.28 ± 0.05	1604^{+51}_{-52}	$0.91^{+0.03}_{-0.01}$	$5.32^{+0.03}_{-0.04}$	58^{+9}_{-7}	-4.70 ± 0.05	1260^{+57}_{-52}	0.91 ± 0.04	5.24 ± 0.10	$1.82^{+0.35}_{-0.18}$
2MASS 1728+39AB	71^{+1}_{-2}	-4.37 ± 0.04	1536^{+30}_{-41}	$0.90^{+0.02}_{-0.01}$	$5.34^{+0.01}_{-0.04}$	68^{+1}_{-4}	-4.52 ± 0.06	1417^{+42}_{-58}	$0.89^{+0.03}_{-0.01}$	$5.33^{+0.01}_{-0.05}$	$2.82^{+0.42}_{-1.24}$
LHS 2397aAB	92±1	-3.34±0.04	2533^{+41}_{-40}	1.07 ± 0.02	5.29 ± 0.01	67^{+1}_{-9}	-4.62 ± 0.02	1342^{+10}_{-39}	$0.88^{+0.04}_{-0.01}$	$5.33^{+0.01}_{-0.10}$	$3.02^{+0.07}_{-1.47}$
2MASS 0850+10AB	28^{+4}_{-5}	-4.49 ± 0.06	1272^{+58}_{-57}	$1.14^{+0.03}_{-0.05}$	$4.72^{+0.11}_{-0.12}$	26^{+5}_{-4}	-4.54 ± 0.09	1234^{+79}_{-77}	$1.15^{+0.03}_{-0.06}$	$4.70^{+0.09}_{-0.11}$	$0.25^{+0.13}_{-0.09}$
SDSS 1021-03AB	29 ± 4	-4.70 ± 0.05	1219^{+48}_{-47}	$1.00^{+0.04}_{-0.03}$	$4.85^{+0.09}_{-0.08}$	23 ± 4	-4.99 ± 0.01	1023^{+20}_{-24}	$1.02^{+0.04}_{-0.03}$	$4.74^{+0.08}_{-0.11}$	$0.47^{+0.08}_{-0.15}$
2MASS 1534-29AB	52 ± 3	-4.94 ± 0.02	1157^{+21}_{-7}	$0.83^{+0.02}_{-0.01}$	$5.27^{+0.03}_{-0.04}$	47 ± 3	-5.08 ± 0.02	1062^{+19}_{-9}	$0.85^{+0.01}_{-0.02}$	5.21 ± 0.04	2.4 ± 0.1

Evolutionary model-derived properties from Saumon and Marley (2008) hybrid grids. For the T dwarfs, SDSS 1021A+B and 2MASS 1534-29A+B, evolutionary properties are from Baraffe et al. (2003) COND grids. Luminosity for LHS 2397aA is from Dupuy and Liu (2017).

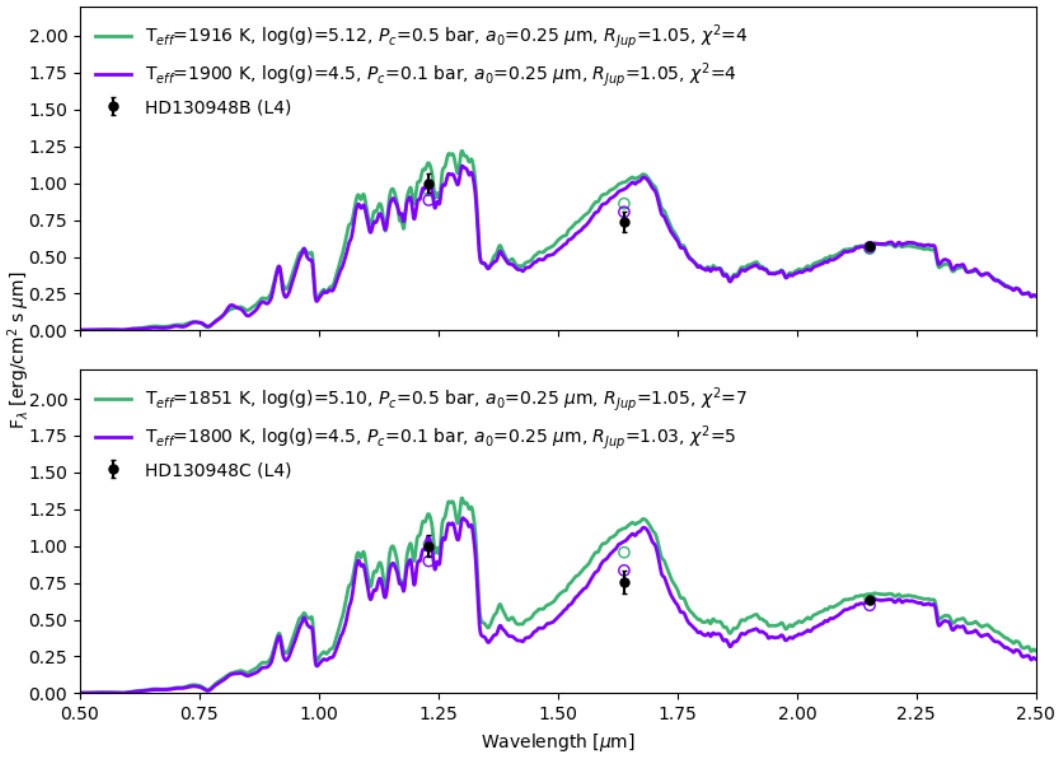

Figure 2.10: New evolutionary fit atmosphere models (green) compared to weighted mean grid fits (purple) for HD 130948B (top) and HD 130948C (bottom). Surface gravity is in cm s^{-2}.

be achieved for HD 130948B with a higher cloud and a_0=0.25 μm grain size. The fits are nearly identical, but the grid fit with lower surface gravity is inconsistent with measured mass compared to the higher surface gravity model ($M_{\rm Jup}$=14.08 and 58.68, respectively). HD 130948C is slightly cooler than the B component yet fit well with the same type of cloud and grain size. Again, the lower surface gravity model can be ruled out by implied mass ($M_{\rm Jup}$=13.54). The new evolutionary fits presented here for both objects are consistent with recent atmospheric properties determined by Briesemeister et al. (2019) which included both J, H, and K photometry with additional ALES L-band spectra from 2.9–4.1 μm. Our updated fits provide additional constraints on the cloud properties of early-to-mid L type dwarfs.

2.7.2 2MASS 0850+10AB

We show our new evolutionary fits compared to our previous best-fitting grid model in Figure 2.11 for 2MASS 0850+10A and B. The initial grid fits significantly over-predicted temperature ($\approx$ 250-500 K) and gravity ($\approx$ 0.75 dex) while under-predicting radius compared to evolutionary predictions. Weighted mean parameters were consistent with evolutionary predictions for the secondary component but not for the primary (Table 2.8). Table 2.9 shows evolutionary predictions for this system have the lowest values of gravity ($\log(g) \leq 4.75$) for all the L dwarfs studied in this sample.

2MASS 0850+10A is fit well when bulk properties are fixed to evolutionary values and clouds include a 1 μm mean grain size. The warmer grid-based model ($T_{\rm eff}$=1800 K) can be ruled out by the larger implied mass ($M_{\rm Jup}$=40.04) and non-physical radius (0.56 $R_{\rm Jup}$) inconsistent with evolutionary models. Figure 2.11 shows how the grid fit for 2MASS 0850+10B compares to a cooler model with fixed evolutionary parameters. We can rule out the warmer 1500 K model because the implied mass (69.91 $M_{\rm Jup}$) is higher than the total measured mass of the entire system ($M_{\rm tot}$ = 54 $\pm$ 8 $M_{\rm Jup}$). For the $T_{\rm eff}$=1234 K model, the fit can be improved at J band if the grain size is increased to 1 μm, but this results in a poor fit to HST photometry near 0.75-1 μm. A deeper cloud can also improve the J-band fit but reddens the H and K bands.

We believed the warmer, initial grid fit for this system, notably the primary, may have been caused by the spacing of our grid since evolutionary-predicted gravities for 2MASS 0850+10AB are near the edge of a boundary. To test this hypothesis and determine if the issue was indeed lack of sufficient grid coverage, we extended the segment of our grid that begins at log(g)=4.75 down to log(g)=4.5, including the same range of temperatures and cloud properties given in row two of Table 2.7. We then recalculated the grid fits for both A and B components. The best grid fit for 2MASS 0850+10A did not change with the addition of new lower gravity grid models. The weighted mean properties remained nearly identical to our previous

findings and inconsistent with evolutionary predictions. The updated best grid fit for 2MASS 0850+10B resulted in an unusually cool model with a non-physical radius. Weighted mean parameters were again consistent with predictions from evolutionary models within the uncertainties, but the average gravity was still higher than expected ($\log(g)=5.25^{-0.77}_{+0.25}$).

Previous work has suggested 2MASS 0850+10A may be an unresolved binary. Burgasser et al. (2011) pointed out the object had unusually bright J and K-band absolute magnitudes for a late L dwarf. Dupuy and Liu (2012, 2017) later determined with an updated system distance absolute magnitudes were similar to other L5-L7 dwarfs. Our HST photometry shows large differences in component brightnesses across multiple bands (ΔF625W = 1.31 dex, ΔF775W = 1.16 dex, ΔF814W = 1.47 dex, and ΔF850LP = 0.86 dex) hinting 2MASS 0850+10A might actually be composed of more than one object after all. The small total system mass of 54 $\pm$ 8 $M_{\rm Jup}$ implies 2MASS 0850+10A would be a pair of objects near the deuterium burning limit ($\approx$ 13.5 $M_{\rm Jup}$) with lower gravity ($\log(g)=4.3$, $R_{\rm Jup}=1.3$) assuming the primary is an equal mass binary, and the B component is a more massive single object with higher gravity ($\log(g)=4.70$, $R_{\rm Jup}=1.15$). The effective temperature in substellar evolutionary models can be quite flat for objects near 20 $M_{\rm Jup}$ at these ages due to clouds, and low-mass objects of similar effective temperatures have been known to look like mid-to-late L dwarfs (Barman et al., 2011b). Fitting the A component as a binary would require more specialized atmosphere models.

2.7.3 2MASS 1728+39AB

The best grid fit for 2MASS 1728+39A is consistent with evolutionary predictions in temperature and radius but gravity is over-predicted resulting in an implied mass that is inconsistent with measured masses ($M_{\rm Jup}=115.22$). By fixing $T_{\rm eff}$, $\log(g)$, and $R_{\rm Jup}$ to evolutionary predictions from Table 2.9 and adjusting the depth of the cloud, we are able to produce a good fit to the data shown in Figure 2.12. The 1536 K model has an implied mass consistent with measured mass ($M_{\rm Jup}=71.54$).

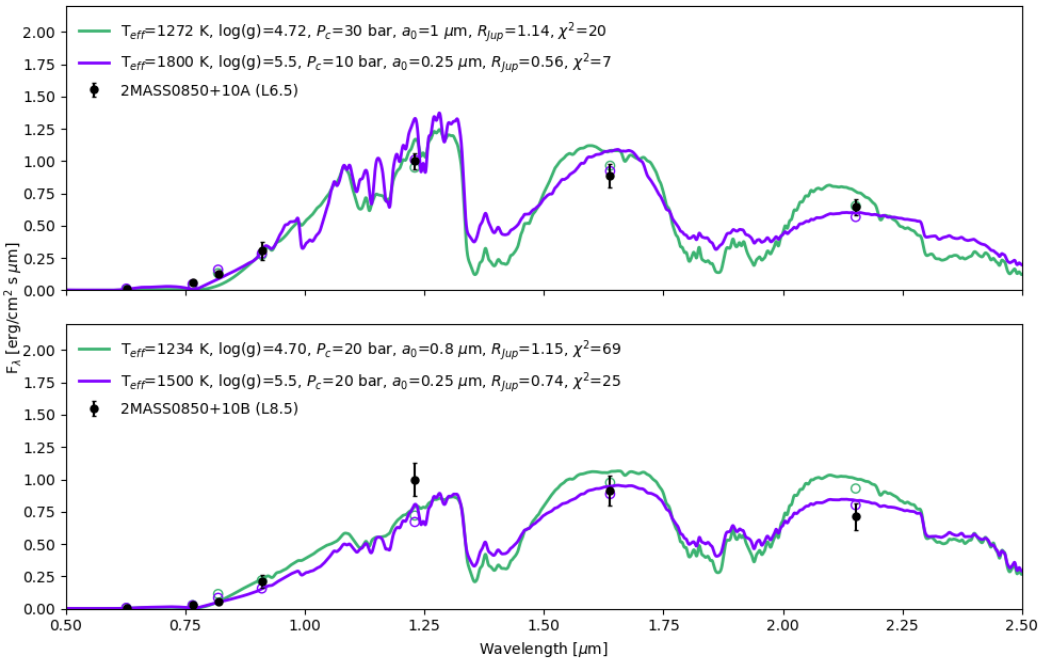

Figure 2.11: New evolutionary fit atmosphere models (green) compared to best grid fits (purple) for 2MASS 0850+10A (top) and 2MASS 0850+10B (bottom). Surface gravity is in cm s^{-2}.

Fitting 2MASS 1728+39B was not as straightforward as fitting the A component. It was difficult to find a model fit that agreed reasonably well with the data simultaneously in both the F814W and F1042W bands even with fixed T_{eff}, log(g), and R_{Jup} to evolutionary predictions. The F814W data point was fit best by models with deeper clouds and 0.25 μm grains whereas the F1042W point preferred models with higher clouds and $\geq$ 1 μm grains. Figure 2.12 shows evolutionary model fits with both cloud preferences compared to our initial grid fit. The lower gravity 1400 K model can be excluded because its implied mass of M_{Jup}=31.98 is less than half of the measured mass. For the remainder of this paper, we use the model fit that excludes the F814W photometric point as our preferred fit because it is more consistent with the majority of the photometric bands.

2MASS 1728+39AB is a flux reversal binary system, which may explain some of the difficulty finding an atmosphere model that fit in all bands. Several binary systems have been discovered with a secondary component brighter than the primary component in the 1.0-1.3 μm range (Gelino et al., 2014). In this system, the B component is brighter in the F1042W band (Δ_{A-B}= 0.25 dex) but not in the J or F814W bands. Looper et al. (2008a) explain the brightening could be the result of a cryptobinary, but it is often an intrinsic property of the object due to weather, unusual cloud properties, or changes in surface gravity. Surface gravity is unlikely to be the culprit because widely varying gravities requires different ages not expected for coeval binaries (Gelino et al., 2014). Our model fits suggest it may be due to differences in cloud location and particle sizes.

2.7.4 2MASS 0920+35AB

Dupuy and Liu (2017) suggest 2MASS 0920+35AB is a triple brown dwarf system given the large total mass of the system (187 $\pm$ 11 M_{Jup}) with over half of the total system mass belonging to the fainter secondary (116^{+7}_{-8} M_{Jup}). In order to obtain evolutionary predictions for the A component of this system, we follow the same approach as Dupuy and Liu (2017) and assume 2MASS 0920+35B is composed of

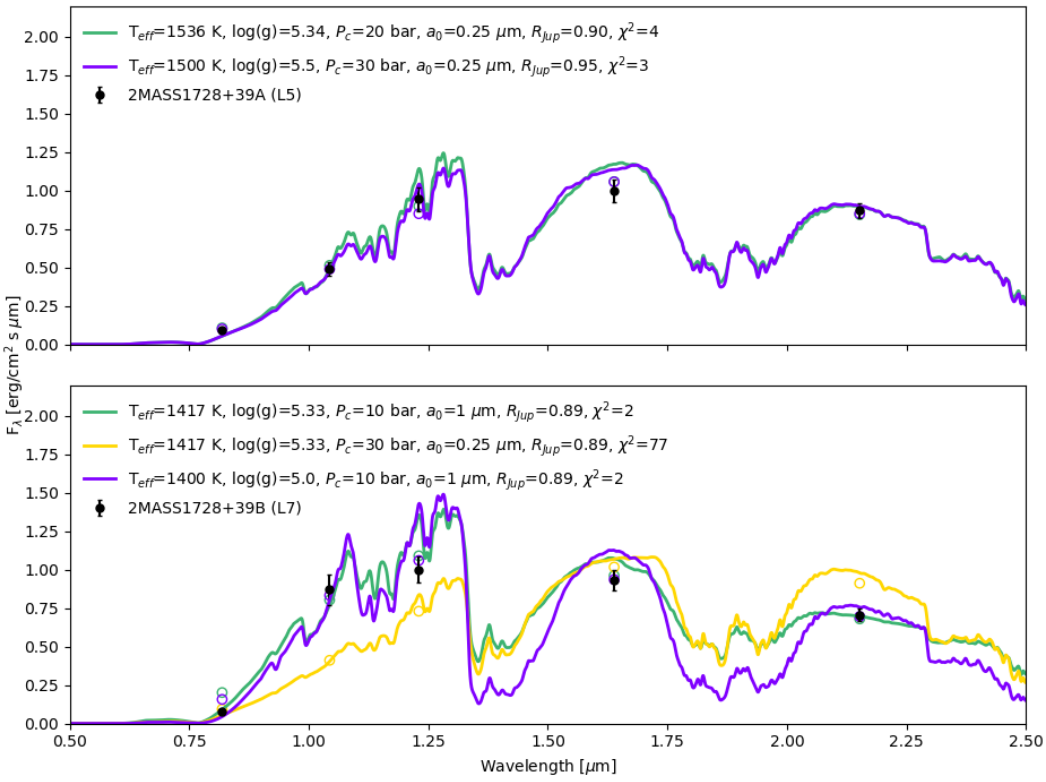

Figure 2.12: New evolutionary fit atmosphere models (green) compared to best grid fits (purple) for 2MASS 1728+39A (top) and 2MASS 1728+39B (bottom). Two fits for 2MASS 1728+39B are provided: one excluding the F814W photometric point (green) and one including it (gold). Surface gravity is in cm s^{-2}.

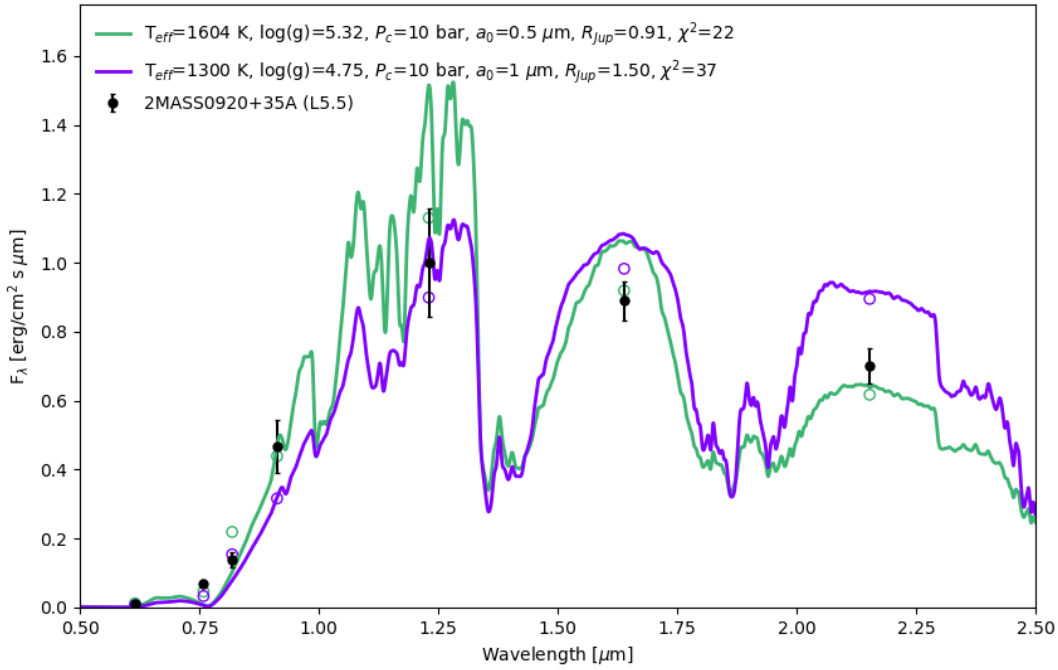

Figure 2.13: New evolutionary fit atmosphere model (green) compared to best grid fit (purple) for 2MASS 0920+35A. Surface gravity is in s^{-2}.

two equal-mass, equal-luminosity components. These predictions are given in Table 2.9.

Figure 2.13 compares our best grid-fit model of 2MASS 0920+35A from Section 2.6 to a new model with fixed $T_{\rm eff}$, log(g), and $R_{\rm Jup}$ from evolutionary predictions. We are able to produce a good fit to the data and remain consistent with evolutionary predictions if the B component is indeed a binary with two equal-mass, equal-luminosity components. We derive a younger age of the system at $1.82^{+0.35}_{-0.18}$ Gyr using SM08 evolutionary models, but our results are consistent within the uncertainties to the system age from Dupuy and Liu (2017) of $2.3^{+0.3}_{-0.4}$ Gyr.

2.7.5 LHS2397aAB

We only studied the L dwarf companion in this system because the A component is a low-mass star and outside the temperature range of our grid fitting ($\geq$ 2000 K).

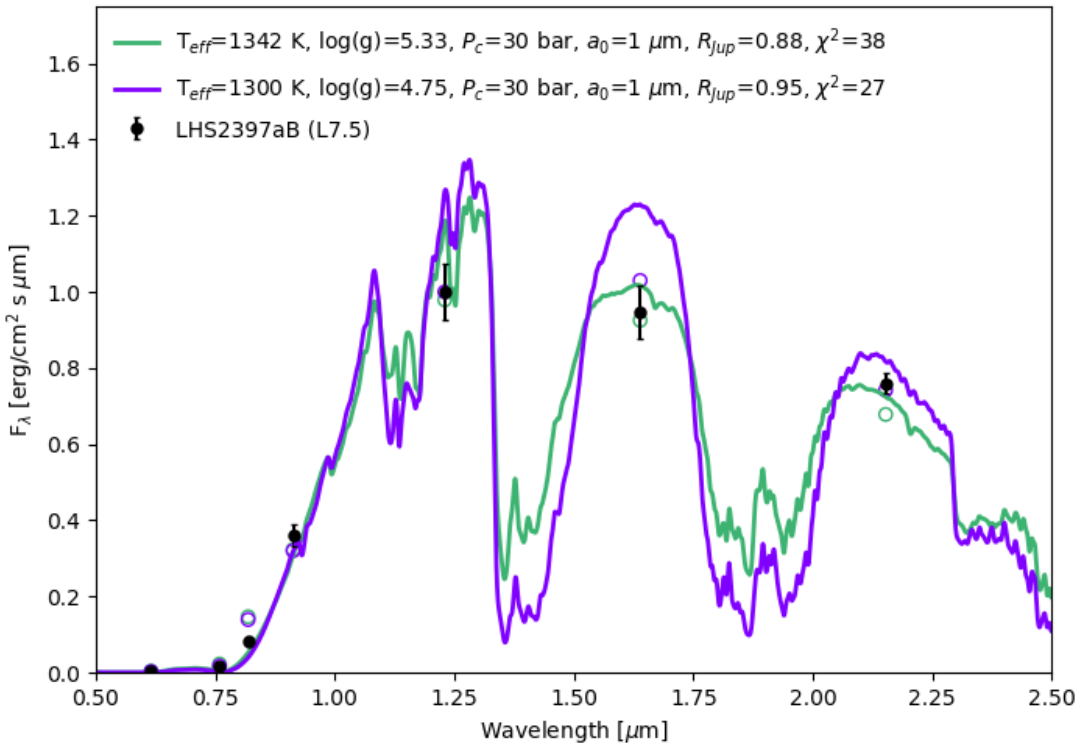

Figure 2.14: New evolutionary fit atmosphere model (green) compared to the best grid fit (purple) for LHS 2397aB. Surface gravity is in cm s^{-2}.

Although the best grid-fitting model for LHS 2397aB was consistent in temperature and radius to evolutionary properties, the lower gravity resulted in an implied mass that was too small ($M_{\rm Jup}$=20.49). By fixing the bulk atmospheric properties of the object to evolutionary-derived properties from Table 2.9, we are able to get a good fit to the data with a new model show in Figure 2.14 that has an implied mass consistent with observations ($M_{\rm Jup}$=66.84).

2.7.6 SDSS 1021-03AB

It became apparent our cloudy atmosphere grids did not sample enough of the parameter space in cloud pressure and grain size to accommodate early-to-mid T dwarfs, particularly at lower values of surface gravity near log(g)=4.75. K-band flux is sensitive to surface gravity (Saumon et al., 2012), and the cooler models in

our grid more appropriate for T dwarfs predicted an overly red H - K color. We were able to obtain improved fits more appropriate for the SDSS 1021-03AB system by testing models outside the grid with larger grain sizes and deeper clouds.

The cloudy model fits presented here help to provide an upper limit to the location of clouds in T dwarf atmospheres, which are traditionally fit with cloud-free models (Baraffe et al., 2003). Figure 2.15 provides a comparison of the best grid models to new evolutionary-based models. The initial grid fits to the system have lower values of χ^2 but significantly over-predicted temperature ($\geq$ 500 K) and under-predicted radius ($\leq$ 0.50 $R_{\rm Jup}$). Although the J-band flux is under-predicted by our evolutionary fit for SDSS 1021-03B, this model is still the preferred model based on mass and radius. If we allow the radius to vary, the fit at J-band can be improved using a model with a deeper cloud and larger grain size (P_c=100 bar, a_0=5 μm) with a radius of 1.25 $R_{\rm Jup}$; however, this results in a 35 M_{Jup} mass inconsistent with observations of 23 $\pm$ 4 M_{Jup}.

2.7.7 2MASS 1534-29AB

Similar to the SDSS 1021-03AB system, the mid-T dwarfs in the 2MASS 1534-29AB system were not fit well by our cloudy atmosphere grids. Grid fits resulted in significantly over-predicted effective temperatures ($\geq$ 500 K) and small, non-physical radii ($\leq$ 0.40 $R_{\rm Jup}$) for both the A and B components.

Using cloud parameters informed from our evolutionary fits to the SDSS 1021-03AB system, we were able to test additional models and find more realistic fits for 2MASS 1534-29AB shown in Figure 2.16. The fits are greatly improved over the original grid-based models and help to provide upper limits to the cloud over cloud-free models.

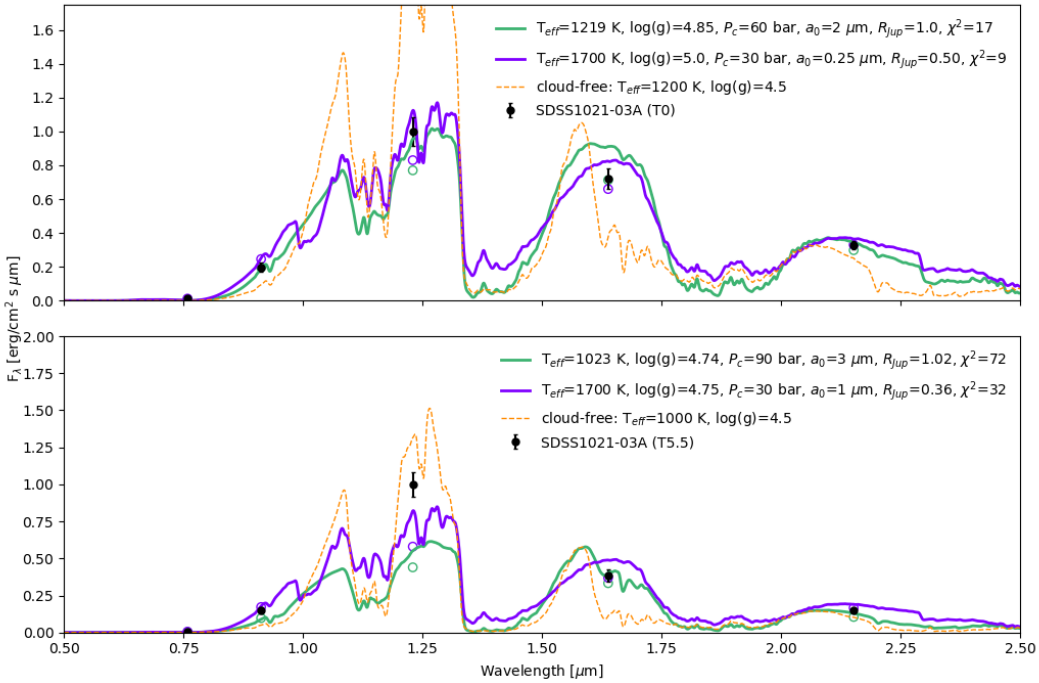

Figure 2.15: New evolutionary fit atmosphere models (green) compared to best grid fits (purple) for SDSS 1021-03A (top) and SDSS 1021-03B (bottom). Plotted in orange is a cloud-free model for comparison. Surface gravity is in cm s^{-2}.

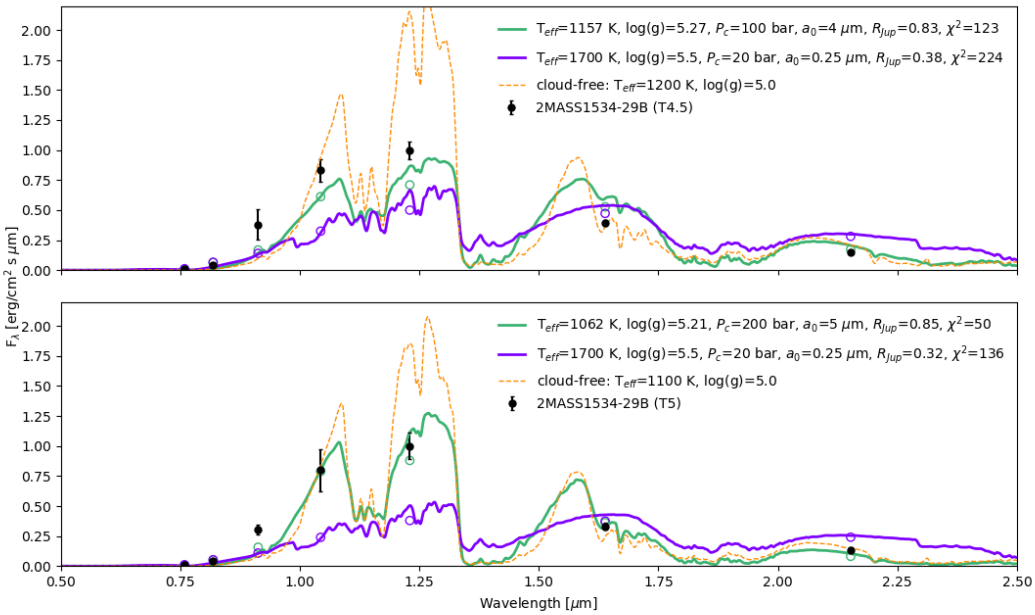

Figure 2.16: New evolutionary fit atmosphere models (green) compared to best grid fits (purple) for 2MASS 1534-29A (top) and 2MASS 1534-29B (bottom). Plotted in orange is a cloud-free model for comparison. Surface gravity is in cm s^{-2}.

2.8 Cloud Properties

Here we discuss detailed cloud properties from our best-fitting atmosphere models. For the remainder of the paper, we consider the best fits those constrained by evolutionary models in the previous section. Model parameters are summarized in Table 2.10. We also include the location of the photosphere, cloud location (top, base), cloud thickness, and peak gas-to-dust ratio in the table for reference. We adopt the approximate location of the spectrum-forming region (photosphere) where the atmospheric temperature equals the effective temperature. This location is also very close to where the Rosseland mean optical depth is ≈ 1.

The model cloud is composed of multiple layers of thermochemically permissible condensate species composed mostly of Fe and Mg-Si grains. Cloud opacity is determined from a heterogeneous mixture of these grains along with a number of minor contributors for which opacities are available rather than using a single grain type as representative of all cloud particles. We report the most abundant condensate species for each object in Table 2.11. While the table is representative of the composition at the cloud top layer, a gradient of condensates is present within the cloud.

Figure 2.17 illustrates how the cloud properties change in our sample for L to mid T-type dwarfs for $T_{\rm eff} \approx$ 1900-1000 K. Cloud formation occurs higher in the atmosphere and shifts to deeper regions as effective temperature decreases. The peak dust-to-gas ratio shifts to deeper regions within the cloud for cooler objects as well. This trend emerges into two distinct clusters in the plot–one containing eight objects ($\approx$ L4-T5) and one containing four objects ($\approx$ L6-T5)–signifying a similar trend for high-gravity and low-gravity objects. It is worth noting all objects in our sample near $T_{\rm eff} \leq 1400$ K have detached convection zones from the radiative-convective boundary with a convective flux greater than 50% of the total flux. Isolated convection zones can emerge as temperatures decrease. These detached convection zones are a result of localized changes to the temperature gradient caused by the cloud opacity. Similar zones, produced for the same reason, were discussed by Burrows

et al. (2006). In addition to the effective temperature and gravity, the location and vertical extent of these zones are sensitive to the detailed cloud properties (e.g., composition, particle size, and cloud morphology) that determine a cloud's contribution to the total opacity.

Sub-micron grains (0.25-0.50 μm) were the most appropriate for L4-L5.5 spectral types with temperatures of ≈1900-1500 K and high surface gravities (log(g) $\geq$ 5.0) and one lower gravity (log(g) $\leq$ 5.0) L8.5 dwarf. Previous work found comparable grain sizes for L dwarfs using a single grain type such as 0.4-0.6 μm for corundum and enstatite grains (Marocco et al., 2014), 0.15-0.3 μm for iron grains (Marocco et al., 2014), and a mean grain size of 0.15-0.35 μm using forsterite grains (Hiranaka et al., 2016). Rotational modulations have also suggested hazes present in L dwarf atmospheres have characteristic grain sizes of ≈0.28-0.4 μm (Lew et al., 2016).

Larger grain sizes ($\geq$ 1 μm) were required for most spectral types later than L6.5-L7 with effective temperatures near 1400 K and cooler. The coolest and latest type objects in our sample required the largest grain sizes (2-5 μm). Similarly, Zhou et al. (2018) found characteristic condensate particle sizes grew for later L types ($\geq$ L8) with larger mean grain sizes required to match observations ($a_0 \geq 1.0$ μm).

We compare our modelled objects to the cooling and color evolution of brown dwarfs across the L/T transition using Saumon and Marley (2008) hybrid evolution models in Figure 2.18. Objects redder than the track were best represented by the smallest grain sizes, whereas objects bluer than the track where those that required the largest grain sizes. Reddened L dwarfs in the L5-L7.5 range can be an important indicator of youth in brown dwarfs, or the redder colors can be indicative of excess dust and clouds in the photosphere (Kirkpatrick, 2005; Filippazzo et al., 2015; Faherty et al., 2012). The reddest object in our sample, 2MASS 1728+39A, is a mid-L dwarf slightly redder than average (J - K_s = 2.07), which we believe is due to excess dust and a small cloud particle size.

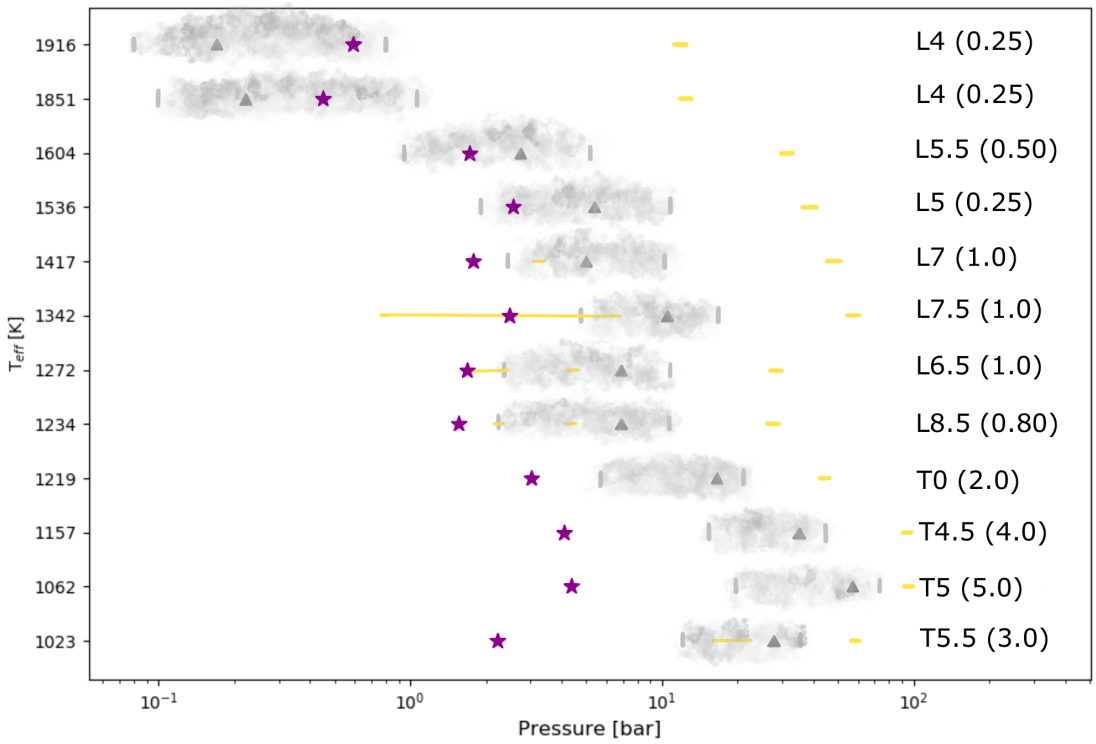

Figure 2.17: Summary of best-fit evolutionary model cloud progression organized by decreasing effective temperature with the warmest objects at the top. The photosphere for each model atmosphere is represented by a star. The cloud top and cloud base are denoted by light grey lines. The peak dust-to-gas ratio is represented by a grey triangle. Regions with a yellow line are indicative of convection with the right-most dash always indicating the radiative-convective boundary. Yellow regions to the left of the this boundary highlight a detached convection zone ($F_{conv}/F_{tot} \geq 50$ %). Spectral type and the model's mean grain size in μm is included on the right-hand side of the plot for reference.

Table 2.10: Summary of Evolutionary Constrained Cloud Properties

Object	T_{eff}	log(g)	a_0	P_c	Photosphere	Cloud Base	Cloud Top	Peak Dust	H_p	SpT
HD 130948B	1916	5.12	0.25	0.5	0.59	0.80	0.08	0.17	1.93	L4 ± 1
HD 130948C	1851	5.10	0.25	0.5	0.45	1.07	0.10	0.22	2.58	L4 ± 1
2MASS 0920+35A	1604	5.32	0.50	10	1.72	5.21	0.94	2.74	2.14	L5.5 ± 1
2MASS 1728+39A	1536	5.34	0.25	20	2.57	10.8	1.89	5.37	2.16	L5 ± 1
2MASS 1728+39B	1417	5.33	1.0	10	1.78	10.2	2.45	5.00	1.90	L7 ± 1
LHS2397aB	1342	5.33	1.0	30	2.49	16.7	4.79	10.5	1.53	L7.5 ± 1
2MASS 0850+10A	1272	4.72	1.0	30	1.68	10.8	2.37	6.90	1.84	L6.5 ± 1
2MASS 0850+10B	1234	4.70	0.8	20	1.56	10.7	2.24	6.84	1.90	L8.5 ± 1
SDSS 1021-03A	1219	4.85	2.0	60	3.04	21.0	5.67	16.5	1.57	T0 ± 1
2MASS 1534-29A	1157	5.27	4.0	100	4.06	44.6	15.4	34.9	1.30	T4.5 ± 1
2MASS 1534-29B	1062	5.21	5.0	200	4.35	73.6	19.6	57.2	1.48	T5 ± 1
SDSS 1021-03B	1023	4.74	3.0	90	2.21	35.4	12.1	27.8	1.26	T5.5 ± 1

Detailed model cloud properties for best evolutionary-derived atmosphere model fits from Section 2.7. Cloud properties are given in bars. H_p is the cloud thickness in pressure scale height. Spectral types listed are from Dupuy and Liu (2017).

Table 2.11: Most Abundant Condensates in Cloud Top Layer

Object	Condensates
HD 130948B	Fe (48%) | $MgSiO_3$, Mg_2SiO_4, MgO, SiO_2 (52%)
HD 130948C	Fe (49%) | $MgSiO_3$, MgO, Mg_2SiO_4, SiO_2 (51%)
2MASS 0920+35A	Fe (48%) | $MgSiO_3$, Mg_2SiO_4, MgO, SiO_2 (52%)
2MASS 1728+39A	Fe (49%) | $MgSiO_3$, MgO, Mg_2SiO_4, SiO_2 (51%)
2MASS 1728+39B	Fe (50%) | MgO, SiO_2, Mg_2SiO_4, $MgSiO_3$, $MgAl_2O_4$ (50%)
LHS2397aB	Fe (45%) | $MgSiO_3$, MgO, SiO_2, Mg_2SiO_4 (55%)
2MASS 0850+10A	Fe (49%) | $MgSiO_3$, MgO, Mg_2SiO_4, SiO_2 (51%)
2MASS 0850+10B	Fe (48%) | $MgSiO_3$, Mg_2SiO_4, MgO, SiO_2 (52%)
SDSS 1021-03A	Fe (47%) | $MgSiO_3$, MgO, Mg_2SiO_4, SiO_2 (53%)
2MASS 1534-29A	Fe (45%) | SiO_2, MgO, Mg_2SiO_4, $MgSiO_3$, $MgAl_2O_4$ (55%)
2MASS 1534-29B	Fe (46%) | SiO_2, MgO, Mg_2SiO_4, $MgSiO_3$, $MgAl_2O_4$ (54%)
SDSS 1021-03B	Fe (47%) | $MgSiO_3$, MgO, SiO_2, Mg_2SiO_4 (53%)

The most abundant dust species are listed for each object at the cloud top layer. Individual condensates species are in order from the most abundant to the least abundant and represent a combination of both solid and liquid phases. Percentages shown are for total iron grains and Mg-Si grains, respectively.

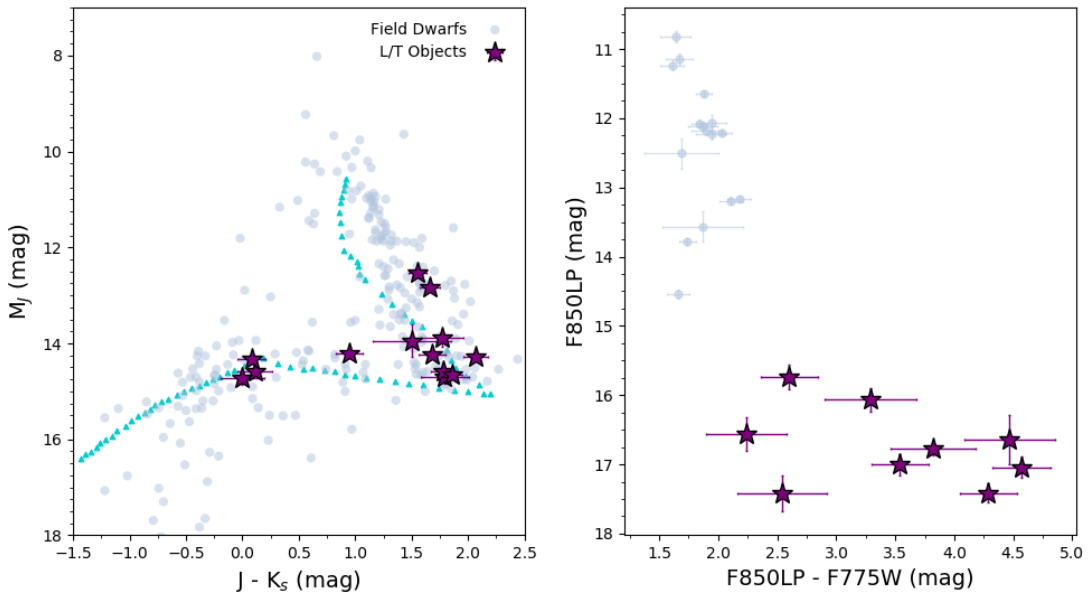

Figure 2.18: Color-magnitude diagrams in near-infrared and optical colors. Saumon and Marley (2008) hybrid evolutionary tracks are overplotted in turquoise triangles. Purple stars show the objects focused on in this paper. Filled light blue circles are low-mass field objects from Faherty et al. (2012) (left) and low-mass objects from Konopacky et al. (2010) (left and right). HST observations on right include both WFC3 and ACS filters.

2.9 Summary and Conclusion

Discrepancies between atmosphere and evolutionary model predictions play a significant role as different stages of condensate cloud evolution greatly influences the overall spectral shape. Previous grid comparisons have led to disagreements between atmosphere models and evolutionary predictions for substellar objects of known mass (e.g., Chabrier and Baraffe, 2000; Dupuy et al., 2014). We are able to produce atmosphere models that match evolutionary predictions for a sample of brown dwarfs ($\approx$ L4-T5) by allowing enough flexibility within the cloud properties.

Determining the bulk properties (e.g., effective temperature and gravity) of stellar and substellar mass objects is an important step along the way to making inferences about more specific properties, such as metallicity, or the relative abundances of key elements. These bulk properties are frequently estimated by comparing photometric or spectroscopic observations to model atmosphere predictions. For many objects such comparisons yield properties consistent with those of interior and evolution models that, at moderate to old ages, are considered reliable and less sensitive to model assumptions (Baraffe et al., 2002). Significant inconsistencies, however, can occur whenever condensate cloud formation greatly influences the overall spectral shape. This situation occurs, for example, across the L/T transition (Cushing et al., 2006) and for most young directly imaged companions (Metchev and Hillenbrand, 2006) where models with a range of temperatures, gravities, and cloud properties are capable of matching a single object's near-IR SED equally well (Barman et al., 2011a). Such ambiguity can often hinder the study of cloudy objects where mass and age are very uncertain.

In this paper we have studied a set of L/T transition ($T_{\rm eff} \approx$ 1900-1000 K) brown dwarf binaries with measured masses, luminosities, and well-determined ages. For these objects comparisons to evolutionary models yield very precise estimates of the bulk properties. Overall, synthetic spectra from our cloudy atmosphere models matched spatially-resolved visible to near-IR photometry of each binary component reasonably well. The cloud parameters included in our grids appear to be most

appropriate for L4-L8 field dwarfs with effective temperatures between 1900-1300 K and log(g) $\geq$ 5.0. The grid fits for these objects were the most consistent with our evolutionary-constrained atmosphere models.

With these atmosphere models we have determined a set of cloud properties across the L/T transition. The warmest objects in the sample ($\approx$1900-1500 K) were fit best by particles with mean grain sizes of 0.25-0.50 μm, whereas objects cooler than 1500 K required larger mean grain sizes 0.80-5 μm. Although the composition at the cloud top remained relatively close to an equal split between Fe and Mg-Si grains for the majority of objects, the overall location of the cloud top shifted to deeper regions within the atmosphere as objects cooled in effective temperature. Near 1400 K clouds began to disappear below the photosphere, which agrees with previous findings (Saumon and Marley, 2008; Marley et al., 2010).

There was some disagreement between our grid-based atmosphere models and the evolutionary-constrained atmosphere models for lower-gravity objects (log(g) $\leq$ 5.0) and the latest T dwarfs included in the sample (T4.5-T5.5; $T_{\rm eff} \leq$ 1200 K). Our grid-based models tended to over-predict temperature, gravity, and under-predict radius. In addition to model-grid aspects (e.g., grid spacing and boundaries), unresolved binarity might play a role in some systems. For example 2MASS 0850+10A may be a pair of objects near the deuterium burning limit, rather than a single L-type brown dwarf, due to the large difference in brightness between A and B components, low total mass of the system, and mixed results from atmosphere model fitting. Giant exoplanets overlap with the range of effective temperatures of brown dwarfs (Faherty et al., 2016) and such objects (e.g., HR8799c) can resemble mid-L spectral types (Marois et al., 2010; Barman et al., 2011b). Binarity is just one possibility and further study, both observationally and modeling, is warranted for this system.

SDSS 1021-03A is the earliest T dwarf in the sample, and evolutionary-constrained models preferred a deeper cloud (P_c=60 bar) and larger grain size (> 1 μm) slightly beyond the parameters in our atmosphere grids. Similarly, the later T4-T5 dwarfs (SDSS 1021-03B, 2MASS 1534-29A, 2MASS 1534-29B) required even deeper clouds (P_c=90-200 bar) and the largest grain sizes (3-5 μm). Evolutionary-

derived fits for these objects suggest our grids should be extended to include a larger range of cloud properties to accommodate early-to-mid T dwarfs and help constrain the limits of homogeneous cloud models for the coolest objects. We observe that condensate growth becomes more important near late-L types, leading to preferred model fits with larger mean grain sizes for T dwarfs. Other work has successfully reproduced T dwarf photometry using thin sulfide clouds (Morley et al., 2012) and inhomogeneous cloud cover with low temperature condensates (Na_2S, KCl) (Charnay et al., 2018). Near $T_{eff} \approx 1000$ K cloud-free models may be a better fit to our data; however, this is the same regime in low-gravity objects where sulfide clouds appear while iron and silicate clouds are simultaneous disappearing (Morley et al., 2012; Charnay et al., 2018). A more diverse grid for these objects will be beneficial in order to untangle the relationship between condensate growth, cloud composition, and surface gravity.

Rapid color changes across the L/T transition have been interpreted as the result of patchy clouds or holes in the cloud deck (Burrows et al., 2003; Ackerman and Marley, 2001; Marley et al., 2010), a sudden collapse of the cloud deck (Tsuji and Nakajima, 2003), or an increase in sedimentation efficiency of clouds (Knapp et al., 2004). By parameterizing the sedimentation efficiency of dust particles to regulate the influence of cloud opacity on the model spectrum, one can reproduce the L/T transition (Saumon and Marley, 2008; Stephens et al., 2009). We are able to reproduce photometric changes across the L/T transition in a similar fashion by parameterizing the vertical extent and mean grain size of a uniform cloud. However, we cannot rule out the existence of patchy clouds in this sample of objects despite our homogeneous cloudy model fits because the presence of cloud holes is very subtle across the near-infrared part of the spectrum for L/T transition objects (Marley et al., 2010; Apai et al., 2013).

Other groups use a more complex treatment of grain nucleation, growth, evaporation, and/or drift. Work from Helling et al. (2008a,c) resulted in mean cloud particle sizes that increased as a function of atmospheric depth, with small particles (≈ 0.01 μm) in high atmospheric layers with a narrow grain size distribution that

broadened to larger particle sizes ($\approx$ 100 μm) and grain size distributions near the cloud base. Charnay et al. (2018) was able to reproduce the spread of near-IR colors across the L/T transition and those observed in reddened low-gravity objects by computing cloud particle radii estimated from simple microphysics. Our models use a constant grain size distribution with cloud height, but similar to more complex treatment of grains, the peak dust-to-gas ratio sinks to deeper regions within the atmosphere, eventually below observable layers.

It has been hinted at that grain size increases as objects cool across the L/T transition (Zhou et al., 2018; Knapp et al., 2004). Burrows et al. (2006) used models with homogeneous forsterite grains with sizes of 3, 10, 30, and 100 μm and identified that atmospheres with larger particles resulted in stronger J-band fluxes near 1400-1500 K due to the natural deepening of the cloud position in the model atmospheres. We observe something similar in our grid models across a smaller range of particle sizes (0.25-1 μm) for our heterogeneous grains. Figure 2.3 shows J-band flux is greater for the largest grain sizes at 1300 K whereas J-band fluxes are similar at 1500 K regardless of grain size. A physical mechanism responsible for this trend in increasing grain size is not well understood. At cooler effective temperatures, it has been suggested that a larger supply of condensate vapor near the base of the cloud could result in runaway particle growth for cooler objects (Gao et al., 2018).

Photometry has limited sensitivity; therefore, future steps will be to improve atmospheric constraints with resolved spectroscopy. Cloud location, mean grain size, surface gravity, and metallicity impact our understanding substellar atmospheres as a function of temperature. Decoupling the degeneracies between these interwoven features is essential to explain observations of objects, particularly across the L/T transition. This work provides valuable insight into the complex evolution of cloud opacity for a range of well-studied brown dwarf binaries. Ideally, the goal is to be able to construct reliable atmosphere models that can account for the drastic color change and physical properties of substellar objects without a reliance on evolutionary models to infer the properties of individual objects. We plan to extend our cloudy grids to both lower and higher cloud top pressures with additional grain

sizes to accommodate the earliest and latest spectral types. Additional exploration of cloud properties is warranted for the warmest and coolest objects for binaries where our atmosphere grids lacked coverage.

Future work would greatly benefit from additional observations, especially at the shortest wavelength portion of the SED. Photometric bands near 0.8-1 μm appear important when investigating flux reversal binary systems and provide insight to differing grain size preferences at optical and near-infrared wavelengths. The next generation of telescopes with higher sensitivity and wavelength coverage will be essential in providing high-quality spectra required to fine tune cloud parameters and address lingering inconsistencies, such as broad, continuous wavelength coverage from the James Webb Space Telescope's NIRSpec instrument (0.6-5.3 μm). Furthermore, variability has been detected in brown dwarfs at the transition region (Radigan, 2014) and will be an important factor for cloud formation and evolution going forward. Rotation-modulated spectral variations will be a key approach toward a more in-depth grasp of the evolving cloud structure in low-mass objects (Apai et al., 2013, 2017). Understanding the relationship between grain size distribution and effective temperature will require a multidimensional approach to grain kinetics and growth connected to convective cloud structure. Atmospheric retrieval results can be compared to those of self-consistent models to better understand the nature of discrepancies (e.g., heterogeneous cloud layers, particle sizes, cloud composition, haze layers). Relatively few brown dwarfs spanning the L/T transition have known masses, and the release of future *Gaia* data will increase parallax precision by 30% (Brown et al., 2018). Objects with independently constrained properties from dynamical mass and luminosity measurements are the strongest candidates for future model comparisons.

2.10 Acknowledgements

Laci is extremely grateful for Kyle Pearson and many helpful discussions of this work. We would also like to thank the anonymous referee for a constructive report.

Support for program 11605 was provided by NASA through a grant from the Space Telescope Science Institute, which is operated by the Associations of Universities for Research in Astronomy, incorporated under NASA contract NAS5-26555. This work was also supported by NSF grants 1405505 and 1614492. Material presented in this work is supported by the National Aeronautics and Space Administration under Grants/Contracts/Agreements No.NNX17AB63G issued through the Astrophysics Division of the Science Mission Directorate. This research makes use of data products from 2MASS, a joint project of the University of Massachusetts and the Infrared Processing and Analysis Center/California Institute of Technology, funded by the National Aeronautics and Space Administration and the National Science Foundation. Some of the data presented herein were also obtained at the W. M. Keck Observatory, which is operated as a scientific partnership among the California Institute of Technology, the University of California, and the National Aeronautics and Space Administration. The Observatory was made possible by the generous financial support of the W. M. Keck Foundation. The authors also recognize and acknowledge the very significant cultural role and reverence that the summit of Mauna Kea has always had within the indigenous Hawaiian community. We are most fortunate to have the opportunity to conduct observations from this mountain. Additionally, this research has benefited from the SpeX Prism Library, maintained by Adam Burgasser at http://www.browndwarfs.org/spexprism.

CHAPTER 3

Properties of the Substellar Benchmark HD 130948B+C with Moderate-Resolution Spectroscopy

3.1 Introduction

The growing population of brown dwarfs over the past two decades has provided critical insight into the complex atmospheric processes that shape the spectral energy distribution of low-mass objects. Photometric studies have established the foundation of substellar evolution on the color-magnitude diagram, identifying trends influenced by effective temperature (Faherty et al., 2012; Dupuy and Liu, 2012; Leggett et al., 2002). Fundamental properties of brown dwarfs can be obtained by fitting spectroscopy to synthetic spectra from atmosphere models and, coupled with evolutionary models, mass and age can be inferred (Cruz et al., 2017; Saumon and Marley, 2008). However, brown dwarfs lack fusion in their cores and cool throughout time, resulting in a degeneracy in mass, age, and luminosity. Secondary parameters beyond temperature including surface gravity, metallicity, cloud opacity, and non-equilibrium chemistry are known to influence the color and spectral morphology of brown dwarfs (Knapp et al., 2004; Lew et al., 2020). It is difficult to confidently

constrain atmospheric properties from spectra alone and challenging to untangle the relationship between multiple parameters for individual, isolated objects (Stephens et al., 2009; Barman et al., 2015).

Brown dwarfs span a vast range of masses from ∼13-80 M_{Jup} in between giant gaseous planets and low-mass stars (Burrows et al., 2001). Although the limits depend upon chemical composition (Baraffe et al., 2002), the boundaries are roughly defined by the mass required for deuterium fusion at the lower end of the spectrum and hydrogen fusion at the upper end. Testing and refining substellar evolutionary and atmosphere models requires a population of well-characterized objects due to the diversity of brown dwarfs. One way to tackle degeneracies is to study brown dwarfs in binary systems by obtaining precise dynamical mass measurements, which allow powerful coevality assumptions about age and composition (Konopacky et al., 2010; Dupuy and Liu, 2017). Several binary systems in the solar neighborhood have been studied via extensive astrometric monitoring and high angular resolution imaging surveys, resulting in total and individual masses for objects that span spectral types M7-T5 (e.g., Lane et al., 2002; Liu et al., 2008; Burgasser, 2007; Konopacky et al., 2010; Dupuy and Liu, 2017).

There appears to be a low occurrence rate ($< 1\%$) of brown dwarfs around sun-like stars compared to stars with planetary companions at close-in orbits (< 5 AU) (Sahlmann et al., 2011; Ma and Ge, 2014; Díaz et al., 2016) commonly referred to as the brown dwarf desert. A few binary systems with well-known masses orbit a stellar companion. The properties of the host star can provide independent system age estimates, metallicity, and help to constrain brown dwarf formation models. Ma and Ge (2014) suggest brown dwarfs from 35-55 M_{Jup} are the most depleted and 42.5 M_{Jup} may be a transitional mass where objects below this threshold form similar to giant planets via core accretion or disk instability (Pollack et al., 1996) and above form like stars via gravitational cloud collapse (Hennebelle and Chabrier, 2008).

Both metal-rich and metal-poor stars have been detected with brown dwarf companions (Sahlmann et al., 2011), but recent work suggests there are separate populations for lower and higher mass brown dwarfs based on metallicity and eccentricity

distributions (Maldonado and Villaver, 2017; Grieves et al., 2021). A study from Maldonado and Villaver (2017) found massive brown dwarfs appear to have similar metallicities as stars, whereas low mass brown dwarfs have a higher metallicity with greater abundances of Sc II, Mn I, and Ni. Model-independent characterizations of brown dwarf atmospheric properties are required to understand the link between composition and different formation scenarios. Atmospheric chemistry in brown dwarfs is greatly influenced by the ratio of carbon to oxygen (C/O) through features of water vapor (H_2O), carbon monoxide (CO), and methane (CH_4). Comparing host star properties to brown dwarf companions, such as the C/O, is one way to understand the formation history and evolution of substellar objects (Madhusudhan et al., 2011).

3.1.1 HD 130948 System

HD 130948 is a hierarchical triple system composed of a pair of L4+L4 brown dwarfs discovered using the Gemini North Telescope separated by ≤ 10 mas in a wide orbit around a Sun-like primary star (G2V) (Goto et al., 2002; Potter et al., 2002). Van Leeuwen (2007) measured a precise distance of 18.17 $\pm$ 0.11 pc using astrometric data from *Hipparcos*. The metallicity of the host star measured by Valenti and Fischer (2005) was close to solar (Fe/H = 0.05). Dupuy et al. (2009a) determined a total dynamical mass of 114 $\pm$ 3 M_{Jup} using a combination of telescope observations totaling approximately 70% of HD 130948BC's orbital period. The total measured mass was updated in Dupuy and Liu (2017) to $115.4^{+2.2}_{-2.1}$ M_{Jup} consistent with results from Konopacky et al. (2010).

The age of HD 130948A has been a point of contention since the age of individual solar-type stars can be difficult to constrain. Early estimates characterizing solar analog samples suggested HD 130948A is in the range of 0.2-0.8 Gyr (Gaidos, 1998). Mamajek and Hillenbrand (2008) estimated an age of 0.5 $\pm$ 0.3 Gyr from chromospheric activity traced by Ca II HK emission. Dupuy et al. (2009a) argue gyrochronology provides the most precise age estimate for HD 130948A and arrive

at a mean age of $0.79^{+0.22}_{-0.15}$ Gyr whereas Barnes (2007) suggest the gyrochronology age may be as young as ∼0.39 Gyr. Mullan and MacDonald (2010) found a similar, younger age of 0.28-0.39 Gyr using magnetic convection models. If the star is indeed 0.79 Gyr, Dupuy et al. (2014) found the luminosity for HD 130948B and C to be brighter than theoretical evolutionary model tracks by a factor of 2-3. Disagreements between atmosphere and evolutionary models could be resolved with extended wavelength coverage with L-band spectra (Briesemeister et al., 2019) or with models that accounted for various cloud properties (Brock et al., 2021). These cloudy model fits preferred a younger system age of 0.42-0.45 Gyr consistent with gyrochronology measurements from Barnes (2007) and chromospheric activity from Mamajek and Hillenbrand (2008).

Both brown dwarfs in the system are considered rapid rotators (v sin $i > 10$ km s^{-1}) with the C component rotating at 30% of its break-up speed. Konopacky et al. (2012) measured the projected rotational velocity (v sin i) of HD 130948B and C as 64 ± 4 and 86 ± 6 km s^{-1}, respectively, and explain the difference in rotational velocity between components may be due to dynamical evolution torquing the system into misalignment. It has been suggested magnetic activity could be significant for these objects as well (Konopacky et al., 2012).

In this work, we present resolved, moderate-resolution spectroscopy (R ∼ 4000) of HD 130948B and HD 130948C. We compare J and K-band spectroscopy to atmosphere model grids to determine the best-fit parameters of effective temperature, surface gravity, metallicity, and cloud properties. We explore how sensitive these bands and spectral features are to the various model parameters. We are able to resolve spectral features of H_2O and CO to determine their molecular abundances and derive C/O ratios for our objects.

3.2 Observations

HD 130948B+C was observed on 2015 July 20 (UT) at the W. M. Keck Observatory using natural guide star adaptive optics and the OH-Suppressing Infra-Red Imaging

Table 3.1: OSIRIS Observations of HD 130948BC

Target	Date	Band	Exposures	Exposure Time (sec)
HD 130948B+C	2015-07-20	Jbb	4	300
HIP73087	2015-07-20	Jbb	3	2
HD 130948B+C	2015-07-20	Kbb	4	300
HIP73087	2015-07-20	Kbb	3	2

Spectrograph (OSIRIS) instrument (Larkin et al., 2006) on the Keck II telescope. Broadband J and K spectra were obtained (1.18-1.42, 1.96–2.38 μm) over a 0".32 x 1".28 patch of the sky with a spaxel scale of 0".02 spaxel^{-1} (where spaex refers to one OSIRIS spatial resolution element). We also obtained appropriate dark, sky, and A0 telluric standard star observations. A summary of the observations is provided in Table 3.1 for reference.

Data were reduced using the standard OSIRIS data reduction pipeline (Krabbe et al., 2004; Lockhart et al., 2019). We follow a similar procedure described in Barman et al. (2011a) for producing basic calibrated data (BCD) cubes. Spectra were obtained by fitting Gaussian point-spread functions (PSFs) to each binary component for each monochromatic slice of the cube. The individual spectra were median-combined, and the uncertainties were determined by calculating the rms between the individual spectra at each wavelength. Images from the data cubes are given in Figure 3.1 and show the separation between the binaries. We flux calibrated our spectra such that the flux at each wavelength when integrated matches the respective J and K-band 2MASS absolute magnitudes from Konopacky et al. (2010). Figure 3.2 shows the flux-calibrated spectra for both B and C components.

3.3 Empirical Comparisons

HD130948 B and C are both L dwarfs (L4 $\pm$ 1) with similar bulk properties (Dupuy and Liu, 2017). The B component is more massive ($\sim$4 M_{Jup}), brighter (0.11 dex), and warmer than the C component by $\sim$100 K. We calculated the average percent difference between components using our OSIRIS data to see if any significant spectral differences were driving the differences between the two brown dwarfs.

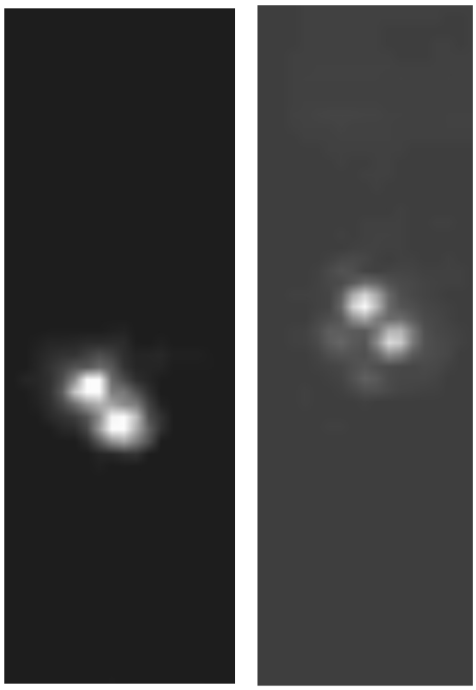

Figure 3.1: Separation of the binary system HD 130948BC in the J (left) and K (right) bands.

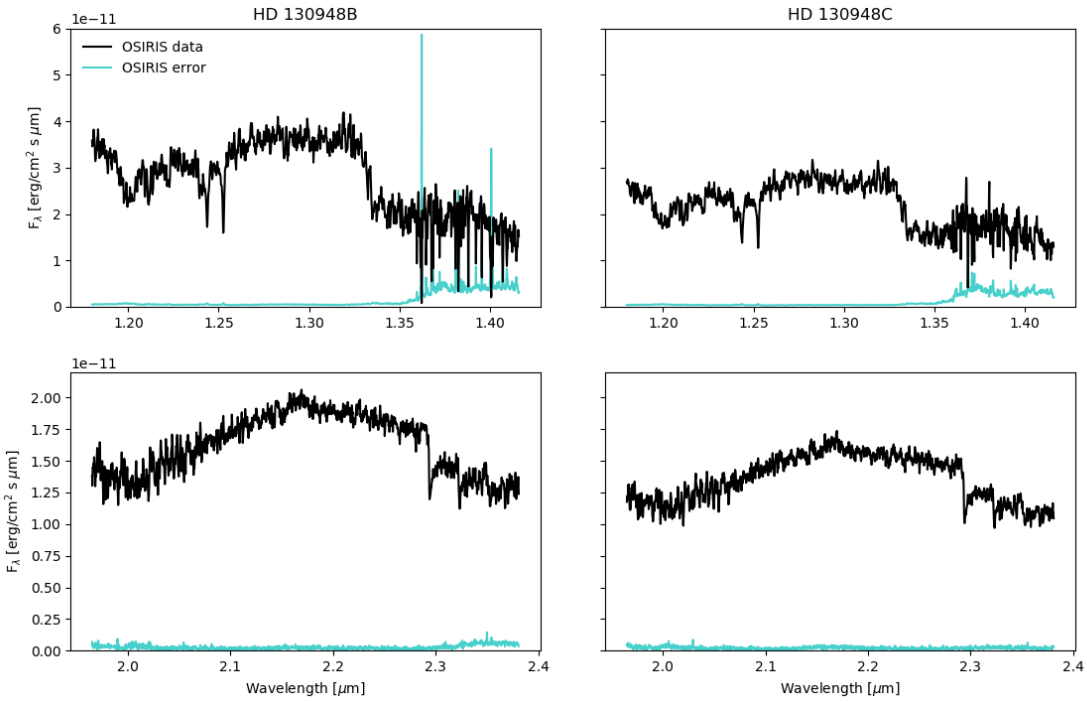

Figure 3.2: Flux-calibrated OSIRIS spectra for HD 130948B and HD 130948C in J (left) and K (right) bands.

Table 3.2: Evolutionary-derived Model Properties

Property	HD 130948B	HD 130948B
SpT	L4 ± 1	
Dupuy and Liu (2017); Dupuy et al. (2014)		
Mass [M_J]	$59.8^{+2.0}_{-2.1}$	$55.6^{+2.0}_{-1.9}$
log(L_{bol}) [$L_\odot$]	-3.85 ± 0.06	-3.96 ± 0.06
$T_{\rm eff}$ [K]	1920^{+70}_{-60}	1800^{+50}_{-70}
log(g) [cm s^{-2}]	5.12 ± 0.03	$5.10^{+0.03}_{-0.04}$
Radius [$R_{\rm Jup}$]	$1.05^{+0.02}_{-0.01}$	$1.06^{+0.01}_{-0.02}$
Age [Gyr]	0.44 ± 0.04	
Briesemeister et al. (2019)		
Mass [M_J]	59.8 ± 0.6	56.4 ± 0.6
log(L_{bol}) [$L_\odot$]	-3.87 ± 0.01	-3.96 ± 0.01
$T_{\rm eff}$ [K]	1900 ± 20	1800 ± 20
log(g) [cm s^{-2}]	5.14 ± 0.01	5.11 ± 0.01
Radius [$R_{\rm Jup}$]	1.037 ± 0.002	1.037 ± 0.002
Age [Gyr]	0.45 ± 0.02	
Brock et al. (2021)		
Mass [M_J]	59 ± 1	56^{+2}_{-1}
log(L_{bol}) [$L_\odot$]	-3.85 ± 0.09	-3.91 ± 0.05
$T_{\rm eff}$ [K]	1916^{+94}_{-90}	1851^{+46}_{-45}
log(g) [cm s^{-2}]	5.12 ± 0.02	$5.10^{+0.02}_{-0.03}$
Radius [$R_{\rm Jup}$]	1.05 ± 0.02	1.05 ± 0.02
Age [Gyr]	$0.42^{+0.06}_{-0.04}$	

We first looked for any differences between the combined J and K-band data. The average percent difference between B and C is ∼5%, which is slightly larger than the average uncertainty for B and C (4 % and 3 %, respectively). By individual band, there is an average difference of 8% between B and C in J band approximately 3% larger than the average uncertainties. The K differences are roughly equal to the average uncertainties (∼2%). Figure 3.3 provides a comparison of the B and C components for each band. The data show spectra are quite similar between the two objects.

The spectra of HD 130948B+C are similar to other field L dwarfs (Figure 3.4). FeH (1.20 μm) and K I alkali lines (1.25 μm) in the J band are the most prominent features in our object and in L dwarfs of spectral types L0-L6 (Cushing et al., 2004). FeH features tend to be strongest in L2-L3 dwarfs and decrease for types later than L3 (Allers and Liu, 2013). The strength of FeH and K I are indicators of gravity and youth. For objects with lower gravity, the photosphere is shifted to regions of

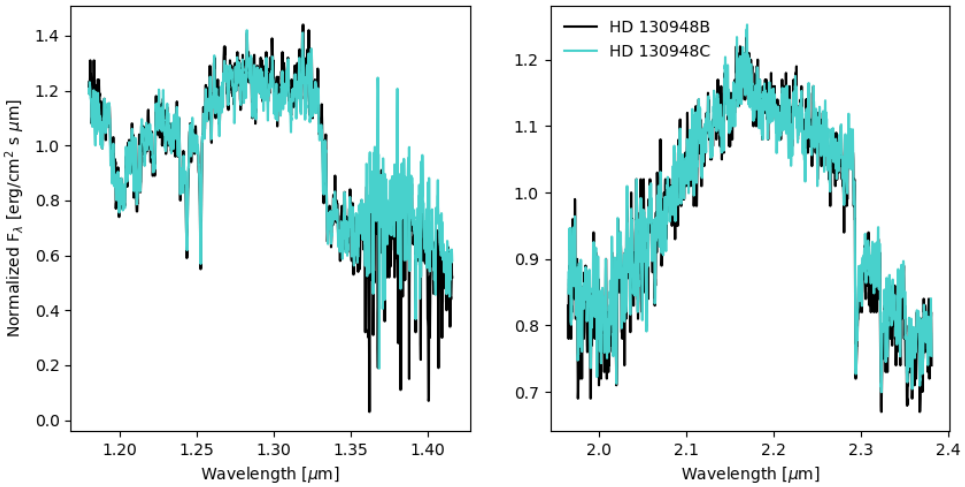

Figure 3.3: Comparison between J and K-band spectra for HD 130948 B and C. Spectra are flux calibrated and normalized.

lower pressure and weakens lines of FeH, Na I, and K I. K I lines are prominent in our object suggesting a field gravity and age. Allers and Liu (2013) suggest signs of weak gravity can also be apparent in the K-band continuum with a more positive slope from 2.15-2.25 μm. There are no apparent spectral indicators in our data that suggests our objects have low gravity or youth.

Because the spectra are quite similar, differences observed between HD 130948 B and C are likely driven by color variations in the J band. Figure 3.5 illustrates HD 130948B is slightly bluer than HD 130948C and places the system in the context of the field dwarf population. Figure 3.6 provides a closer look at color dispersal of L3-L5 dwarfs including those classified as intermediate gravity (Cruz et al., 2009). HD 130948 B and C both have an average J - K near-infrared color representative of L3-L4 types and therefore do not show any signs of youth (Faherty et al., 2012).

3.4 Spectral Modeling

Our goal is to constrain the atmospheric properties of HD 130948B and C using new spectral data presented in this paper. Additionally, we explore how sensitive

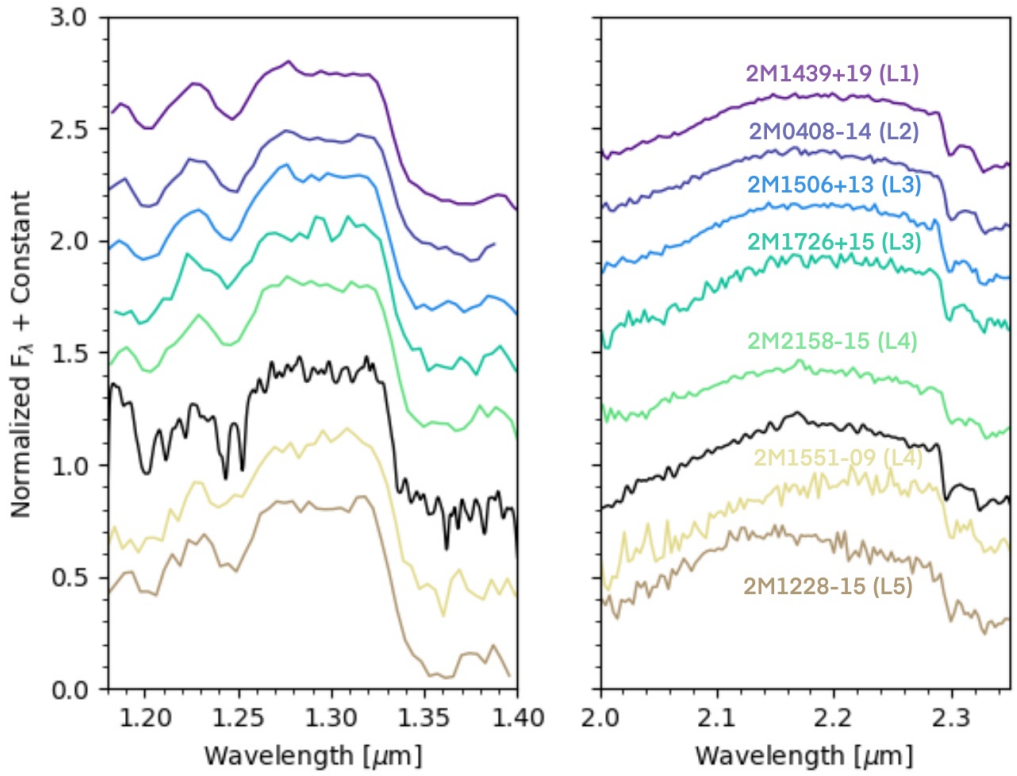

Figure 3.4: An example of L dwarf spectra is shown from L1-L5 [1-4]. Moderate-resolution spectra of HD 130948 B is smoothed with a Gaussian to a resolution of 200. The J and K bands are plotted separately and normalized by the mean flux at 1.18-1.41 and 1.97-2.38 μm, respectively. 2M1726 and 2M1551 are classified as intermediate and low gravity. **References:** [1] (Allers and Liu, 2013), [2] Kirkpatrick et al. (2010), [3] Cruz et al. (2017), [4] Burgasser et al. (2007), [5] Burgasser et al. (2010)

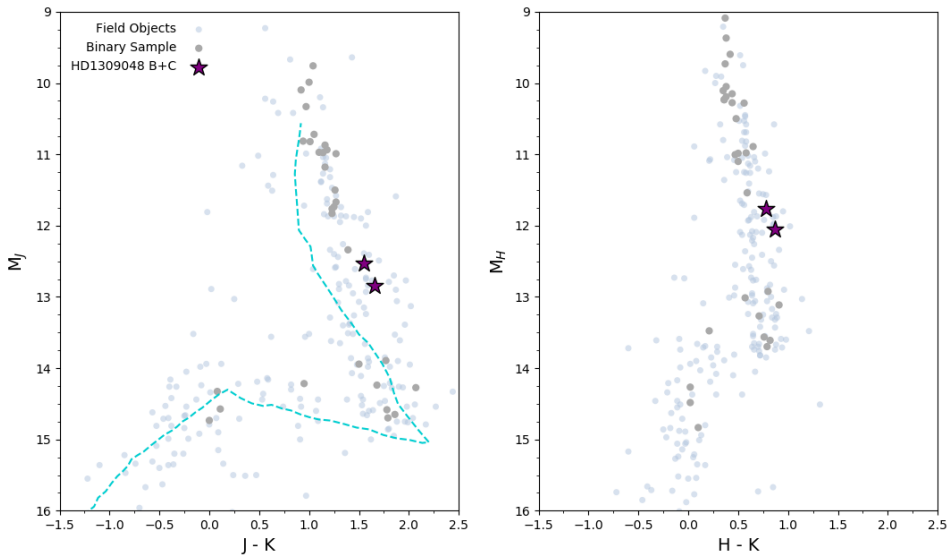

Figure 3.5: Near infrared color-magnitude diagram with field dwarfs from Faherty et al. (2012) and the full sample of low mass binaries from Konopacky et al. (2010). HD 130948B+C are plotted as purple stars. Saumon and Marley (2008) hybrid evolutionary tracks are over-plotted in turquoise.

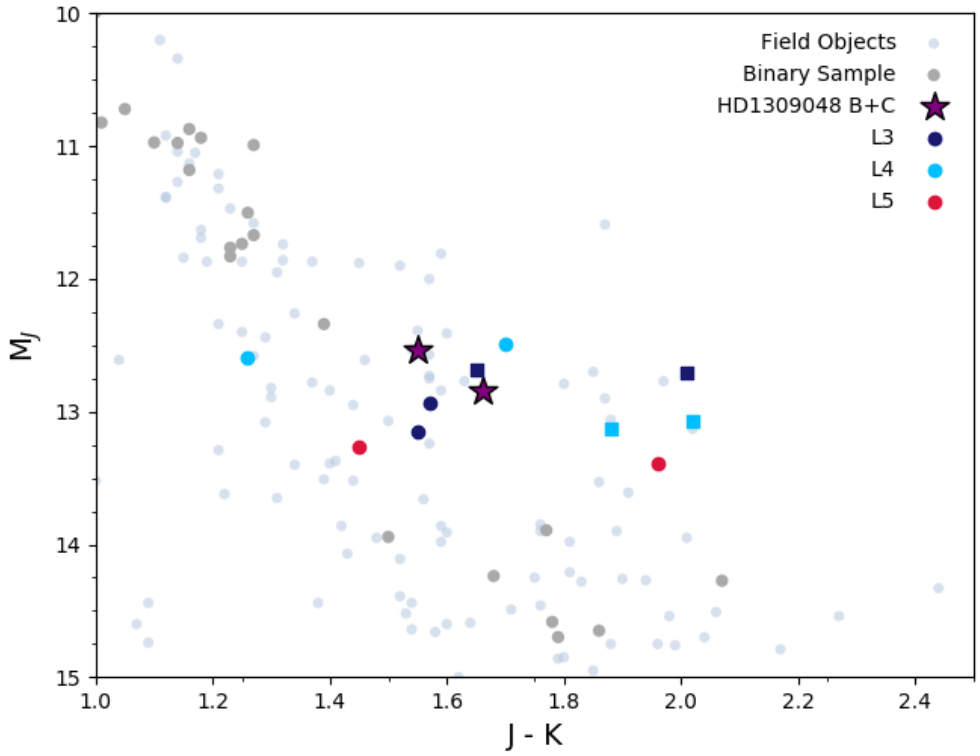

Figure 3.6: Comparison of colors across a sample of L3-L5 dwarfs. Intermediate gravity objects are plotted as square symbols for their respective spectral type. Data from Faherty et al. (2016).

Table 3.3: Model Parameters

$T_{\rm eff}$ [K]	log(g) [cm s^{-2}]	P_c [bar]	a_0 [μm]	Increments
1700-2000	4.5-5.5	0.1, 0.5	0.25, 0.50, 1.0	100 K; 0.5 in log(g)

spectral features are to small changes in model parameters of temperature, gravity, metallicity, and cloud properties.

In Brock et al. (2021) we created grids of synthetic spectra using the PHOENIX 1D model atmosphere code assuming radiative-convective equilibrium. Our models included parameterized clouds composed of multiple condensates that contribute to the total atmospheric opacity. Clouds are described by two parameters: the cloud pressure, P_c, and the mean grain size, a_0. A more detailed discussion of the model can be found in Barman et al. (2011a). Models were calculated with an updated line list from Tennyson and Yurchenko (2012) with a sampling of 1 Å between 0.9 and 5 μm.

First, we required model grids that spanned the expected values of our objects (Table 3.3). We used a small grid from our previous work with a temperature range of 1700-2000 K and log(g) from 4.5-5.5 dex that included two values for cloud pressure (P_c=0.1, 0.50 bar) and three values for grain size (a_0=0.25, 0.50, 1 μm). Another grid was created with the same properties but using metallicity of the host star, HD 130948A. Elemental abundances were obtained from the Hypatia Catalog (Hinkel et al., 2014). Abundances for 25 elements were available and incorporated into our PHOENIX models. The remaining elements were kept at their respective solar values.

3.4.1 Model Atmosphere Fits

For each brown dwarf, we fit solely the J band, solely the K band, and a joint fit of both near-infrared bands combined with H-band photometry. We determined the best atmosphere model for each object using a χ^2-fitting approach. Models are by $(R/D)^2$, where R is the radius of the object to be fit, and D is 10 parsecs to ensure fluxes are at absolute values.

The best-fitting atmosphere models and weighted mean values were determined for both solar and stellar metallicity grids. Results from the grid fitting are provided in Tables 3.4 and 3.5. We allowed models at the 68% confidence level ($\Delta\chi^2 < 11.3$) taking χ^2 distributed with five degrees of freedom. Parameters fit include those listed in Table 3.3 and the object's radius.

Weighted mean parameters were calculated using a similar approach to Stone et al. (2016)

$$\bar{m} = \frac{\Sigma_i W_i m_i}{\Sigma_i W_i}, \tag{3.1}$$

where the weight W_i for each model m_i is given by

$$W_i = e^{-0.5\chi^2}, \tag{3.2}$$

Uncertainties were calculated using sided variance estimates with

$$\sigma_m = \frac{\Sigma_i W_i (m_i - \bar{m})^2}{\Sigma_i W_i}, \tag{3.3}$$

where the sum is calculated using parameters above (+) or below (-) the mean values. In cases where the edge of the grid boundary was approached, we report an upper/lower limit for our uncertainty.

A summary of the weighted mean grid fits are provided for HD130948 B in Table3.4 and for HD130948 C in Table 3.5. In Figures 3.7 and 3.8, the joint JHK best-fitting models are shown. The model parameters we arrived at for B and C were identical to each other for both solar and stellar metallicity (T_{eff} = 1900 K, P_c = 0.10 bar, a_0 = 0.25 μm); however, the solar fit prefers a surface gravity of log(g)=5.0 whereas the stellar fit is greater by 0.5 dex. Although the model parameters are the same, HD 130948B is brighter with a larger radius than the C component in both solar and stellar cases. Overall, the shape of the H band appears to be the largest diagnostic difference between these model fits.

Individual band fits for each object were consistent within the uncertainties across solar and stellar metallicity grids in most cases. Weighted mean fits for solar models preferred effective temperatures ∼1800-1900 K. Stellar metallicity fits were similar. The surface gravity for K-band fits leaned toward lower values (log(g) ∼

4.90) for solar models compared to stellar models ($\log(g) \sim 5.25$), which occurred for HD 130948B and C. We were unable to constrain surface gravity for stellar models as well as we hoped; thus, for J-band and JHK fits we quote the uncertainty of the lower grid boundary. Similarly, weighted mean cloud properties were difficult to constrain for J-band and JHK fits. We plot the best-fitting model spectra compared to the individual J and K-bands for added insight in Figure 3.9. The J band prefers a smaller 0.25 μm mean grain size, and the K-band fits lean toward grain sizes of approximately 0.45-0.60 μm both at a cloud pressure of 0.1 bar.

The results presented here are an overall improvement from our previous paper in which grid fits for HD 130948B and HD 130948C could not be formally constrained by resolved JHK photometry and required a prior on radius from evolutionary models (Brock et al., 2021). However, the uncertainties do suggest our objects are bumping up against the lower edge of our grid boundary. A combination of models with clouds at higher pressures and smaller grain sizes would be required to test this further. Changes in metallicity that deviate from solar can also influence the location of the cloud deck and radiative-convection boundary; therefore, additional exploration beyond the given parameter space would be beneficial and will be discussed later in the paper.

J and K-band spectra and H-band photometry grid fits for HD 130948B are shown for solar (purple) and stellar (cyan) metallicity compared to OSIRIS data (black). In the bottom panel, we also include the H-band portion of the model fits assuming a wavelength range from OSIRIS.

3.4.2 Evolutionary Model Properties

We derived evolutionary model-inferred properties using the weighted mean luminosity from our joint JHK atmosphere model fits and the total measured mass of the B+C components. Only the evolutionary properties were determined for the solar case because the luminosity derived from stellar metallicity was nearly identical and well within the uncertainties. The results are provided in Table 3.6. HD 130948 B

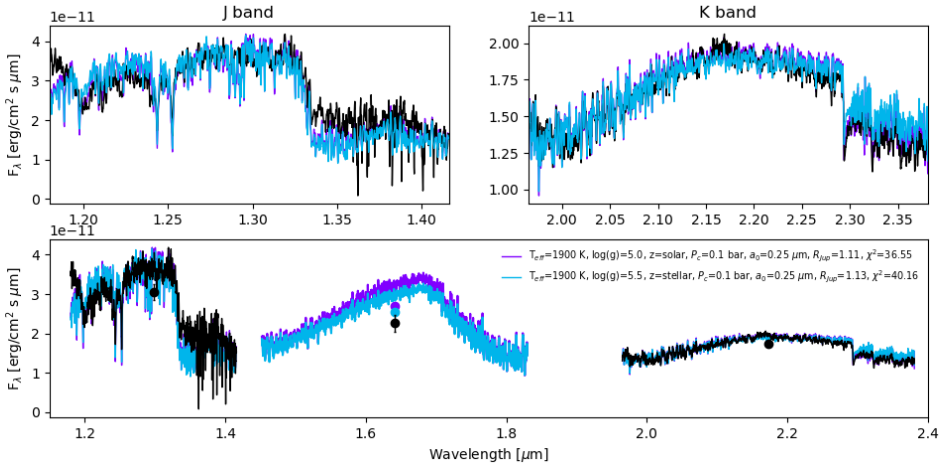

Figure 3.7: J and K-band spectra and H-band photometry grid fits for HD 130948B are shown for solar (purple) and stellar (cyan) metallicity compared to OSIRIS data (black). In the bottom panel, we also include the H-band portion of the model fits assuming a wavelength range from OSIRIS.

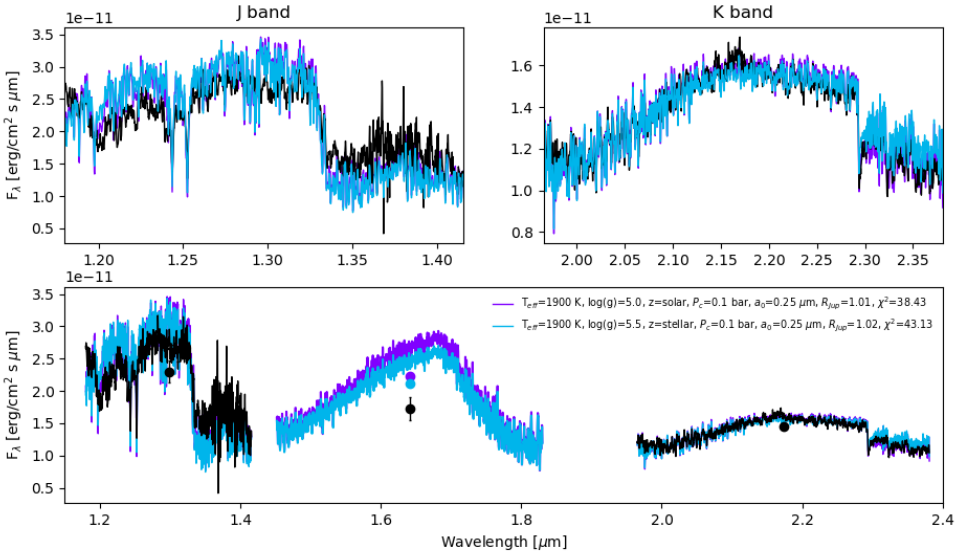

Figure 3.8: J and K-band spectra and H-band photometry grid fits for HD 130948C are shown for solar (purple) and stellar (cyan) metallicity compared to OSIRIS data (black). In the bottom panel, we also include the H-band portion of the model fits assuming a wavelength range from OSIRIS.

Table 3.4: HD 130948B: Atmosphere Model Inferred Properties

Property	J	K	JHK	JHK best fit
Solar Metallicity				
T_{eff} [K]	1900^{+100}_{-92}	1885^{+69}_{-117}	1900^{+100}_{-200}	1900
log(g) [cm s^{-2}]	$4.53^{+0.47}_{-0.03}$	$4.96^{+0.04}_{-0.46}$	$5.01^{+0.49}_{-0.01}$	5.0
Radius [R_J]	$1.14^{+0.30}_{-0.15}$	$1.18^{+0.09}_{-0.10}$	$1.11^{+0.02}_{-0.01}$	1.11
log(L_{bol}) [$L_\odot$]	$-3.81^{+0.09}_{-0.05}$	$-3.78^{+0.03}_{-0.05}$	$-3.81^{+0.02}_{-0.01}$	-3.82
P_c [bar]	$\leq$0.50	$0.23^{+0.27}_{-0.13}$	$0.11^{+0.39}_{-0.01}$	0.10
a_o [μm]	$\leq$1	0.46 $\pm$ 0.21	$\leq$ 1	0.25
Stellar Metallicity				
T_{eff} [K]	1797^{+3}_{-97}	1916^{+84}_{-127}	1900^{+100}_{-200}	1900
log(g) [cm s^{-2}]	$\geq$4.5	$5.27^{+0.23}_{-0.45}$	$\geq$ 4.5	5.5
Radius [R_J]	$1.40^{+0.31}_{-0.01}$	$1.19^{+0.19}_{-0.11}$	$\cdots$	1.13
log(L_{bol}) [$L_\odot$]	$-3.71^{+0.08}_{-0.01}$	$-3.75^{+0.02}_{-0.05}$	$\cdots$	-3.80
P_c [bar]	$0.11^{+0.39}_{-0.01}$	$0.19^{+0.31}_{-0.09}$	$\leq$ 0.50	0.10
a_o [μm]	$\leq$1	$0.60^{+0.40}_{-0.21}$	$\leq$ 1	0.25

Weighted mean grid fits for HD130948 B with 2-σ uncertainties are provided for fits to J-band spectra, K-band spectra, and a joint fit of both near-infrared bands plus H-band photometry. Only one model was within 2-σ for the JHK stellar metallicity fit; therefore, we report upper/lower limits for model parameters constrained by the grid where possible.

Table 3.5: HD 130948C: Atmosphere Model Inferred Properties

Property	J	K	JHK	JHK best fit
Solar Metallicity				
T_{eff} [K]	$\leq$ 2000	1818^{+113}_{-67}	1900^{+100}_{-200}	1900
log(g) [cm s^{-2}]	$5.49^{+0.01}_{-0.49}$	$4.89^{+0.13}_{-0.39}$	$5.17^{+0.33}_{-0.17}$	5.0
Radius [R_J]	1.59 $\pm$ 0.06	$1.16^{+0.12}_{-0.10}$	1.02 $\pm$ 0.01	1.01
log(L_{bol}) [$L_\odot$]	-3.70 $\pm$ 0.03	$-3.86^{+0.03}_{-0.04}$	-3.89 $\pm$ 0.01	-3.90
P_c [bar]	$0.12^{+0.38}_{-0.02}$	$0.17^{+0.33}_{-0.07}$	$\leq$ 0.50	0.10
a_o [μm]	$\leq$ 1	$0.45^{+0.23}_{-0.20}$	$\leq$ 1	0.25
Stellar Metallicity				
T_{eff} [K]	1800 $\pm$ 100	1897^{+84}_{-148}	1900^{+100}_{-200}	1900
log(g) [cm s^{-2}]	$\geq$ 4.5	$5.25^{+0.25}_{-0.43}$	$\geq$ 4.5	5.5
Radius [R_J]	$1.25^{+0.30}_{-0.01}$	$1.12^{+0.17}_{-0.12}$	$\cdots$	1.02
log(L_{bol}) [$L_\odot$]	$-3.81^{+0.09}_{-0.01}$	$-3.82^{+0.02}_{-0.05}$	$\cdots$	-3.89
P_c [bar]	$\leq$ 0.50	$0.15^{+0.36}_{-0.04}$	$\leq$ 0.50	0.10
a_o [μm]	$\leq$ 1	$0.63^{+0.37}_{-0.20}$	$\leq$ 1	0.25

Weighted mean grid fits for HD130948 C with 2-σ uncertainties are provided for fits to J-band spectra, K-band spectra, and a joint fit of both near-infrared bands plus H-band photometry. Only one model was within 2-σ for the JHK stellar metallicity fit, so we again report upper/lower limits for model parameters constrained by the grid where possible.

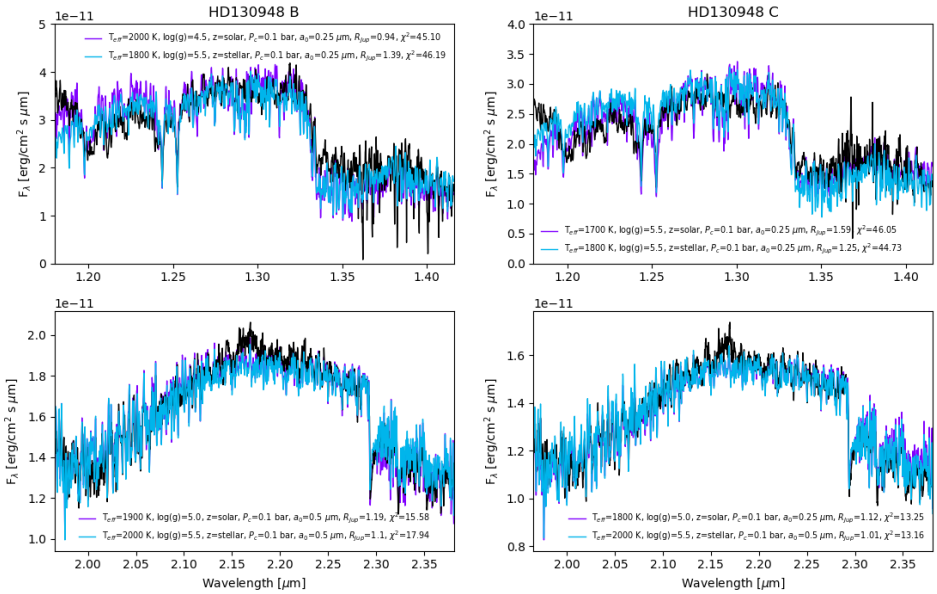

Figure 3.9: The best-fitting models to the individual J and K-bands are shown for solar (purple) and stellar (cyan) metallicity compared to OSIRIS data (black) for HD 130948B (left) and HD 130948C (right).

Table 3.6: Evolutionary Derived Model Properties

Property	HD 130948B	HD 130948C
Mass [M_{Jup}]	59.2 ± 1.2	56.2 ± 1.2
log(L_{bol}) [$L_{\odot}$]	-3.81 ± 0.02	-3.89 ± 0.01
T_{eff} [K]	1957^{+26}_{-25}	1868 $/pm$ 13
log(g) [cm s^{-2}]	5.12 ± 0.01	$5.10^{+0.01}_{-0.02}$
Radius [R_{Jup}]	1.05 ± 0.01	1.05 ± 0.01
Age [Gyr]	0.40 ± 0.03	

Evolutionary parameters were derived using SM08 hybrid models. Input parameters include a total measured mass of 115.4 ± 2.1 M_{Jup} and the weighted mean luminosity determined from atmospheric grid fitting for JHK data.

and C have similar bulk properties with C being slightly cooler and fainter compared to B. Our overall findings are consistent with previous work, which is summarized in Table 3.2.

3.4.3 Cloud Condensates

The process of cloud formation removes gases from the atmosphere as condensation occurs, introducing solid or liquid cloud particles. Optical and infrared spectra of substellar objects thus depends strongly on the presence and distribution of atmospheric condensates. A large variety of materials can condense; L dwarfs like HD 130948B+C tend to have thick clouds composed of rock-forming elements such as iron, magnesium, and silicon which condense in substellar atmospheres as iron metal (Fe), forsterite (Mg_2SiO_4), and enstatite ($MgSiO_3$) (Allard et al., 2001; Marley et al., 2002; Cushing et al., 2008; Visscher et al., 2010). The exact composition and structure of these clouds, however, are often model dependent and remain among one of the greatest uncertainties in the field (Marley and Robinson, 2015). Being able to identify the dominant mineral species can greatly improve interpretations of observed spectra and provide empirical constraints on the substellar condensation sequence. Determining which oxygen-bearing species is more abundant is needed to constrain derived C/O ratios from atmosphere models and test planetary formation mechanisms.

The way clouds are implemented in our PHOENIX models is a straight-forward approach that assumes the atmosphere is in thermochemical equilibrium. Cloud opacity is determined from a heterogeneous mixture of grains at a specified distribution of particle sizes. The resulting cloud is composed of multiple layers of permissible condensate species composed of mostly Fe and Mg-Si grains as expected for L dwarfs with T_{eff} = 1800-1900 K. The approach of equilibrium clouds has been called into question recently due to differing nucleation and sedimentation timescales (Gao et al., 2020). Furthermore, recent atmospheric retrieval results have suggested optically thick clouds composed of iron and corundum particles, or perhaps just iron, were responsible for the spectrum of two L dwarfs (1700-1800 K, log(g)=5.2-5.3) and an unusually red L4.5 dwarf preferred cloud particles of enstatite and quartz at shallow pressures with a deep iron cloud deck (Burningham et al., 2017, 2021).

We explored how varying the type of cloud used in our models impacted spectral morphology by recalculating our best-fit models with several different combinations of condensate species (Table 3.7), including those described above. Model parameters were held constant with stellar metallicity to generate synthetic spectra. Figure 3.10 shows how the spectra of various cloud types compare to our heterogeneous clouds. Overall, the greatest differences in flux are observed in the J-band portion of the spectrum with each new cloud model deviating from the model that includes all condensates. The largest differences in the SED occur for cloud types with grains composed of enstatite, iron/corundum, and enstatite/quartz/iron. These models have the greatest flux in the 0.8-1.3 μm wavelength region and a stronger H-band flux but a reduced K-band flux. Clouds composed of individual forsterite or corundum grains deviate the least from the heterogeneous cloud model in all bands. Figure 3.11 provides temperature-pressure profiles for each cloud type model.

3.4.4 Mole Fractions of H_2O and CO

The resolution of OSIRIS (R $\sim$ 4000) allows us to resolve important spectral features in the atmospheres of HD 130948B and C. The K I doublet becomes a prominent

Table 3.7: Cloud Condensate Type

Condensate	Photosphere [bar]	Cloud Base [bar]	Cloud Top [bar]	Peak Dust [bar]
All Condensates	0.51	0.96	0.04	0.11
Iron	4.75	8.61	0.30	0.60
Enstatite	6.02	10.04	0.27	1.41
Forsterite	0.95	1.67	0.17	0.35
Iron + Corundum	1.36	3.39	0.22	0.58
Quartz	6.09	10.14	0.27	1.43
Corundum	1.42	3.46	0.24	0.62
Enstatite + Quartz + Iron	4.75	8.61	0.30	0.60

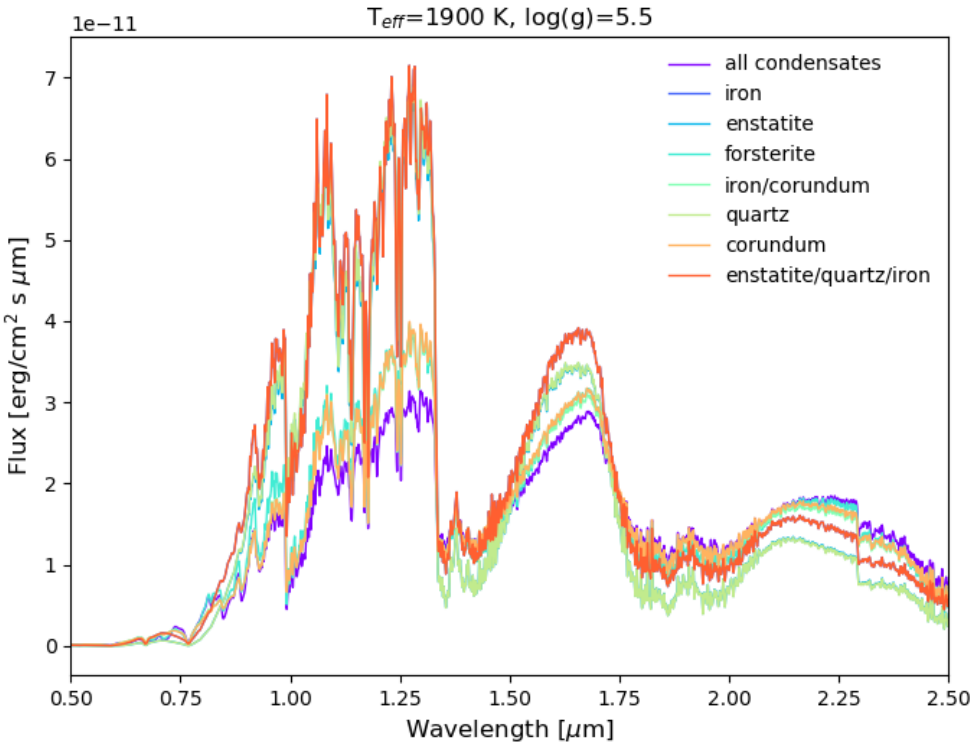

Figure 3.10: Comparison of near-infrared synthetic spectra for various cloud types. Original best-fit model with heterogeneous clouds plotted in purple. All parameters were held constant with P_c=0.50 bar and a_0=0.25 μm.

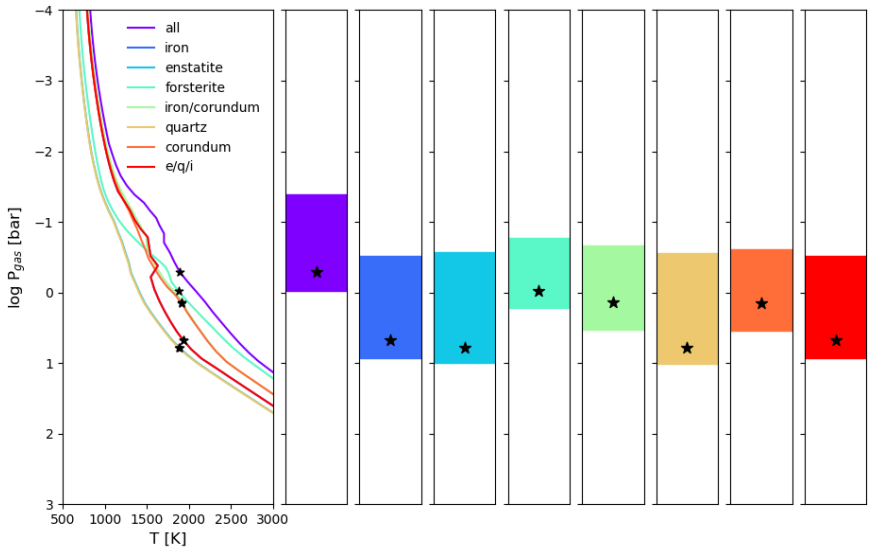

Figure 3.11: Temperature-pressure profiles for each cloud type model. Heterogeneous clouds shown in purple. The cloud base and cloud bottom are shown as individual bars. The photosphere is labeled with a black star.

feature in early-to-mid L dwarfs and decays for later spectral types. These features are clearly visible in J band near 1.24 and 1.25 μm and are deeper for HD 130948B compared to the C component (Figure 3.12). The line depth can show considerable scatter for objects of the same spectral type (Mclean et al., 2007). FeH features reach a peak line depth for L3-L4 spectral types around 1.20 μm (Cushing et al., 2004; Mclean et al., 2000). Updated FeH line lists have improved comparisons between observations and synthetic spectra, but reproducing observed FeH absorption features remains a lingering challenge for atmosphere models (Rice et al., 2010).

Perhaps the most important absorption features are molecules of H_2O and CO in the J and K bands, which can be used to constrain the carbon-to-oxygen (C/O) ratio. The CO line is prominent in the K band at 2.29 μm. We used the best-fit values of effective temperature ($T_{\rm eff}$ = 1900 K), surface gravity (log(g) = 5.5), and cloud properties (P_c= 0.10 bar, a_o= 0.25 μm) from our stellar metallicity grid fitting to derive abundances of H_2O and CO. The above model parameters were fixed

Table 3.8: Mole Fractions

Molecule	Band	Stellar	HD 130948B	HD 130948C
H_2O	J	-3.26	-3.26	-3.04
H_2O	K	-3.26	-3.26	-3.26
CO	K	-3.38	-3.16	-3.16

and used to generate a grid of synthetic spectra with scaled molecular abundances similar to work from Barman et al. (2015) and Wilcomb et al. (2020). The molecular abundances of H_2O and CO were scaled relative to their initial stellar values using uniform logarithmic sampling. The mole fractions can be determined by comparing the synthetic spectra to observations with the continuum removed.

The mole fraction of H_2O was determined first, holding CO constant at the stellar value. Comparisons were first made with the J-band spectrum and repeated for the K band. Next, we held H_2O constant at the stellar value and fit for the mole fraction of CO using the K-band spectrum. This exercise was done for both HD 130948B and HD 130948C. The abundance of CH_4 was held constant at the stellar value throughout this process because significant amounts of CH_4 are not expected to be present in objects with such warm temperatures.

The χ^2 distributions for all H_2O and CO mole fraction comparisons is shown in Figure 3.15. The K band clearly provides a tighter constraint on the abundance of water than the J band. The true minimum implies a slightly higher abundance for CO than the stellar value from K-band spectra for HD 130948B and HD 130948C. Figures 3.12 and 3.13 show the best H_2O abundance models for our objects at J and K band, respectively. At J band HD 130948B was best fit to a stellar abundance and HD 130948C preferred a value greater than the stellar abundance by 1.66. The water abundance at K band was identical to the stellar value for both objects. In Figure 3.14 we show the best-fitting models for the CO abundance in K band. Each object resulted in a fit with stellar abundances.

3.4.5 C/O Ratio

Elemental abundances are an important tracer of formation history in giant planets and brown dwarfs. Brown dwarfs in binary systems are thought to form from gravitational instability, and it is expected each object will inherit the bulk composition from the molecular cloud. The same should be true for a pair of brown dwarfs within the presence of a host star. One way to test this assumption is by constraining the abundances of the dominant carbon and oxygen-bearing molecules and deriving the carbon-to-oxygen (C/O) ratio, which can provide insight into the formation mechanism of substellar objects.

We calculated the C/O ratio for each brown dwarf component using the atmospheric mole fractions (N) determined in Section 3.4.4. The mole fraction of CH_4 is small and negligible because the temperature of our objects are near $\sim$ 1900 K and methane becomes important when $T_{eff} \leq 1100$ K (Zahnle and Marley, 2014). The following equation was used:

$$\frac{C}{O} = \frac{N_{CH_4} + N_{CO}}{N_{H_2O} + N_{CO}}. \tag{3.4}$$

Valenti and Fischer (2005) determined the carbon-to-oxygen ratio of the host star, HD 130948A, was C/O=0.43. The abundances and C/O values we determined in the previous section are provided in Table 3.8 and consistent within 1 σ uncertainties to the stellar value. The C/O ratios derived from our models fit to the H_2O abundance in J band between B and C were not statistically different.

Atmospheric retrieval is another technique to directly determine molecular abundances and C/O ratios for brown dwarfs but unlike our approach differs in that it does not rely on equilibrium chemistry. Some papers have determined abundances and C/O ratios through this method that deviate from the stellar population, resulting in a large spread of C/O values even at solar metallicity (Line et al., 2017). For example, Burningham et al. (2017) found much higher CO abundances than expected in a small sample of L dwarfs and Zalesky et al. (2019) arrived at slightly enhanced metallicities for Y dwarfs that were only broadly consistent with the FGK

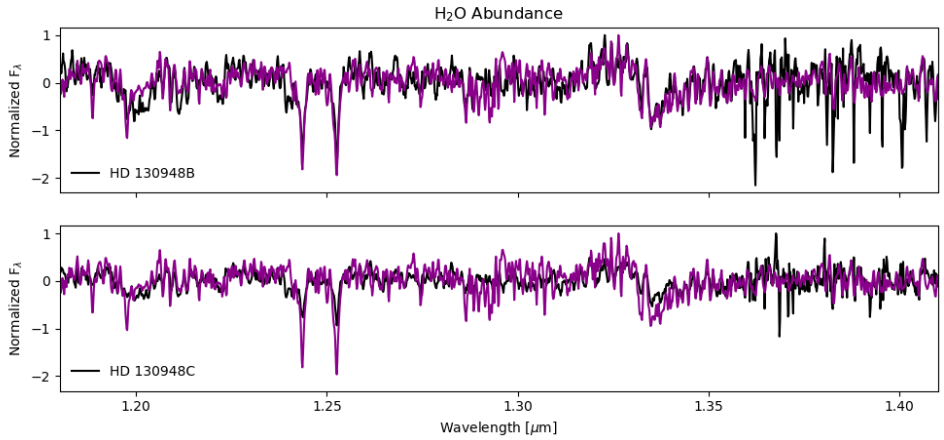

Figure 3.12: Continuum-subtracted J-band spectra for HD 130948B (top) and HD 130948C (bottom) in black compared to best-fitting H_2O abundance models (purple). HD 130948B preferred a stellar value and HD 130948C preferred a slightly larger abundance by a factor of 1.66.

stellar population. Field brown dwarfs often have unknown metallicities and ages, which can make it quite a challenge to constrain abundances. In our case, we measured the abundances of two L4 dwarfs using medium-resolution spectra and compare the results to the host star with known metallicity and do not find any significant differences.

3.5 Conclusion

We obtained resolved moderate-resolution (R $\sim$ 4000) J and K-band spectra of HD 130948B+C, a system of L4+L4 brown dwarf binaries orbiting a solar type star. We modelled the atmospheres of these objects using stellar metallicity and find bulk properties consistent with the Saumon and Marley (2008) evolutionary models and previous work (Dupuy and Liu, 2017; Briesemeister et al., 2019). We were able to resolve spectral features and determine molecular abundances of H_2O and CO in both components. The C/O ratios we derived are similar to the host star's metallicity (C/O=0.43). This is different from some atmospheric retrieval results that find abundances and C/O ratios that deviate from the stellar population

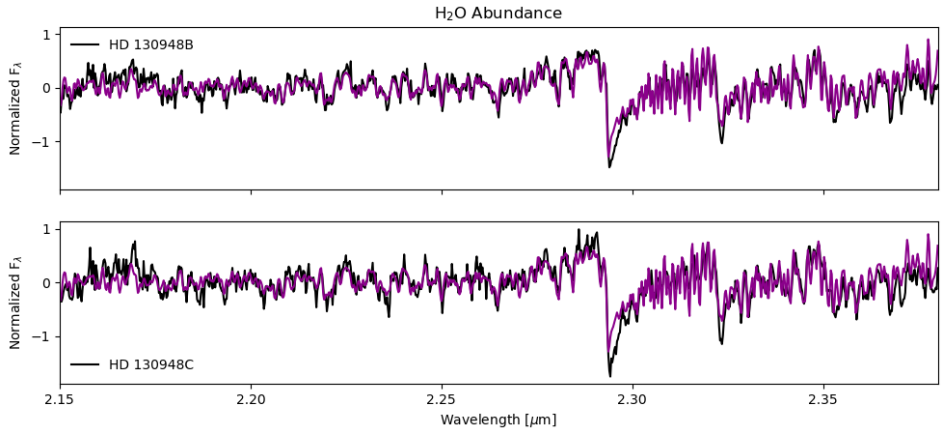

Figure 3.13: Continuum-subtracted K-band spectra for HD 130948B (top) and HD 130948C (bottom) in black compared to best-fitting H_2O abundance models (purple). Both brown dwarfs preferred a water abundance equal to the stellar value.

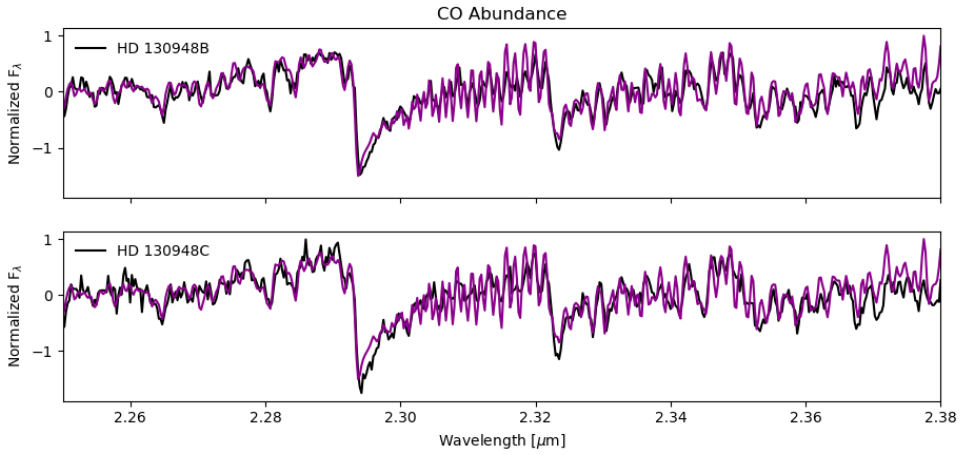

Figure 3.14: Continuum-subtracted K-band spectra for HD 130948B (top) and HD 130948C (bottom) in black compared to best-fitting CO abundance models (purple). Both components preferred an abundance greater than the stellar value by a factor of 1.66.

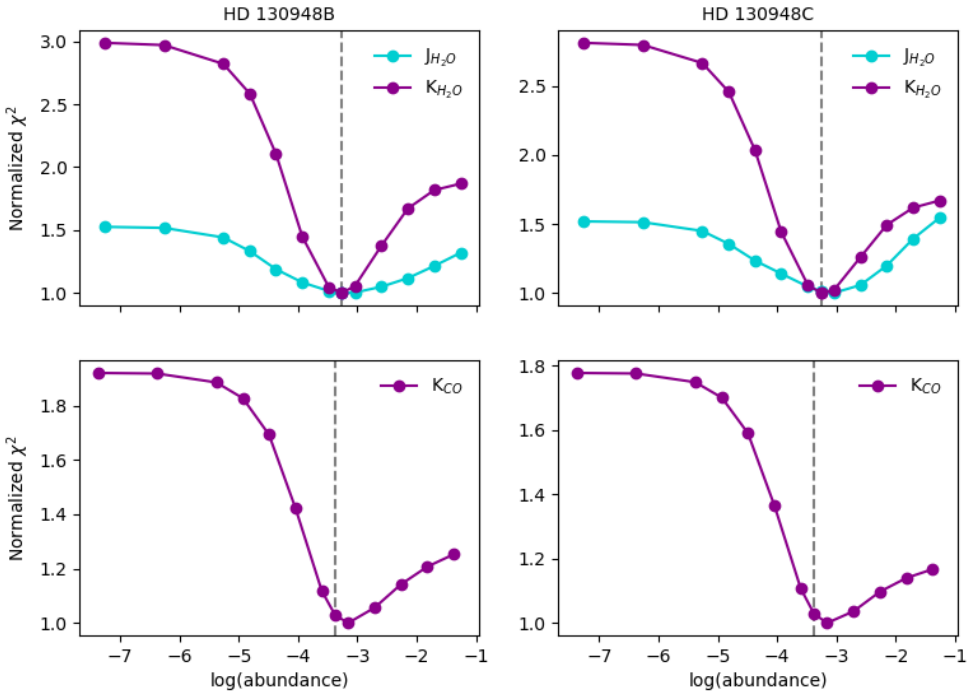

Figure 3.15: Summary of χ^2 distributions for H_2O and CO mole fractions when fitting model spectra. Both J and K bands are shown. The stellar mole fractions are indicated by a vertical dotted line. HD 130948B and HD 130948C prefer abundances very close to the stellar value.

(Line et al., 2017; Burningham et al., 2017; Zalesky et al., 2019). Going forward, comparisons between the results of self-consistent models like those presented here with those of retrievals will be increasingly important to identify where atmosphere and evolutionary models succeed and fail, particular for benchmark systems with measured properties.

Future observations with JWST will provide additional data to help constrain cloud composition and particle sizes for brown dwarfs. Characterizing clouds will be particularly important for L/T dwarfs to separate cloud evolution in the color-magnitude diagram from important secondary influences of gravity and metallicity (Burrows et al., 2001; Knapp et al., 2004).

CHAPTER 4

Finding The Time: Exploring A New Perspective on Students' Perceptions of Cosmological Time and Efforts to Improve Temporal Frameworks in Astronomy

Some of the contents of this chapter were published in Brock et al. (2018)

4.1 Introduction

Understanding time is a cross-disciplinary endeavor uniting the disciplines of astronomy, cosmology, geology, evolutionary biology, and natural history. The ability to comprehend and synthesize temporally related events has been cited as a significant component of scientific and numerical literacy, as well as a critical component of science education standards from kindergarten through the collegiate level. As humans, we are only able to experience and perceive time in short anthropomorphic forms of measurement, such as days or years; however, the perception of cosmic evo-

lutionary time—from the origin of the Universe 13.8 billion years ago to the present day—remains intangible and abstract. Grasping (and accepting) such enormous scales of time as beings who live relatively short lifetimes in comparison is a unique cognitive challenge.

Integrating such macroevolutionary timescales into one's framework is essential in order to learn astronomy. Astronomy can be a challenging discipline to teach and learn—it deals with unimaginably large objects separated by vast, untraveled distances that form and evolve on immense timescales much longer than human lifetimes. Researchers have investigated how students of all ages construct their knowledge of astronomical phenomena for over a century (Piaget, 1929; Piaget and Gabain, 1930; Piaget, 1969). Astronomy education reviews cite students' conceptions of observational topics including objects in the sky, motions within the Earth-Moon-Sun system (e.g., lunar phases, eclipses, day-night cycle), gravity, and the cause of seasons (Bailey and Slater, 2003; Lelliott and Rollnick, 2010). Though these aforementioned topics are among the most commonly taught in introductory astronomy courses (Slater et al., 2001), contemporary work includes research beyond Solar System topics such as students' ideas about stars (Bailey et al., 2009), cosmology (Wallace et al., 2012), planet formation, and exoplanets (Simon et al., 2018). Missing from the literature is how students conceive cosmological and geological time in an astronomical context. Acquiring knowledge of such timescales requires students to develop and apply temporal and spatial reasoning skills, which ultimately shapes a perception of Earth and its place in space and time in the Universe.

Astronomical research continues to demonstrate that Earth is only one of potentially billions of planets in our galaxy alone. Exoplanets, planets in other solar systems, are being discovered at a rapid rate, and the question of whether we are alone in the Universe has finally come into focus. This current era of astronomical research has led to the inclusion of new topics within astronomy. Astrobiology——a relatively new interdisciplinary field of science studying the origin, evolution, and distribution of life in the Universe— has made its way into both high school and

college science classrooms. Implementing astrobiology courses has recently been viewed as an ideal way to engage students and adults in science due to the subject's multidisciplinary nature and appeal (Fergusson et al., 2012; Oliver and Fergusson, 2007; Staley, 2003). Our understanding of the origin, formation, and evolution of the Universe has increased drastically over the past few decades as well, and cosmology has become more widely incorporated into existing astronomy courses (Wallace et al., 2012). Further, more disciplines are including the event that formed our Universe, the big bang, even outside the context of astronomy courses (Delgado, 2013).

Incorporating new astronomical topics into the classroom are not without challenges. Deeper investigations have shown that students often describe the Big Bang in a manner that is not consistent with the modern cosmological model instead describing it as a phenomenon organizing preexisting matter (e.g., subatomic particles, molecules, stars, or planets). Students also conflate the Big Bang with later planetary formation events (Wallace et al., 2012; Plummer et al., 2015; Prather et al., 2002; Simon et al., 2018), which are fundamentally different physical processes.

In this generation in the classroom, students' pre-instructional knowledge upon entering introductory astronomy courses may be beginning to shift to incorporate topics that have recently become more commonplace——astrobiology, cosmology, and exoplanets. Students are now faced with a larger pool of information to comprehend when discussing Earth's place in space and time in the Universe in the astronomy classroom. Instructors are equally challenged, tasked with deciding what content to teach and how to most effectively convey the information. This new framing of astronomy establishes a new trajectory for research in science education. Thus, it is of critical importance to investigate how learners are constructing knowledge of Earth and its relationship to the Universe to develop effective curricula and instruction in astronomy courses at all levels.

4.2 Framing The Research

Before we investigate any prior research findings, it is important to establish the framework of our work. This research is informed by a constructivist learning perspective. Constructivism suggests that learners develop their understanding of the physical world through personal experiences, observations, and the integration of new concepts and information (Bransford, 2004). We briefly highlight three facets of constructivism——mental models, phenomenological primitives, and resource framing——that most appropriately guide our agenda.

Collective factors that shape one's representation and understanding of the physical world have been referred to as "mental models" (Gentner and Stevens, 1983; Vosniadou and Brewer, 1992; Johnson-Laird, 1983). Vosniadou and Brewer (1992) explain mental models are generated from and constrained by students' underlying conceptual structures and are used to provide causal explanations of scientific phenomena. As we look toward our research, we will see students constructing mental models influenced by their underlying assumptions of cosmic events prior to Earth's formation.

Students do not always form coherent representations of Earth nor the events that took place prior to Earth's formation and often use their fragmented scientific knowledge to explain astronomical phenomena. DiSessa (1988) developed phenomenological primitives, or p-prims, as a means to explain how students also rely on more abstract or intuitive knowledge structures. This can be observed when students use the p-prim of "closer means more" to explain Earth's seasons (i.e., the naive concept that it is Earth's distance to the Sun that is the cause of seasons) (Hammer, 1996).

In order for students to consider when Earth formed in relation to the formation of the Universe, they must be able to apply knowledge from multiple disciplines—astronomy, chemistry, physics, and biology, for example—and extrapolate back through cosmological time. Hammer et al. (2004) explored how students apply what they know from one scientific context to another based on an activation of

resources. Hammer's approach, called resource framing, views learning as a state rather than the acquisition of a specific set of scientifically correct ideas. In other words, this approach focuses less about whether students have misconceptions or not and more on how students integrate their knowledge into future learning. The idea of misconceptions are framed in positive light as a step to grasp complex topics and may be able to help frame the ideas of Earth's place in cosmological time, an abstract concept that cannot be physically experienced.

As we look toward our research, we will see the aforementioned facets of constructivist learning being used. Our new research agenda incorporates an approach to astronomy education from both a philosophical and literal perspective of Earth's place in time and space in the Universe. When we talk about Earth's place in time, we are referring to cosmic events that occurred before and after Earth's formation. Place here refers to Earth's physical location in the Universe (i.e., Earth orbits the Sun in the Solar System, which is part of the Milky Way Galaxy, Local Group, and Local Supercluster) but also the significance of Earth and humanity in this new era of exoplanet detection and discovery. Thus, the work presented here is guided by the following research questions:

1. What are students' ideas when asked questions related to Earth's place in space and time?

2. What are students' conceptions about the formation of the Universe and its relationship to the formation of Earth and the Solar System?

In order to explore our research questions, we must first place it in the context of prior work. Results from past studies informed the direction of our work, which ultimately sets a new course for investigating students' ideas related to how Earth fits into the scale of cosmological time. After a literature review, I will discuss the methodology and results from our study. Finally, I will wrap up with a discussion and recommendations for future work.

4.3 Unpacking Prior Research About Earth, Space, and Time

Studies regarding temporal knowledge of learners within Earth and space sciences span multiple research areas including cognitive science, psychology, and science education. This section will first highlight the motivation for our research and summarize past work relevant to our research agenda. We first consider work that illustrates how learners in general think about the ideas of time and Earth without applying them to the idea of the Universe. We then consider research which examines learners' ideas related to how time and Earth are connected to the larger concept of the Universe. For clarity, we use the word time or temporal to refer to the essence of time, or more concretely, the existence of both cosmological and geological timescales. The use of the word space or spatial describes both physical location and an awareness of Earth from a space-based frame of reference.

4.3.1 Motivation For Research: The Missing Link

At the heart of appreciating Earth's relationship with the Universe is the concept of time. All physical science disciplines require their learners to possess some grasp of time—be it the time required for an event to happen, or for change to occur (Lee et al., 2011). Time is inherent in order to grasp Darwin's theory of evolution, piece together Earth's geological history, approach the concept of climate change, predict the eventual death of our Sun, or observe a chemical reaction. Time is a central and fundamental component of describing how a system functions, but its importance stretches far beyond science. Cervato and Frodeman (2012) highlight the cultural, economic, religious, and political relevance of time in addressing the looming environmental crises that require a perspective and appreciation of immense timescales. Temporal knowledge has been cited as a significant component of scientific literacy (Catley and Novick, 2009; Dodick and Orion, 2003b) and listed in science education standards from K-12 (American Association for the Advancement of Science

(AAAS), 1993; Schweingruber et al., 2007; States, 2013) through the collegiate level (College Board, 2009); yet, it is often overlooked in the classroom, or expected to become obvious within the context of the scientific content being taught.

Time as a teaching and learning topic has continued to elude students and instructors. Available literature demonstrates students' conceptual difficulties with time at the elementary (Ault, 1982; Trend, 1998), high school (Dodick, 2007; Trend, 2001b), and college levels (Delaughter and Stein, 1998; Libarkin et al., 2007, 2005; Libarkin and Anderson, 2005; Schoon, 1992). Students' knowledge of geological time has been widely explored and equally so have children's perspectives of Earth (Vosniadou and Brewer, 1992, 1994). Students commonly struggle with absolute and/or relative timescales and distinguishing between orders of magnitude for both large and small numbers (e.g., millions vs. billions).

The missing link in the research is studies exploring students' understanding of time in an astronomical context, which are lacking, as well as investigations on more interdisciplinary topics regarding Earth's place in time and space in the Universe (Lelliott and Rollnick, 2010). Investigations on students' perceptions of Earth's place in time and space in the Universe may help to break down disciplinary borders within Earth and space sciences through efforts that consider how both Earth and humanity fit into the cosmic landscape. Students and the general public must develop causal, chronological frameworks that more closely mirror scientific understandings of the relationship between cosmological and geological time——as well as knowledge of Earth's place in the Universe——to become both quantitative and scientifically literate citizens able to deal with global issues of the future.

4.3.2 Earth as an Astronomical Body

All people encounter Earth and space science phenomena prior to any formal instruction—observing the Sun, Moon, and stars; experiencing weather, the changing seasons. This leads to initial ideas and beliefs of the larger picture of how Earth fits into the cosmic landscape. Time is a related but rather abstract concept, espe-

cially across large timescales central to the disciplines of Earth and space sciences. While scientists' knowledge of Earth's age and the age of the Universe was first developing, some of the earliest studies by psychologists and cognitive scientists investigated the acquisition of spatially related knowledge in astronomy (Piaget, 1929; Piaget and Gabain, 1930). Piaget's work suggests young children construct explanations that resemble scientific theories based on studies that use open-ended questions. Children's perspectives of Earth as both a physical and astronomical object were explored by Nussbaum and Novak (1976); Nussbaum (1979). They found children have many different conceptions of Earth as a cosmic body that often begin with the concept of a flat Earth and progress to more science-like explanations with variations on a spherical Earth. These early studies probing student-constructed knowledge of astronomy helped to shape the constructivist learning movement (Bransford, 2004), leading conceptual change researchers to form theoretical approaches to explain how humans learn. Two of these approaches, colloquially known as "knowledge as theory" and "knowledge as elements" or "pieces," explain how learners might progress from naive to scientific understandings of phenomena (Johnson-Laird, 1983; DiSessa, 1988; Özdemir and Clark, 2007; Gentner, 2001).

Notable work was conducted by Nussbaum and Novak (1976) and Vosniadou and Brewer (1994) who argued students construct mental models, or theory-like structures, to explain scientific phenomena. Individual mental models spanned a spectrum from scientifically accurate to inaccurate. This approach has been used to examine children's conceptions of Earth's shape, the day-night cycle, and gravity. The studies found that young children's initial perceptions of Earth, its place in the Solar System, and its position in space closely resembled that of Ancient Greek's geocentric perspectives. For example, elementary school-aged children were more likely to conceptualize a flat, un-moving Earth reminiscent of a pre-Aristotelian view (Vosniadou and Brewer, 1992). Children aged 10 to 11 years were more likely to acknowledge Earth is both spherical and rotating, suggesting that some scientific explanations of astronomical phenomena had been acquired by this age (Vosniadou and Brewer, 1992). A more detailed discussion of work on Earth's shape and related

topics——including articles not discussed here——can be found in the review paper by Bailey and Slater (2003) and is also summarized in more recent work by Jelinek (2021).

Since the aforementioned review was published, additional work has expanded upon the efforts of Vosniadou and colleagues. Straatemeier et al. (2008) investigated how young children in Netherlands constructed mental models of Earth utilizing mental models from Vosniadou and Brewer (1992) and found conflicting results. In their work, Straatemeier and colleagues evaluated a larger sample size of children and concluded children's presuppositions are not strong enough to suggest children actually do construct mental models, rather the children's knowledge is more fragmented and inconsistent. A longitudinal study by Hannust and Kikas (2010) used open-ended questions and drawing tasks similar to Vosniadou and Brewer to examine two and three year old children's knowledge of Earth over four years. Hannust and Kikas (2010) concluded, much like Straatemeier et al. (2008), that there were few indications to suggest children did form mental models of Earth at this age. More recent work from Jelinek (2021) with Polish children aged 5-10 found consistent results with Vosniadou but highlighted that cultural influences could pose a significant difference. In summary, collective findings suggest some novice learners may draw from mental models while others may only have fragmented ideas of a phenomenon. When we examine how learners might perceive Earth's place in time and space in the Universe, it is important to consider these aforementioned studies. However, it is important to note the population in many of these studies is younger children from different countries and cannot be generalized to our population.

Other work has explored spatial thinking through students' views of Earth-based and space-based frames of reference. Plummer and colleagues (Plummer, 2014; Plummer et al., 2016; Plummer, 2011) have investigated children's perceptions of the daily apparent motion of the Sun, Moon, and stars. Plummer (2011) found that children often explained that the Sun moved across the sky rather than Earth rotating, which was also similar to studies by Vosniadou and colleagues. However, it was observed that even children that could explain the Sun's apparent motion correctly

often could not apply the knowledge of Earth's rotation to account for the motion of the stars. The researchers concluded, "knowing the scientific description of both an Earth-based phenomenon and how objects move in space does not necessarily lead to an understanding why motion in one frame of reference causes the appearance of motion in the other" (Plummer, 2011).

4.3.3 Conceptualizing Time and Spatial Reasoning

It is critical for the work we are pursuing to consider past research in psychology and cognitive science on how time is viewed metaphorically. Chrysikou and Ramey (2006)'s work on language related to time provides some interesting results that may be relevant to our research on time in the context of science. Participants' responses to ambiguous questions related to the rescheduling of events were evaluated, and the researchers observed biases in responses based on the attractiveness of the event. Chrysikou and Ramey argued time perception is complicated by the interaction of many variables and suggest subjective factors can control a person's perception of time. Kurby and Zacks (2011) explain how people without intentionally meaning to hierarchically break down events to build mental representations and remember what happened, such as separating the act of making a sandwich into discrete events (e.g., collecting ingredients, assembling the sandwich, and clean-up). Therefore, in order to understand the hierarchical structure of an event, one must be able to separate the event into smaller, more meaningful segments (Kurby and Zacks, 2011).

Researchers in psychology have also demonstrated a key link in the conceptual understanding of time through its relationship with spatial thinking. Levin (1992) found that preschool children shape their sense of time by temporally sequencing familiar events into the space of their day, such as snack time or recess time. Cognitive studies show the abstract perception of time is acquired through metaphorical mappings in language from the domain of space; these conceptualizations of time often vary for different cultures and languages. In English, time is commonly perceived through ego-moving or time-moving metaphors. Gentner (2001) explains the

ego-moving metaphor as a mapping where the observer progresses along a timeline toward the future. Most English speakers tend to conceptualize ego-moving metaphors, by placing time on a horizontal axis and expressing they are looking ahead to the future or back into the past (Boroditsky, 2000). The time-moving metaphor is a projection where events move from the future to the past via a river or conveyor belt (Gentner, 2001). Time-moving metaphors focus on placing events on a timeline with regards to when the event occurred or will occur rather than how the event occurred in relation to an individual's location.

Work on time perception shows a link between temporal and spatial association related to the concepts of scale and environment. Grondin (2010) found recalling past events requires location-based associations to determine how recent an event is, as well as a distance-based association to determine how much time has elapsed between a past and present event. Radvansky and Zacks (2011) further explain how spatio-temporal location is a major organizing factor in memory for events and serves as the basis for the representation of a real-world event. For example, these "event models" can be dependent on a particular perspective in which the information was learned such as experiencing a space from a bird's eye view or a first person perspective (Radvansky and Zacks, 2011). Hegarty and Waller (2004) found a correlation with being in a memorized environment and people's self-reported sense of direction. In other words, the more familiar a person is with their environment, the more likely a person is able to succeed at large-scale spatial cognition tasks (e.g., planning or navigating a route), which requires the individual to imagine themselves in a particular place or orientation and determine the direction of travel from one location to another in the given environment. It is clear how this can be problematic when asking students to consider a timeline prior to Earth's existence or a time after Earth has formed but from a location requiring a space-based perspective as these perspectives in time and space cannot be experienced directly. Surprisingly, Hegarty and Waller (2004)'s work showed that successful planning or navigation could occur whether the situation was viewed or imagined, which is promising for our agenda related to Earth's place in time or space.

Research on spatial thinking in the science education community may provide a meaningful pathway toward incorporating more research and instruction on spatio-temporal location. Spatial reasoning skills have previously predicted achievement in science, technology, engineering, and mathematics (STEM) fields; however, these skills seem to be infrequently taught or opportunities to practice honing these skills in the classroom are lacking (Uttal et al., 2012). The likelihood that children and college-aged students will construct scientifically accurate astronomical explanations related to Earth's location in time and space requires the spatial skills of mental rotation, spatial perception, and spatial visualization (Kikas, 2006; Black, 2005; Heyer et al., 2013; Wilhelm, 2003); in other words, students must possess or learn the ability to extrapolate in three dimensions. Black (2005) found a possible relationship between poor spatial abilities in college students——most specifically mental rotation—— and Earth science misconceptions. Similarly, Heyer et al. (2013) measured spatial thinking abilities in undergraduate non-science majors and found results which suggested the relationship between spatial reasoning and astronomical reasoning ability can explain roughly 25% of variation in student achievement. Thus, fostering spatial reasoning skills at all grade levels may help to improve conceptual difficulties related to Earth's location in time and space.

Eriksson et al. (2014) suggest the ability to perceive the Universe in multiple dimensions calls for more than is provided in traditional instruction and often requires the use of hands-on experiences, computer simulations, and other virtual tools to enhance astronomical learning. In their work, Eriksson et al. (2014) explored students' abilities to discern the multidimensional structure of the Universe and found this ability was relatively rare for undergraduate students. Visual representations of the Universe in new and different ways has been particularly promising to help students grasp the 3D structure and hierarchy of the Universe. For example, Schneps et al. (2014) provided high school students with virtual astronomy simulations on iPads to see if immersive, hands-on technology could help students to learn spatial scales. The students engaged in brief interactions with 3D simulations with a pinch-to-zoom interface, and these simulations helped students to develop spatial

skills with minimal instructional support. These studies highlight how improving knowledge and awareness on relative sizes and distances in the Universe are limited when only using two dimensions.

It should be cautioned that technology alone does not rectify students' difficulties with spatial reasoning. Eriksson et al. (2014) warn that without providing an opportunity to experience motions of parallax, for example, students may not be successful when attempting to extrapolate from 2D to 3D representations of the Universe, even with the use of computer simulations. Schneps et al. (2014) reported that unstructured 3D simulations did not help students overcome their naive ideas about the seasons, and the presence of misconceptions would require scaffolding specifically designed to address the implications of such naive ideas. Mental rotation, such as a spatial transformation of an object and the ability to take in a scene from a different viewpoint (i.e., perspective taking), are simultaneously required in astronomy courses. Incorporating new technologies into the astronomy classroom may be helpful to aid students in developing spatial awareness but must be accompanied by effective teaching strategies to aid students in constructing accurate scientific representations of the Universe.

4.3.4 Geological, Biological, and Cosmological Time

In this section we discuss research into learners' conceptions of geological and biological time. It should first be noted that there is some disparity regarding the definition of the term geological time within the literature. We use geological time to refer to the time period from Earth's formation to the present day, encompassing all of Earth's ∼4.5 billion year geological and biological history. We use the term cosmological time to refer to the much larger span of time stretching back approximately 13.8 billion years (to the age of the known Universe) to present day. Some researchers use geological time interchangeably with the term deep time, though the beginning point in time varies from either the origin of the Universe or the formation of Earth. Clearly, a rather vast span of time exists between these two origin

events. This nomenclature may not have implications for researchers who focus on a starting point and proceed to investigate students' knowledge of time restricted to post-Earth formation and related events; however, it is important to clarify terminology for future studies attempting to incorporate students' understanding of cosmological time into the existing literature. For clarity, we refrain from using the term deep time but feel it most appropriately encompasses both cosmological and geological timescales.

Studies exploring geological time have been both qualitative and quantitative, asking subjects to respond to open-ended questions, recall certain events or dates, select an appropriate age range, or organize events or dates in chronological order. Studies of this nature help to gather information regarding learners' knowledge of absolute ages and their relative relationships within a time frame. A great deal of research on geological time identifies that learners struggle to provide the age of Earth as well as place Earth events from formation to present day in appropriate timescales within a timeline.

A study from Trend (2001b) determined in-service teachers of 7 to 11 year old children developed their own individual chronological order of key events and dates, which greatly differed from a scientific acceptance. Another study from Trend (2001a) found similar results for children aged 10 to 11 years old. Trend's work shows these aforementioned groups often favor qualitative terms to describe time such as ancient, less ancient, or recent (Trend, 1998, 2001b,a). When asked about Earth's age, Marques and Thompson (1997) found younger students 10-11 years old typically provided estimates of hundreds or thousands of years, whereas older students 14-15 years old typically responded with millions, billions, or sometimes even trillions.

Studies with college-aged students show similar difficulties reporting absolute ages and organizing events in time. Libarkin and Anderson (2005) analyzed 265 questionnaires and conducted 105 interviews with college students enrolled in introductory science courses and concluded that fewer than 50% of all students in the study believed that Earth was 4–5 billion years old and, at some institutions, this

was less than 10%. Another study from Libarkin et al. (2007) of college students across 43 institutions found that the majority of students could not create time-lines of geological events that were ordered correctly, nor did they have scientifically accurate time-spacings for events.

Students' conceptions of how time functions in an evolutionary biology context is related to geological time, and knowledge of these individual topics has been shown to impact each other. If one does not believe or understand that Earth is billions of years old, the same disparity could be applied to the subsequent age of life and its evolution on Earth. Students' knowledge of the first appearance of various life forms on Earth (e.g., dinosaurs) has been investigated at different grade levels. Marques and Thompson (1997) found students in secondary school often perceived life arising concurrently with the formation of Earth. In a study of 149 college students in an introductory Earth science course, Delaughter and Stein (1998) found approximately 25% of students reported dinosaurs died out long before life even began on Earth. Another study by Catley and Novick (2009) evaluated college students' knowledge of seven key macroevolutionary events related to life on Earth (e.g., first appearance of prokaryotic life, eukaryotic life, dinosaurs, hominid lineage). Results showed that students provided extreme variability in their estimates of ages with a tendency to provide dates closer to the present and struggled to differentiate between orders of magnitudes, such as millions or billions. Another interesting finding from this study was students with a greater biology background, even those who had taken a prior course on evolution, did not fare better with ordering and appropriately spacing biological events in time. Furthermore, related work from Cotner et al. (2010) demonstrated that college students' beliefs of the age of Earth also impacted their ability to accept evolution. Collective findings reveal a disconnect between the relative relationships of the age of Earth, the time and characteristics of life's first appearance on Earth, and the subsequent evolution of life on Earth (Catley and Novick, 2009; Delaughter and Stein, 1998; Libarkin and Anderson, 2005; Marques and Thompson, 1997).

Dodick and Orion (Dodick and Orion, 2003b; Dodick, 2007; Dodick and Orion,

2003a,c, 2006) have dedicated significant research efforts exploring how students' perceive geological time cognitively. Dodick and Orion (2003b) and Dodick and Orion (2003a) examined how 343 Israeli middle and high school students reconstructed geological transformations over time. They focused on the strategies students in grades 7-9 and 9-12 used when faced with temporal problems and what factors might interfere with the process, notably students' prior geological knowledge and spatial visualization. They found students have the most success reconstructing geological phenomena when they are able to use diachronic thinking, in other words, the ability to situate an event or physical object within a temporal dimension and grasp how the event/object changes throughout time (Montangero, 1985).

The quantitative aspect of large numbers required to understand geological events can be problematic and cause further difficulties. Work by (Cheek, 2012) and Cheek (2013) with 35 students aged 13-24 identified how large numbers can place limits on a student's ability to understand associated geological processes. Landy et al. (2013) investigated how difficulty with large numbers interferes with an understanding of concepts that require their use. Their work shows that people tend to treat thousands, millions, billions, and trillions as a uniformly spaced list in magnitude on a number line. The outcome is that any associated scientific events that occur on timescales using such numbers become misrepresented. Lee et al. (2011) also found that students tended to overestimate durations of time for large temporal magnitude categories; however, students also tended to overestimate durations of time smaller than one millisecond. In related work, Tretter et al. (2006) explored students' conceptions of spatial scales and noticed students had difficulty providing accurate sizes of objects at the microscopic scale. This research suggests both temporal and spatial magnitude scales outside of the human experience range—both large and small—can pose challenges for learners.

The formation of Earth and its subsequent evolution is arguably at the transition between astronomical and geological timescales. A handful of geologically-focused studies included cosmological events. Work from Trend (2001b) asked 51 in-service teachers of 7-11 year old children to rank events in time and included the formation

of Earth's Moon, Earth, the formation of the Sun, and the formation of the Universe (e.g., the Big Bang). Results showed that the majority of teachers did not see the formation of the Sun and the Big Bang as separate events in time, with 82% of teachers reporting the Sun's formation as the first event rather than the Big Bang. Delgado (2013) evaluated 66 undergraduate students' abilities to estimate events in time related to major cosmological, geological, and historical events. Delgado was able to show that college-aged students could successfully provide the approximate time estimates for the Big Bang and the age of Earth.

Related work regarding the Big Bang and our Universe, though not directly focused on cosmological time, has shown that students possess a variety of nonscientific ideas about the origin of the Universe that likely influence students' conceptions of time or vice versa. In a study exploring nearly 1000 students' ideas about the Big Bang from middle school through college, Prather et al. (2002) found that 70% of students responded that matter existed prior to the Big Bang. In this study as well as others (Bailey and Slater, 2003; Wallace et al., 2012; Plummer et al., 2015; Simon et al., 2018), it is commonly observed that students describe the Big Bang as a process that formed Earth or our Solar System in a variety of different ways. We now move from reviewing the literature to talking about our own research.

4.4 Research Background and Methods

4.4.1 Pilot Studies

The work presented in this dissertation chapter is informed from two pilot studies. The first pilot study is a museum exhibit and accompanying curriculum that focused on connecting spatial and temporal scales as part of my master's thesis (Brock, 2015). The exhibition centered on a "walking timeline" of Earth's biological and geological history in which visitors would view Earth from a space-based perspective at different distances, and thus, points in time throughout the history of the Universe. The curriculum component was developed by asking undergraduate stu-

dents astronomy questions related to time, distance, and scale. Students were asked to respond to a mix of multiple choice and open-ended questions approximately once per week throughout the semester. All data were collected anonymously and without any personal identifiers. The students were enrolled in a three credit First Year Learning Initiative (FLYI) course at Northern Arizona University in Flagstaff, Arizona. FYLI courses are typically taken by first-year college students with a variety of majors. Enrollment at the start of the course was 23 students, which fluctuated at times due to absences. From analysis of responses to the multiple-choice and open-ended questions, we learned that students struggled to explain how the Solar System formed and were unsure of the age of the Universe.

The second pilot study was conducted at The University of Arizona, a public university located in Tucson, Arizona. A total of 52 undergraduate students enrolled in an eight-week preceptor workshop responded to the two questions provided below. In general preceptors are undergraduate teaching assistants that are selected to help out in large enrollment introductory courses after previously performing well in the course. Students were not graded on their responses to the questions and all data were collected anonymously. From prior research, we learned it was important not to use the term Big Bang when inquiring about the origin or formation of the Universe as it may bias student responses. These questions were developed with distinctly different content focus to ensure that we would elicit students' ideas about 'how' the Solar System and Earth formed—independently from their thinking about 'when' Earth formed—relative to the formation of the Universe. Preceptors were asked to respond to the following open-ended questions:

1. Describe how you think the Solar System, including Earth, formed.

2. Do you think the Earth formed before, during, or after the Universe formed? Explain your reasoning.

The responses from students to question two often involved convoluted and contradictory information. Students seemed to struggle to unpack their ideas in a coherent manner. This led us to design our final research questions in a set that separated

"before, during, and after the Universe formed" by focusing their attention on what needed to exist and what events needed to happen before Earth formed. These results informed the next phase of our research that constitutes the bulk portion of the dissertation and is described in the next section.

4.4.2 Question Development and Participants

The overarching goal of this research was to inform our research questions:

1. What are students' ideas when asked questions related to Earth's place in space and time?

2. What are students' conceptions about the formation of the Universe and its relationship to the formation of Earth and the Solar System?

We developed questions that gave learners the opportunity to share their ideas about when Earth formed, what existed before Earth formed, and how Earth relates to other planets (exoplanets) in the Universe. The four questions developed were:

1. When do you think the Earth formed in relation to the formation of the Universe?

2. Which events had to occur before the Earth formed?

3. Which materials had to exist before the Earth formed?

4. Did all planets in the Universe form at the same time as Earth? Explain why or why not.

The questions were issued to a total of 170 students enrolled at The University of Arizona. All participants in the study were undergraduate students enrolled in an introductory astronomy course. The questions were administered to students prior to instruction on these topics. Students enrolled in these courses are typically non-science majors fulfilling their general education requirements. Students were told they were not being graded on their responses and were encouraged to provide

thoughtful responses when answering questions even if they felt they did not have a correct or robust idea of the topic. Any personal identifiers were removed prior to analysis of the responses. Students were asked to respond to one of the four questions above rather than all four questions for the sake of class time and to help ensure students would respond as thorough as possible. The survey questions were distributed roughly evenly among all participants to ensure we got the same sample size of responses for each question.

4.4.3 Data Analysis

Student-supplied responses to all four questions were analyzed using grounded theory (Glaser and Strauss, 1967). Although the questions touch on similar concepts, all four questions were analyzed separately from each other. Each student response was read and common themes and ideas were recorded. This progressed in an iterative fashion assigning each theme a specific code until no new codes emerged. Multiple themes, or codes, could result from a single student response and were arranged into main and sub-codes for clarity if needed. Another education researcher conducted an independent check of the data to ensure its validity before progressing to the next step. A summary and discussion of the responses are broken down by question in the next section.

4.5 Results

4.5.1 Question 1: When do you think the Earth formed in relation to the formation of the Universe?

A scientifically accurate response to the question of when Earth formed in relation to the formation of the Universe would include the Earth forming billions of years after the Universe forms in two unrelated (and different) physical processes. An ideal response would include the absolute age of the Universe ($\sim$ 14 billion years)

and/or the age of the Earth ($\sim$ 4.5 billion years). There were 44 students who responded to the question. Of these students, three did not address when Earth formed and instead described a formation mechanism. The remaining 41 students did provide some type of description of time. Students' responses were analyzed and coded to characterize if they described Earth as forming before, during, or after the Universe formed. A sub-category regarding the duration of time was incorporated to summarize responses that stated Earth formed after the Universe formed in more detail. The results are summarized in Table 4.1.

Two students were able to answer this question with a scientific response. The first student stated that the Universe was 14.5 billion years old, Earth was 4 billion years old, and Earth formed 10.5 billion years after the universe. Although this student slightly over and underestimated the ages respectively, there was a clear awareness of the span of time between the two events. The second student provided the correct age of the Earth and stated the Big Bang happened billions of years before this. Providing absolute timeframes in response to this question was extremely rare; only three students did so—the two described above and one other student who provided a completely incorrect number.

Many students (25%, n=11) believed that the Earth formed during the formation of the Universe. Although students do not always provide numerically accurate responses of the timescales involved, they do appear to be clear on a more conceptual grasp of the subject. The majority (66%, n=29) of students described the Earth forming after the Universe formed. It was clear that some students had conceptual difficulties with the time between these two formation events, often conflating when the Earth formed with a description of how the Earth formed. Of the 29 students who described the Earth forming after the Universe, 28% of responses included a vague description of time such as "a long time after" or "much later". When students did describe an order of magnitude estimate, the most common response was millions, which was observed in 25% of the responses.

Within the description of a formation mechanism, several students described Earth forming at the same time of the Universe or shortly after. For example, one

Table 4.1: Student responses to the question *When do you think the Earth formed in relation to the formation of the Universe?*

Response	Number
Before Universe formed	1
During formation of Universe	11
After Universe formed	29
years	2
millions	7
millions to billions	3
billions	4
vague description	8
other	5
Did not address time	3
Total	**N=44**

student stated that Earth formed "toward the end of the formation of the Universe" but did not specify a timeframe. It appears that at least some of the students answering this survey question are unsure of how long the formation of the Universe lasted and if Earth's formation is or is not related to this. We also frequently observed students conflating planetary formation processes with the process of the Big Bang in their responses to this question. Some students chose not to include descriptions of time in their responses, avoiding it in favor of describing a formation mechanism. It should also be noted that the student with the most scientifically accurate response to this question did not discuss a formation mechanism whatsoever.

4.5.2 Question 2: Which events had to occur before the Earth formed?

A scientifically accurate response to the question of which events had to occur before the Earth formed could include a variety of events such as the formation of the Universe or the Big Bang, the first stars, the first galaxies, the formation of the Sun, or even the formation of other planetary systems. Out of 40 students who responded to this question, one student's response stood out and is the most in-line

with a scientific response. In this response, the student specifically mentioned the fact that the Universe needed to expand, cool, and stars needed to form and is much more advanced than the other responses to this question. The student stated:

> Big bang, Universe expanded and cooled, stars formed from gas, nuclear fusion created new elements, finally after billions of years tiny pieces of matter from exploded stars collected and snowballed into planets. Earth was one of those planets.

Responses from the remainder of the students were not this complete or coherent. It was more common for a student to describe the formation of the Universe and then jump to Earth's formation, leaving out several important events in between. However, students were often capable of incorporating at least one component of a scientifically accurate response even if their overall response was incoherent. Student responses to this question provide interesting insight into how undergraduate students think about astronomical events that occur prior to Earth's formation. Future questions will likely need to be more explicit or ask students to order events to gauge a better understanding. A summary of all responses to this question is provided in Table 4.2 in more detail.

The two most commonly cited events were the formation of the Sun and the Big Bang. Several students (38%) cited that the Sun had to form first, and over half of the responses (60%) explicitly mentioned the Big Bang as an event that occurred previously. Fewer responses (18%) mentioned that the Universe formed first, but these did not always explicitly name the Big Bang. This suggests that many students are familiar with some type of event in which the Universe formed. However, of the students who mentioned the Big Bang (n=24), 25% described Earth forming from this event. This was similarly observed in the first survey question. Furthermore, students who provided the Big Bang as an event did not always explain it correctly. It was commonly described as a mechanism to form planets, which is consistent with other literature (Simon et al., 2018). Other responses to this question provided a description of some type of event or process rather than explicitly naming one. For

Table 4.2: Student responses to the question *Which events had to occur before the Earth formed?*

Response	Number
Earth has always existed	10
Universe formed first	7
Mentioned Big Bang	24
Earth formed during Big Bang	6
Sun forms first	15
Description of materials	
macro	17
micro	9
Description of processes	
collisions	12
explosion	9
gravity	5
orbits	4
religious	4
expansion	2
magnetic	2
Total	**N=40**

example, many students described explosions, collisions, or the inception of gravity.

Although the question specifically asked for an event that occurred before Earth formed to be named, approximately 25% of students described an event or process that required a Earth to already exist. These Earth-centric descriptions of events included scientifically inaccurate descriptions of Earth being formed. These responses were generally religious in nature or described Earth undergoing an interaction of some sort in a preformed state.

4.5.3 Question 3: Which materials had to exist before the Earth formed?

A scientifically accurate response to the question of which materials had to exist before Earth formed would include abundant elements in the Universe such as hydrogen, helium, carbon, oxygen, nitrogen. Ideally we would like students to be able

to expand on this further and discuss the creation of heavy elements from stars (e.g., iron) as one of the key ingredients required to form a rocky planet like Earth. When analyzing these responses, students were less likely to describe a formation mechanism compared to the previous two survey questions. The responses to this question were helpful in uncovering what students' understood regarding materials within the Universe. A total of 43 students responded to this question and a summary of responses is provided in Table 4.3.

The most common response (33%) provided was the element hydrogen. Surprisingly, helium was mentioned far less often with only 7% of the responses including this element, whereas more students answered carbon (19%) or nitrogen (12%). Many students (23%) provided oxygen as an element that existed before Earth. Some students mentioned water (19%), carbon dioxide (7%), or ozone (5%). Discussion of heavy elements was only observed in 9% of the responses–three students specifically mentioned iron whereas one student said "heavy elements".

Some students included formation mechanisms in their descriptions, with 12% of students discussing the Big Bang or a type of explosion and 19% of students talking about gravity or some kind of interaction of material. It is unclear if this is because students were unsure what is considered a material or if they see gravity as a type of material. Many student responses discussed what we classified as micromaterial. For example, 23% of responses discussed matter at the atomic level, while others (21%) said dust or provided vague descriptions of 'particles'. Other responses included much larger materials, which were referred to as macromaterials such as responses that mentioned the Sun (21%), stars or galaxies (28%), asteroids/planets/moons (14%), or vague descriptions of rocky materials (21%).

A handful of students (16%) said that organic materials like dirt or life existed before Earth formed. It is unclear from the responses if students mean the ingredients for life existed or if they specifically mean life evolved before Earth was formed. It would be worthwhile in the future to tease this out more to get a better idea of what students are thinking.

Table 4.3: Student responses to the question *Which materials had to exist before the Earth formed?*

Response	Number
Elements	
hydrogen	14
helium	3
carbon	8
nitrogen	5
oxygen	10
sulfur/phosphorus	1
"heavy elements“	1
iron	3
Molecules	
H_2O	8
CO_2	3
O_3	2
Micro materials	
matter/atoms	10
dust/particles	9
Macro materials	
rocky materials	9
organic (e.g., dirt, life)	7
asteroids/planets/moons	6
Sun	9
stars	6
galaxies	6
Formation Mechanisms	
Big Bang/explosion	5
Gravity/interactions	8
Total	**43**

Table 4.4: Student responses to the question *Did all planets in the Universe form at the same time as Earth? Explain why or why not.*

Response	Number
No	31
Yes	12
Total	**43**

4.5.4 Question 4: Did all planets in the Universe form at the same time as Earth? Explain why or why not.

The final survey question asks students to consider the age of the Universe, the age of Earth and the Solar System, as well as the ages of exoplanetary systems. The correct response to this question is 'no' and students could explain why with a few different approaches. In order to answer this question correctly, students have to recognize that the formation of the Universe and planet formation are entirely different physical processes, ideally citing the age differences between these events. Another approach is to discuss the evidence of exoplanets detected around stars of different ages than our Sun. Even though the question appears simple, the question asks students to unpack a lot of concepts and synthesize them together. At its core, this question investigates students' ideas related to cosmological time as well as how planet formation is or is not connected to the Big Bang.

A total of 43 students responded to this question (Table 4.4). The majority of students (72%) correctly responded 'no' but could not back up their choice with a scientific explanation of why or contradicted their choice in the explanation. For example, one student said "No, because they were part of how earth was formed" and another student said "No, because they were part of how earth was formed." Incoherent responses and contradictions made it difficult to identify whether students truly meant no. Similar to their responses to the other questions, students favored vague explanations of collisions, explosions, or material drifting around the Universe.

Approximately 28% (n=12) of students responded 'yes' incorrectly. The majority

(67%) explained that all planets (including Earth) formed during the Big Bang. One student backed up their choice with a religious explanation, and the remaining three students provided incoherent explanations that could not be coded in more detail. This student who responded 'yes' to the question contradicted their choice in the second part of their response:

> Yes because when the Big Bang happened in our solar system, all the planets were created from the debris (which all occured [sic] at once). Other planets in the universe were formed at different times because stars are always dying and being reborn.

The wording of this question was specifically chosen to avoid the term exoplanet to reduce confusion or bias in student responses. In other words, we did not want students' to possess an incorrect definition of what an exoplanet is and bring it into their response. It is possible that students were still confused with what we meant by "other planets" in this context, or perhaps students are unclear about the differences between solar systems, galaxies, and the Universe. However, our findings presented here are similar to results from previous studies and suggest the issue is students' misconceptions regarding the Big Bang and not the wording of our question. Previous work highlights that undergraduate students often describe the Big Bang as an explosion of pre-existing matter (Prather et al., 2002; Wallace et al., 2012; Simon et al., 2018). The misconceptions students posses about the Big Bang seem to make it more difficult for students to provide a scientific explanation for our question about when exoplanets formed in relation to Earth's formation.

4.6 Time in the Future: Recommendations for Research and Instruction

It would be naive to make the assumption that students come to our classrooms essentially as blank slates when it comes to the idea of Earth's place in space and time

in the Universe. Rather, in looking at how students respond to questions in the previous section, it appears that many students do possess adequate building blocks to reach a more scientific understanding with proper, targeted instruction. The above results highlight the potential power of time-related knowledge in astronomy and further support the notion that interdisciplinary instruction connecting astronomy with chemistry, geology, and physics in the classroom is worthy of more research. Many students even at the college level with prior astronomy coursework appear to be unclear how Earth fits into the cosmic landscape. This content area has largely remained a focus in the literature on younger age groups, but our research suggests explorations of student perceptions on Earth's place in time and space in the Universe may be pertinent to investigate for older populations of students and is worthy of more research as well.

New research strategies that target curricula and instruction related to Earth's place in time and space in the Universe are essential in order to improve how students construct temporal knowledge in an astronomical context. Topics such as astrobiology and the ongoing search for and study of exoplanets already exist in the astronomical realm and provide excellent pathways for incorporating education related to temporal and spatial scales. Astrobiology inherently includes the large temporal scales required to describe how life first arose and evolved on Earth nearly 4 billion years ago, as well as discussion of spatial scales at the microscopic level in order to become familiar with Earth's first life at the cellular level. Furthermore, both astrobiology and exoplanetary science require a grasp of the large orders of magnitude in distance to bodies in our Solar System and beyond.

One way to improve students' fragmented and incorrect knowledge is through the use of learning progressions. Plummer et al. (2015) developed a hypothetical learning progression as a first step that could lead students to explain the formation of our Solar System through a big idea approach. A big idea approach connects multiple scientific concepts together and would inherently be connected to an understanding of cosmological time. In other words, this learning strategy provides a map of the fundamental astronomical and physical concepts involved in the planetary

formation process——such as gravitational cloud collapse and angular momentum in the disk——that can guide students and teachers of different levels and backgrounds throughout the learning process, focusing on the big ideas of the topics rather than specific details. This is a new approach for astronomy courses, and explicitly incorporating components of cosmological time into learning progressions may help to tie big ideas in astronomy together in the future.

Despite general difficulties with concepts related to Earth's place in time and space in the Universe, students were clearly able to activate the resources they possessed in the context of questions asked. Introducing Hammer's notion of resource framing into classrooms may help students highlight their existing astronomical knowledge (Hammer et al., 2004), and explicitly dedicating classroom time to learning about new space-based frames of reference and non-geocentric perspectives of time may provide means for students to continue to build upon their existing knowledge resources.

Extrapolating data from studies on geological time provides reasonable evidence to support the fact that students of all ages, teachers, as well as the general public struggle to grasp the span of immense timescales——such as Earth's age or the age of the Universe——in both absolute and relative timescales. Catley and Novick (2009) eloquently highlighted some of the common overarching complications observed from temporal reasoning: (1) subjects provided time frames that spanned unimaginably large periods of time (e.g., trillions), (2) the ability to discriminate between very large numbers was rare (e.g., millions vs billions), (3) the frequency of time estimates to the correct order of magnitude was rare, and (4) it was a common misconception among school children and college students that life arose concurrently with the formation of Earth. These findings are easily extended to time in astronomy from our work and recent literature, with both children and college students: defining the origin event that formed the Universe as an event that formed Earth and/or our Solar System, and underestimating/overestimating the age of the Universe by millions or billions of years.

Timescales of this size are not easy to comprehend or relate to admittedly, and

are far outside the range of human experience as Landy et al. (2013) point out, which may explain why the majority of people fail to provide sufficient knowledge of these scales and their associated events. Yet, the ability to construct scientifically accurate temporal frameworks remains necessary for learning about and truly understanding astronomy at its core, and effectively building these knowledge structures may help students to grasp astronomical concepts more concretely. Learners' perceptions of cosmological time or geological time depend not only on scientific content knowledge and quantitative reasoning skills, but also individual feelings and motivations toward the subject, interest in learning it, and concern for its importance in the scale of their personal lives. We have observed behavior representative of these hierarchical arrangements in our pilot research, notably when we asked undergraduate students to respond to an open-ended question and temporally relate the formation of the Universe to the formation of Earth. Students frequently unify these two formation events in their responses, describing that Earth and the Universe came into existence at the same time. Students who did provide numerical estimates and separated the formation events, however, commonly responded "millions or billions of years apart," seemingly unaware of the three order of magnitude difference between these numbers. Yet, the students knew in the context of their personal lives millions or billions of years were both large numbers.

An approach toward improving students' grasp of the geological timescale and its relationship to cosmological time might require initially removing the quantitative aspect of time, instead focusing on the connection between past and present events. By making the sequence and order of events that occur on large timescales more concrete, large scales of time can become a more approachable concept for students. Furthermore, providing relevant, qualitative points of interest in time—such as the fact there is more time between *Tyrannosaurus rex* and *Stegosaurus* than human's entire existence on Earth—is perhaps far more profound and relatable to students than a memorization of dates on a timeline.

Suggestions from the literature have been provided from all facets of Earth and space science community. In evolutionary biology, Catley and Novick (2009) used

an instructional strategy that also incorporated visualizations of large evolutionary events through the use of phylogenetic trees, or trees which showed evolutionary relationships. They explain these trees serve as markers that may help incorporate instruction on spacing and make it relatable to evolutionary time. Similarly, Delgado (2013) suggested time landmarks to function as pinpoints across learning disciplines so students can orient themselves to specific points in time. Conversely, Trend (2001b) said timelines may be appropriate for historical events but not for cosmological and geological events, as the scale cannot be conceptualized onto a single timeline if ongoing and consistent change is to be expressed.

Prior research has illustrated that learners have a difficult time accounting for motions of the night sky appropriately using Earth as a moving reference frame (Plummer, 2009, 2014). Hegarty and Waller (2004) highlight a dissociation between spatial abilities that require both mental rotation and the ability to take on a different visual perspective that might explain why spatial reasoning difficulties often occur in astronomy. Approaches toward developing students' abilities to construct representations of Earth's place in time and space will require attention to both mental rotation and perspective taking. Plummer and colleagues have dedicated significant efforts with perspective taking that connect the view of Earth from the Sun in both Earth- and space-based reference frames (Plummer et al., 2016; Liben and Downs, 1993). For example, students must be able to comprehend why our Earth-based perspective of the Sun's motion around Earth is opposite in a space-based reference frame. Future work will require an extension to perspective taking that incorporates Earth's location in both time and space in the Universe. Adding the fourth dimension of time increases the complexity of mental rotation and perspective taking, but coupling temporal and spatial awarenesses can be used to introduce students to different points in time throughout cosmological history. Time often influences how an event is perceived and stored into memory (Radvansky and Zacks, 2011), such as the case when students conflate Earth forming at the same time as the Universe, which suggests students' temporal perspectives influence the relative orientation and hierarchy of astronomical events in the past,

present, and future. We believe it is worthwhile to investigate perspective taking that incorporates a temporal point of view.

We encourage future work that helps students build an understanding of scientific evidence explaining the causality related to major astronomical events in cosmological time so students may make more robust connections of concepts (e.g., when and where the ingredients come from for rocky planets to form and how do we know this). Past work suggests that finding ways to connect large points in time to students' personal lives rather than memorization of ages, dates, or a list of events can be beneficial when learning about large timescales (Delgado, 2013; Chaisson, 2011, 2014a,b). We have synthesized the following take-away guidelines as recommendations for future research and instruction related to time at the undergraduate level:

- Explicit instruction through visualizations and guided active learning strategies that explore the relationship between cosmological and geological spatio-temporal scales (i.e., the age of the Universe versus the age of Earth; the sizes of Earth and the Solar System versus the sizes of galaxies and the Universe) and how the age of Earth and the Universe were determined.

- Unpacking and connecting cosmic events including the Big Bang and after, leading up to Earth's formation (e.g., cosmic microwave background, formation of first stars, expansion of space-time, the formation of elements including heavy elements needed for rocky planets).

- Instruction on the composition of the Universe and visualizations of the large-scale hierarchical structure of planets, stars, solar systems, and galaxies.

- Increased instructional attention on processes of stellar nucleosynthesis including where, when, and how the elements on the periodic table arose and how this is related to astronomy and Earth's composition.

- Increased attention on the interdisciplinary knowledge related to physics, particularly gravity and its influence on processes across large spatial scales (e.g.,

expansion of the Universe, planet formation) and how this is related to time.

- Building connections to other findings in astrobiology, the study of exoplanets, and geology to help build bridges between topics such as the origin of life on Earth and how scientists search for life elsewhere in the Solar System.

Our results suggest developing effective curricula and instruction that helps produces temporally literate learners in astronomy may further help students to construct accurate scientific representations of astronomical phenomena. Those in the astronomy and physics education communities, as well as others in the broad community of the physical sciences, are encouraged to pursue study related to our new research agenda described in this paper. We appreciate the incorporation of time-related research and instruction into teaching and look forward to reports on successful methodologies that investigate temporal perceptions as related to the larger picture of Earth's place in time and space in the Universe.

CHAPTER 5

Conclusions and Future Work

Here I summarize the major results of this dissertation. First, I provide the key points from my research on brown dwarf atmospheres followed by a summary of key points from my educational work.

1. **Chapter 2: It is possible to produce atmosphere models that match substellar evolutionary model predictions if enough flexibility is allowed within the cloud properties.** I reported the atmospheric properties of 12 brown dwarf binary objects spanning from mid-L to mid-T in spectral type ($T_{eff} \approx$ 1900-1000 K). Clouds with sub-micron particles (≤ 1 μm) can describe the spectral energy distribution of dusty L dwarfs, but larger particle sizes and deeper clouds are needed for T dwarfs.

2. **Chapter 3: I derive bulk atmospheric properties for HD 130948B+C, a L4+L4 benchmark brown dwarf binary system orbiting a solar-type host star, and find C/O ratios consistent with a stellar metallicity.** I am able to fit cloudy atmosphere models to moderate-resolution J and K-band spectroscopy of HD 130948B and HD 130948C that are consistent with evolutionary-model predictions.

A major goal of this work was to explore cloud properties in detail across a broad range of temperatures, surface gravities, and cloud parameters. I

use spatially-resolved photometry in optical and near-infrared wavelengths and moderate-resolution J and K-band spectroscopy coupled with theoretical models to characterize the atmospheric properties of benchmark brown dwarf binary systems. I created new atmosphere model grids in PHOENIX extending clouds to deeper regions with smaller mean grain sizes (≤ 1 μm). The results from my work show these grids were best suited for L dwarfs ($\sim$ L3-L8) but can also be used to fit L-band observations from directly-imaged substellar objects like κ Andromedae b (Stone et al., 2020). Bolometric luminosity constraints from grid fits were used with measured dynamical masses to derive predictions from evolutionary models including hybrid grids from Saumon and Marley (2008) for mid-to-late L dwarfs and the COND grids from Baraffe et al. (2003) for T dwarfs with $T_{eff} < 1300$ K. A combination of appropriate cloud properties and metallicity can further be used to constrain benchmark systems that have a stellar companion. Molecular abundances for H_2O and CO can be used to derive C/O ratios and confirm coeval assumptions for binary systems.

In Chapter 4, we presented an analysis of student-supplied response questions related to astronomy education. We identified a range of conceptions learners possess that will help inform future research-based curricula. We ended the chapter with a discussion on how future teaching and instructional efforts could improve how learners construct temporal and spatial frameworks in introductory astronomy courses. The key points are summarized below.

1. **Chapter 4: Our results showed that students posses a variety of non-scientific ideas about Earth's place in space and time in the Universe.** Students struggled to separate astronomical events in time (e.g., the Big Bang versus the formation of our Solar System) and often could not recognize the different hierarchies in space (e.g., a solar system, galaxy, the Universe). The following reasoning difficulties stood out in the data the most: (1) difficulties grasping absolute and relative timescales related to events in cosmological history; (2) difference in orders of magnitude (thousands, millions, billions), (3) relationship in time between formation of the Universe, first galaxies/stars,

the Sun, and Earth; (4) materials and conditions required for stars, planets, and life to form.

Similarly, as with scientific reasearch, educating undergraduate students on topics related to astronomy is an ever-changing field. Updated materials and methods are required that reflect students' conceptions as they enter the classroom. The results from my educational work can be utilized to develop effective materials that can easily be implemented into undergraduate classrooms.

5.1 Looking Ahead

Clouds in brown dwarf atmospheres are challenging to model and, although the work presented in this dissertation contributes significantly to the field of study, there remains several lingering questions. Below I discuss a few of these questions. Continued astrometric monitoring of binary systems will provide orbital constraints and dynamical masses for new systems, and the next *Gaia* data release will provide precise parallaxes, both of which will increase the number of brown dwarfs with independently measured masses and distances. Future observations will extend wavelength coverage, such as with the upcoming launch of the James Webb Space Telescope. Below a few of these questions are discussed.

5.1.1 How does the cloud particle size distribution change for late-L through early-to-mid T dwarfs?

In Brock et al. (2021) I explored how the location and grain size of clouds varied for L through T spectral types. Evolutionary-constrained atmosphere models preferred larger grain sizes for T dwarfs (≥ 1 μm) than L dwarfs. The later mid-T dwarfs in my sample required even larger grain size models (≥ 3 μm) and deeper clouds. The trend that emerged suggested cooler dwarfs with later spectral types grow in mean grain size. It will be important to test the results from this photometric study on resolved spectroscopy of benchmark T dwarf systems. Recent work has found dynamical

masses for T dwarfs that are in conflict with evolutionary parameters (Kasper et al., 2009; King et al., 2010; Cheetham et al., 2018). Extending atmosphere grids to more diverse properties may help reduce this tension as well as comparing T dwarfs to the newest generation of evolutionary models (Marley et al., 2021).

5.1.2 How can observations be used to constrain the precise condensate cloud compositions?

Luna and Morley (2021) explain the compositions of condensate clouds are dependent upon the modelling framework used and have not been empirically constrained. Models with heterogeneous grains based on the assumptions of chemical equilibrium have been successfully used to model brown dwarf (Brock et al., 2021) and exoplanet atmospheres (Stone et al., 2020). However, atmospheric retrieval results have suggested optically thick clouds might be composed of only a select few types of grains, such as combinations of deep iron or iron/corundum cloud decks with shallow pressure enstatite/quartz clouds (Burningham et al., 2017, 2021). This calls the approach of equilibrium clouds into question (Gao et al., 2020). Future work will benefit from comparing the results from self-consistent atmosphere models to those from atmospheric retrievals for the same objects. This is especially important for benchmark systems with well known properties of distance, mass, and luminosity. Furthermore, additional observations with longer wavelength coverage from JWST will help to constrian bulk atmospheric properties.

REFERENCES

Ackerman, A. S. and M. S. Marley (2001). Precipitating condensation clouds in substellar atmospheres. *Astrophysical Journal*, **556**(1), pp. 872–884. ISSN 15384357. doi:10.1088/0004-637X/765/1/75.

Allard, F. (1990). *Model Atmospheres for M Dwarfs*. Ph.D. thesis, Ruprecht Karls University.

Allard, F., D. R. Alexander, and P. H. Hauschildt (1998). Model Atmospheres of Very Low Mass Stars and Brown Dwarfs. In *Cool Stars, Stellar Systems and the Sun*.

Allard, F. and P. H. Hauschildt (1995). Model Atmospheres for M (Sub)dwarf Stars I. The Base Model Grid. *The Astrophysical Journal*, **445**, pp. 433–450.

Allard, F., P. H. Hauschildt, D. R. Alexander, and S. Starrfield (1997). Model Atmospheres of Very Low Mass Stars and Brown Dwarfs. *Annu. Rev. Astron. Astrophys*, **35**, pp. 137–177.

Allard, F., P. H. Hauschildt, D. R. Alexander, A. Tamanai, and A. Schweitzer (2001). The Limiting Effects of Dust in Brown Dwarf Model Atmospheres. *The Astrophysical Journal*, **556**(1), pp. 357–372. ISSN 0004-637X. doi:10.1086/321547.

Allers, K. N. and M. C. Liu (2013). A near-infrared spectroscopic study of young field ultracool dwarfs. *Astrophysical Journal*, **772**(2). ISSN 15384357. doi:10.1088/0004-637X/772/2/79.

American Association for the Advancement of Science (AAAS) (1993). Benchmarks for science literacy.

Anderson, J. and I. R. King (2006). PSFs, Photometry, and Astronomy for the ACS/WFC. Technical report, STsCI.

Apai, D., T. Karalidi, M. S. Marley, H. Yang, D. Flateau, S. Metchev, N. B. Cowan, E. Buenzli, A. J. Burgasser, J. Radigan, E. Artigau, and P. Lowrance (2017). Zones, spots, and planetary-scale waves beating in brown dwarf atmospheres. *Science*, **357**(6352), pp. 683–687. ISSN 10959203. doi:10.1126/science.aam9848.

Apai, D., J. Radigan, E. Buenzli, A. Burrows, I. N. Reid, and R. Jayawardhana (2013). HST spectral mapping of L/T transition brown dwarfs reveals cloud thickness variations. *Astrophysical Journal*, **768**(2). ISSN 15384357. doi:10.1088/0004-637X/768/2/121.

Ault, C. R. (1982). Time in geological explanations as perceived by elementary-school students. *journal of geological education*, **30**, pp. 304–309.

Auman, J. (1967). The Infrared Opacity of Hot Water Vapor. *The Astrophysical Journal*, **149**, pp. 171–206.

Bailey, J. M., E. E. Prather, B. Johnson, and T. F. Slater (2009). College students' preinstructional ideas about stars and star formation. *Astronomy Education Review*, **8**(1), pp. 010110–010117.

Bailey, J. M. and T. F. Slater (2003). A Review of Astronomy Education Research. *Astronomy Education Review*, **2**(2), p. 20. ISSN 1539-1515. doi:10.3847/AER2003015.

Baraffe, I. and G. Chabrier (1995). New Evolutionary Tracks for Very Low Mass Stars. *The Astrophysical Journal*, **446**, pp. L35–L38.

Baraffe, I., G. Chabrier, F. Allard, and P. H. Hauschildt (2002). Evolutionary models for low-mass stars and brown dwarfs: Uncertainties and limits at very young ages. *A&A*, **382**, pp. 563–572. ISSN 0004-6361. doi:10.1051/0004-6361:20011638.

Baraffe, I., G. Chabrier, T. S. Barman, F. Allard, and P. H. Hauschildt (2003). Evolutionary models for cool brown dwarfs and extrasolar giant planets. The case of HD 209458. *Astronomy and Astrophysics*, **402**(2), pp. 701–712. ISSN 00046361. doi:10.1051/0004-6361:20030252.

Barman, T. (2007). Identification of Absorption Features in an Extrasolar Planet Atmosphere. *The Astrophysical Journal*, **661**(2), pp. L191–L194. ISSN 0004-637X. doi:10.1086/518736.

Barman, T. S., P. H. Hauschildt, and F. Allard (2001). Irradiated Planets. *The Astrophysical Journal*, **556**(2), pp. 885–895. ISSN 0004-637X. doi:10.1086/321610.

Barman, T. S., Q. M. Konopacky, B. Macintosh, and C. Marois (2015). Simultaneous detection of water, methane, and carbon monoxide in the atmosphere of Exoplanet hr 8799 b. *Astrophysical Journal*, **804**(1), pp. 1–10. ISSN 15384357. doi:10.1088/0004-637X/804/1/61.

Barman, T. S., B. MacIntosh, Q. M. Konopacky, and C. Marois (2011a). Clouds and chemistry in the atmosphere of extrasolar planet HR8799b. *Astrophysical Journal*, **733**(1). ISSN 15384357. doi:10.1088/0004-637X/733/1/65.

Barman, T. S., B. MacIntosh, Q. M. Konopacky, and C. Marois (2011b). The young planet-mass object 2M1207b: A cool, cloudy, and methane-poor atmosphere. *Astrophysical Journal Letters*, **735**(2), pp. 2–6. ISSN 20418205. doi: 10.1088/2041-8205/735/2/L39.

Barnes, S. A. (2007). Ages for Illustrative Field Stars Using Gyrochronology: Viability, Limitations, and Errors. *The Astrophysical Journal*, **669**(2), pp. 1167–1189. ISSN 0004-637X. doi:10.1086/519295.

Best, W. M. J., M. C. Liu, E. A. Magnier, and T. J. Dupuy (2020a). A Volume-limited Sample of Ultracool Dwarfs. I. Construction, Space Density, and a Gap in the L/T Transition. *The Astronomical Journal*, **161**(1), p. 42. ISSN 0004-6256. doi:10.3847/1538-3881/abc893.

Best, W. M. J., M. C. Liu, E. A. Magnier, and T. J. Dupuy (2020b). The Hawaii Infrared Parallax Program. IV. A Comprehensive Parallax Survey of L0–T8 Dwarfs with UKIRT. *The Astronomical Journal*, **159**(6), p. 257. ISSN 0004-6256. doi: 10.3847/1538-3881/ab84f4.

Best, W. M. J., E. A. Magnier, M. C. Liu, K. M. Aller, Z. Zhang, W. S. Burgett, K. C. Chambers, P. Draper, H. Flewelling, N. Kaiser, R.-P. Kudritzki, N. Metcalfe, J. L. Tonry, R. J. Wainscoat, and C. Waters (2017). Photometry and Proper Motions of M, L, and T Dwarfs from the Pan-STARRS1 3pi Survey. *The Astrophysical Journal Supplement Series*, **234**(1), p. 1. ISSN 1538-4365. doi: 10.3847/1538-4365/aa9982.

Black, A. A. (2005). Spatial Ability and Earth Science Conceptual Understanding. *Journal of Geoscience Education*, **53**(4), pp. 402–414. ISSN 1089-9995. doi: 10.5408/1089-9995-53.4.402.

Boroditsky, L. (2000). Metaphoric structuring: Understanding time through spatial metaphors. *Cognition*, **75**(1), pp. 1–28. ISSN 00100277. doi:10.1016/S0010-0277(99)00073-6.

Borysow, A., U. G. Jørgensen, and C. Zheng (1997). Model atmospheres of cool, low-metallicity stars: The importance of collision-induced absorption. *Astronomy and Astrophysics*, **324**(1), pp. 185–195. ISSN 00046361.

Bouy, H., G. Duchêne, R. Köhler, W. Brandner, J. Bouvier, E. L. Martín, A. Ghez, X. Delfosse, T. Forveille, F. Allard, I. Baraffe, G. Basri, L. Close, and C. E. McCabe (2004). First determination of the dynamical mass of a binary L dwarf. *Astronomy & Astrophysics*, **423**(1), pp. 341–352. ISSN 0004-6361. doi:10.1051/0004-6361:20040551.

Bowler, B. P., M. C. Liu, and T. J. Dupuy (2010). SDSSJ141624.08+134826.7: A nearby blue L dwarf from the sloan digital sky survey. *Astrophysical Journal*, **710**(1), pp. 45–50. ISSN 15384357. doi:10.1088/0004-637X/710/1/45.

Brandt, G. M., T. D. Brandt, T. J. Dupuy, Y. Li, and D. Michalik (2021). Precise Dynamical Masses and Orbital Fits for β Pic b and β Pic c. *The Astronomical Journal*, **161**(4), p. 179. ISSN 0004-6256. doi:10.3847/1538-3881/abdc2e.

Brandt, T. D., T. J. Dupuy, B. P. Bowler, D. C. Bardalez Gagliuffi, J. Faherty, G. M. Brandt, and D. Michalik (2020). A Dynamical Mass of 70 $\pm$ 5 M Jup for Gliese 229B, the First T Dwarf. *The Astronomical Journal*, **160**(4), p. 196. ISSN 0004-6256. doi:10.3847/1538-3881/abb45e.

Bransford, J. (2004). *How People Learn*. Washington, DC: National Academy Press, Washington, DC. ISBN 0309070368. doi:10.17226/9853.

Briesemeister, Z. W., A. J. Skemer, J. M. Stone, T. S. Barman, P. Hinz, J. Leisenring, M. F. Skrutskie, C. E. Woodward, and E. Spalding (2019). High Spatial Resolution Thermal Infrared Spectroscopy with ALES: Resolved Spectra of the Benchmark Brown Dwarf Binary HD 130948BC. *The Astronomical Journal*, **157**(6), p. 244. ISSN 0004-6256. doi:10.3847/1538-3881/ab1901.

Brock, L. S. (2015). *To the Universe and Back: Increasing Earth and Space Science Literacy Through a Deep Time Exhibition*. Ph.D. thesis, Northern Arizona University.

Brock, L. S., T. Barman, Q. M. Konopacky, and J. M. Stone (2021). Cloud Properties of Brown Dwarf Binaries Across the L/T Transition. *The Astrophysical Journal*, **914**(2), p. 124. ISSN 1538-4357. doi:10.3847/1538-4357/abfc46.

Brock, L. S., E. Prather, and C. Impey (2018). Finding the time: Exploring a new perspective on students' perceptions of cosmological time and efforts to improve temporal frameworks in astronomy. *Physical Review Physics Education Research*, **14**(1). ISSN 24699896. doi:10.1103/PhysRevPhysEducRes.14.010138.

Brown, A. G. A., A. Vallenari, T. Prusti, D. B. J. H. J, C. Babusiaux, M. Biermann, D. W. Evans, L. Eyer, F. Jansen, C. Jordi, S. A. Klioner, U. Lammers, L. Lindegren, X. Luri, F. Mignard, C. Panem, D. Pourbaix, S. Randich, P. Sartoretti, H. I. Siddiqui, C. Soubiran, V. L. F, N. A. Walton, F. Arenou, U. Bastian, M. Cropper, R. Drimmel, D. Katz, M. G. Lattanzi, J. Bakker, C. Cacciari, J. Castañeda, L. Chaoul, N. Cheek, D. A. F, C. Fabricius, R. Guerra, B. Holl, E. Masana, R. Messineo, N. Mowlavi, K. Nienartowicz, P. Panuzzo, J. Portell, M. Riello, G. M. Seabroke, P. Tanga, F. Thévenin, G. Comoretto, D. Teyssier, M. Altmann, R. Andrae, M. Audard, K. Benson, J. Berthier, R. Blomme, P. Burgess, G. Busso,

B. Carry, A. Cellino, G. Clementini, M. Clotet, O. Creevey, M. Davidson, D. R. J, L. Delchambre, D. O. A, C. Ducourant, M. Fouesneau, Y. Frémat, L. Galluccio, E. Gosset, L. P. Guy, J. Halbwachs, N. C. Hambly, D. L. Harrison, J. Hernández, D. Hestroffer, S. T. Hodgkin, A. Hutton, G. Jasniewicz, S. Jordan, A. J. Korn, A. C. Lanzafame, T. Lebzelter, W. Löffler, M. Manteiga, P. M. Marrese, A. Moitinho, A. Mora, K. Muinonen, J. Osinde, E. Pancino, T. Pauwels, J. Petit, P. J. Richards, L. Rimoldini, A. C. Robin, L. M. Sarro, C. Siopis, M. Smith, A. Sozzetti, M. Süveges, J. Torra, V. R. W, U. Abbas, A. A. A, S. Accart, C. Aerts, G. Altavilla, M. A. Álvarez, R. Alvarez, J. Alves, R. I. Anderson, A. H. Andrei, A. V. E, E. Antiche, T. Antoja, B. Arcay, T. L. Astraatmadja, N. Bach, S. G. Baker, P. Balm, C. Barache, C. Barata, D. Barbato, F. Barblan, P. S. Barklem, D. Barrado, M. Barros, M. A. Barstow, B. M. S, J. Bassilana, U. Becciani, M. Bellazzini, A. Berihuete, S. Bertone, L. Bianchi, O. Bienaymé, T. Boch, C. Boeche, A. Bombrun, R. Borrachero, D. Bossini, S. Bouquillon, G. Bourda, A. Bragaglia, L. Bramante, M. A. Breddels, A. Bressan, N. Brouillet, T. Brüsemeister, E. Brugaletta, B. Bucciarelli, A. Burlacu, D. Busonero, A. G. Butkevich, R. Buzzi, E. Caffau, R. Cancelliere, G. Cannizzaro, R. Carballo, T. Carlucci, J. M. Carrasco, L. Casamiquela, M. Castellani, P. Charlot, L. Chemin, A. Chiavassa, G. Cocozza, G. Costigan, S. Cowell, F. Crifo, M. Crosta, C. Crowley, J. Cuypers, C. Dafonte, Y. Damerdji, A. Dapergolas, P. David, M. David, D. L. P, D. L. F, D. M. R, D. M. D, D. S. R, D. T. A, J. Debosscher, E. Pozo, M. Delbo, A. Delgado, H. E. Delgado, D. M. P, S. Diakite, C. Diener, E. Distefano, C. Dolding, P. Drazinos, J. Durán, B. Edvardsson, H. Enke, K. Eriksson, P. Esquej, E. B. G, C. Fabre, M. Fabrizio, S. Faigler, A. J. Falcão, F. C. M, L. Federici, G. Fedorets, P. Fernique, F. Figueras, F. Filippi, K. Findeisen, A. Fonti, E. Fraile, M. Fraser, B. Frézouls, M. Gai, S. Galleti, D. Garabato, A. Garofalo, N. Garralda, A. Gavel, P. Gavras, J. Gerssen, R. Geyer, P. Giacobbe, G. Gilmore, S. Girona, G. Giuffrida, F. Glass, M. Gomes, M. Granvik, A. Gueguen, A. Guerrier, J. Guiraud, R. Haigron, D. Hatzidimitriou, M. Hauser, M. Haywood, U. Heiter, A. Helmi, J. Heu, T. Hilger, D. Hobbs, W. Hofmann, G. Holland, H. E. Huckle, A. Hypki, V. Icardi, K. Janßen, J. D. F. G, P. G. Jonker, Á. L. Juhász, F. Julbe, A. Karampelas, A. Kewley, J. Klar, A. Kochoska, R. Kohley, K. Kolenberg, M. Kontizas, E. Kontizas, S. E. Koposov, G. Kordopatis, P. Koubsky, S. Lambert, A. F. Lanza, Y. Lasne, J. Lavigne, L. F. Y, L. P.-l. C, Y. Lebreton, S. Leccia, N. Leclerc, H. Lenhardt, F. Leroux, S. Liao, E. Licata, H. E. P. Lindstrøm, T. A. Lister, E. Livanou, A. Lobel, M. López, S. Managau, R. G. Mann, G. Mantelet, O. Marchal, J. M. Marchant, M. Marconi, S. Marinoni, G. Marschalkó, D. J. Marshall, M. Martino, G. Marton, N. Mary, D. Massari, G. Matijevič, T. Mazeh, P. J. Mcmillan, S. Messina, D. Michalik, N. R. Millar, D. Molina, R. Molinaro, L. Molnár, P. Montegriffo, R. Mor, R. Morbidelli, T. Morel, D. Morris, A. F. Mulone, T. Muraveva, I. Musella, G. Nelemans, L. Nicastro, L. Noval, O. W. Mullane, C. Ordénovic, P. Osborne, C. Pagani, I. Pagano, F. Pailler, H. Palacin,

L. Palaversa, A. Panahi, M. Pawlak, A. M. Piersimoni, F. Pineau, E. Plachy, G. Plum, E. Poggio, E. Poujoulet, A. Prša, L. Pulone, E. Racero, S. Ragaini, N. Rambaux, S. Regibo, C. Reylé, F. Riclet, V. Ripepi, A. Riva, A. Rivard, G. Rixon, T. Roegiers, M. Roelens, N. Rowell, F. Royer, G. Sadowski, S. S. T, J. Sahlmann, J. Salgado, E. Salguero, N. Sanna, M. Sarasso, H. Savietto, M. Schultheis, E. Sciacca, M. Segol, J. C. Segovia, D. Ségransan, S. I-c, L. Siltala, A. F. Silva, R. L. Smart, K. W. Smith, E. Solano, F. Solitro, R. Sordo, S. N. S, J. Souchay, A. Spagna, F. Spoto, U. Stampa, I. A. Steele, H. Steidelmüller, C. A. Stephenson, H. Stoev, F. F. Suess, J. Surdej, L. Szabados, D. Tapiador, F. Taris, G. Tauran, M. B. Taylor, R. Teixeira, D. Terrett, P. Teyssandier, W. Thuillot, A. Titarenko, T. C. F, C. Turon, A. Ulla, E. Utrilla, S. Uzzi, M. Vaillant, G. Valentini, V. Valette, V. E. A, V. H. E, V. L. M, M. Vaschetto, A. Vecchiato, J. Veljanoski, Y. Viala, D. Vicente, S. Vogt, V. E. C, H. Voss, V. Votruba, S. Voutsinas, G. Walmsley, M. Weiler, O. Wertz, T. Wevers, Ł. Wyrzykowski, A. Yoldas, M. Žerjal, H. Ziaeepour, J. Zorec, S. Zschocke, S. Zucker, C. Zurbach, and T. Zwitter (2018). Astrophysics Special Issue Gaia Data Release 2. *Astronomy & Astrophysics*, **616**(A1), pp. 1–22.

Buenzli, E., M. S. Marley, D. Apai, and R. E. Lupu (2014). Cloud structure of brown dwarfs from spectroscopic variability observations. *ArXiv e-prints*, **1406**, p. 210.

Burgasser, A., M. C. Liu, M. J. Ireland, K. L. Cruz, and T. J. Dupuy (2008a). Subtle Signatures of Multiplicity in Late-Type Dwarf Spectra :. *Astrophysical Journal*, **681**, pp. 579–593.

Burgasser, A. J. (2007). Binaries and the L Dwarf/T Dwarf Transition. *The Astrophysical Journal*, **659**(1), pp. 655–674. ISSN 0004-637X. doi:10.1086/511027.

Burgasser, A. J. (2014). The SpeX Prism Library: 1000+ Low-resolution, Near-infrared Spectra of Ultracool M, L, T and Y Dwarfs. **10**(1995), pp. 1–10.

Burgasser, A. J., D. C. Bardalez-Gagliuffi, and J. E. Gizis (2011). HUBBLE space telescope imaging and spectral analysis of two brown dwarf binaries at the L dwarf/T dwarf transition. *Astronomical Journal*, **141**(3). ISSN 00046256. doi: 10.1088/0004-6256/141/3/70.

Burgasser, A. J., K. L. Cruz, M. Cushing, C. R. Gelino, D. L. Looper, J. K. Faherty, J. D. Kirkpatrick, and I. N. Reid (2010). SpeX Spectroscopy of unresolved very low mass binaries. I. Identification of 17 candidate binaries straddling the L dwarf/T dwarf transition. *Astrophysical Journal*, **710**(2), pp. 1142–1169. ISSN 15384357. doi:10.1088/0004-637X/710/2/1142.

Burgasser, A. J., T. R. Geballe, S. K. Leggett, J. D. Kirkpatrick, and D. A. Golimowski (2006). A Unified Near-Infrared Spectral Classification Scheme for T Dwarfs. *The Astrophysical Journal*, **637**(2), pp. 1067–1093. ISSN 0004-637X. doi:10.1086/498563.

Burgasser, A. J., J. D. Kirkpatrick, J. Liebert, and A. Burrows (2003). The Spectra of T Dwarfs. II. Red Optical Data. *The Astrophysical Journal*, **594**(1), pp. 510–524. ISSN 0004-637X. doi:10.1086/376756.

Burgasser, A. J., D. L. Looper, J. D. Kirkpatrick, K. L. Cruz, and B. J. Swift (2008b). Clouds, Gravity, and Metallicity in Blue L Dwarfs: The Case of 2MASS J112639915003550. *The Astrophysical Journal*, **674**(1), pp. 451–465. ISSN 0004-637X. doi:10.1086/524726.

Burgasser, A. J., D. L. Looper, J. D. Kirkpatrick, and M. C. Liu (2007). Discovery of a High Proper Motion L Dwarf Binary: 2MASS J152002244422419AB. *The Astrophysical Journal*, **658**(1), pp. 557–568. ISSN 0004-637X. doi:10.1086/511518.

Burgasser, A. J., M. S. Marley, A. S. Ackerman, D. Saumon, K. Lodders, C. C. Dahn, H. C. Harris, and J. D. Kirkpatrick (2002). Evidence of Cloud Disruption in the L/T Dwarf Transition. *The Astrophysical Journal*, **571**(2), pp. L151–L154. ISSN 0004637X. doi:10.1086/341343.

Burgasser, A. J. and M. W. McElwain (2006). Resolved Spectroscopy of M Dwarf/L Dwarf Binaries. I. DENIS J220002.05-303832.9AB. *The Astronomical Journal*, **131**(2), pp. 1007–1014. ISSN 0004-6256. doi:10.1086/499042.

Burgasser, A. J., M. W. McElwain, J. D. Kirkpatrick, K. L. Cruz, C. G. Tinney, and I. N. Reid (2004). The 2MASS Wide-Field T Dwarf Search. III. Seven New T Dwarfs and Other Cool Dwarf Discoveries. *The Astronomical Journal*, **127**(5), pp. 2856–2870. ISSN 0004-6256. doi:10.1086/383549.

Burgasser, A. J., J. C. Wilson, J. D. Kirkpatrick, M. F. Skrutskie, M. R. Colonno, A. T. Enos, J. D. Smith, C. P. Henderson, J. E. Gizis, M. E. Brown, and J. R. Houck (2000). Discovery of a Bright Field Methane (T-Type) Brown Dwarf by 2MASS. *The Astronomical Journal*, **120**(2), pp. 1100–1105. ISSN 00046256. doi:10.1086/301475.

Burningham, B., J. K. Faherty, E. C. Gonzales, M. S. Marley, C. Visscher, R. Lupu, J. Gaarn, M. Fabienne Bieger, R. Freedman, and D. Saumon (2021). Cloud busting: Enstatite and quartz clouds in the atmosphere of 2M2224-0158. *Monthly Notices of the Royal Astronomical Society*, **506**(2), pp. 1944–1961. ISSN 13652966. doi:10.1093/mnras/stab1361.

Burningham, B., M. S. Marley, M. R. Line, R. Lupu, C. Visscher, C. V. Morley, D. Saumon, and R. Freedman (2017). Retrieval of atmospheric properties of cloudy L dwarfs. *Monthly Notices of the Royal Astronomical Society*, **470**(1), pp. 1177–1197. ISSN 13652966. doi:10.1093/MNRAS/STX1246.

Burrows, A., W. B. Hubbard, and J. I. Lunine (1989). Theoretical Models of Very Low Mass Stars and Brown Dwarfs. *The Astrophysical Journal*, **345**, pp. 939–958.

Burrows, A., W. B. Hubbard, J. I. Lunine, and J. Liebert (2001). The theory of brown dwarfs and extrasolar giant planets. *Reviews of Modern Physics*, **73**(3), pp. 719–765. ISSN 00346861. doi:10.1103/RevModPhys.73.719.

Burrows, A., M. Marley, W. B. Hubbard, J. I. Lunine, T. Guillot, D. Saumon, R. Freedman, D. Sudarsky, and C. Sharp (1997). A Nongray Theory of Extrasolar Giant Planets and Brown Dwarfs. *The Astrophysical Journal*, **491**(2), pp. 856–875. ISSN 0004-637X. doi:10.1086/305002.

Burrows, A., D. Sudarsky, and I. Hubeny (2006). The L to T dwarf transition. *The Astrophysical Journal*, **640**, pp. 1063–1077. ISSN 03796566.

Burrows, A., D. Sudarsky, and J. I. Lunine (2003). Beyond the T Dwarfs: Theoretical Spectra, Colors, and Detectability of the Coolest Brown Dwarfs. *The Astrophysical Journal*, **596**(1), pp. 587–596. ISSN 0004-637X. doi:10.1086/377709.

Catley, K. M. and L. R. Novick (2009). Digging deep: Exploring college students' knowledge of macroevolutionary time. *Journal of Research in Science Teaching*, **46**(3), pp. 311–332. ISSN 00224308. doi:10.1002/tea.20273.

Cervato, C. and R. Frodeman (2012). The significance of geologic time: Cultural, educational, and economic frameworks. *Geological Society of America*, **2486**(03), pp. 19–27. ISSN 00721077. doi:10.1130/2012.2486(03).

Chabrier, G. and I. Baraffe (1996). Mass-Luminosity Relationship and Lithium Depletion for Very Low Mass Stars. *The Astrophysical Journal*, **459**(L91-94), pp. L91–94.

Chabrier, G. and I. Baraffe (1997). Structure and evolution of low-mass stars. *Astronomy and Astrophysics*, **327**(3), pp. 1039–1053. ISSN 00046361.

Chabrier, G. and I. Baraffe (2000). Theory of Low-Mass Stars and Substellar Objects. *Annual Review of Astronomy and Astrophysics*, **38**, pp. 337–377.

Chaisson, E. J. (2011). Cosmic Evolution – More Than Big History by Another Name. In *Evolution: A Big History Perspective*, pp. 37–48. Uchitel Publishing House.

Chaisson, E. J. (2014a). Big History's Risk and Challenge. *Expositions*, **81**, pp. 85–95.

Chaisson, E. J. (2014b). The natural science underlying big history. doi:10.1155/2014/384912.

Charnay, B., B. Bézard, J. L. Baudino, M. Bonnefoy, A. Boccaletti, and R. Galicher (2018). A self-consistent cloud model for brown dwarfs and young giant exoplanets: comparison with photometric and spectroscopic observations. *The Astrophysical Journal*, **854**(2), p. 172. ISSN 23318422. doi:10.3847/1538-4357/aaac7d.

Cheek, K. A. (2012). Students' Understanding of Large Numbers As a Key Factor in Their Understanding of Geologic Time. *International Journal of Science and Mathematics Education*, **10**(5), pp. 1047–1069. ISSN 15710068. doi:10.1007/s10763-011-9312-1.

Cheek, K. A. (2013). Exploring the Relationship between Students' Understanding of Conventional Time and Deep (Geologic) Time. *International Journal of Science Education*, **35**(11), pp. 1925–1945. ISSN 09500693. doi:10.1080/09500693.2011.587032.

Cheetham, A., D. Ségransan, S. Peretti, J. B. Delisle, J. Hagelberg, J. L. Beuzit, T. Forveille, M. Marmier, S. Udry, and F. Wildi (2018). Direct imaging of an ultracool substellar companion to the exoplanet host star HD 4113 A. *Astronomy and Astrophysics*, **614**. ISSN 14320746. doi:10.1051/0004-6361/201630136.

Chiu, K., X. Fan, S. K. Leggett, D. A. Golimowski, W. Zheng, T. R. Geballe, D. P. Schneider, and J. Brinkmann (2006). Seventy-One New L and T Dwarfs from the Sloan Digital Sky Survey. *The Astronomical Journal*, **131**(5), pp. 2722–2736. ISSN 0004-6256. doi:10.1086/501431.

Chrysikou, E. G. and C. H. Ramey (2006). Factors Influencing the Adoption of Temporal Metaphors. *Cognitive Development*, pp. 19104–19104.

College Board, T. (2009). College Board Standards for College Success ™ Science. p. 242.

Cotner, S., D. C. Brooks, and R. Moore (2010). Is the age of the earth one of our "sorest troubles?" students' perceptions about deep time affect their acceptance of evolutionary theory. *Evolution*, **64**(3), pp. 858–864. ISSN 00143820. doi:10.1111/j.1558-5646.2009.00911.x.

Crepp, J. R., D. A. Principe, S. Wolff, P. A. Giorla Godfrey, E. L. Rice, L. Cieza, L. Pueyo, E. B. Bechter, and E. J. Gonzales (2018). GPI spectroscopy of the mass, age, and metallicity benchmark brown dwarf HD 4747 B. *The Astrophysical Journal*, **853**(2), p. 192. ISSN 23318422. doi:10.3847/1538-4357/aaa2fd.

Cruz, K. L., J. D. Kirkpatrick, and A. J. Burgasser (2009). Young l dwarfs identified in the field: A preliminary low-gravity, optical spectral sequence from L0 to L5. *Astronomical Journal*, **137**(2), pp. 3345–3357. ISSN 00046256. doi: 10.1088/0004-6256/137/2/3345.

Cruz, K. L., A. Núñez, A. J. Burgasser, E. Abrahams, E. L. Rice, I. N. Reid, and D. Looper (2017). Meeting the Cool Neighbors. XII. An Optically Anchored Analysis of the Near-infrared Spectra of L Dwarfs. *The Astronomical Journal*, **155**(1), p. 34. ISSN 1538-3881. doi:10.3847/1538-3881/aa9d8a.

Cruz, K. L., L. Wang, D. Baade, P. Ho, J. C. Wheeler, K. Kawabata, and K. Nomoto (2004). 2MASS J051859952828372: DISCOVERY OF AN UNRESOLVED L/T BINARY, 2004 March 20 2004. pp. 2002–2005.

Cushing, M., W. Vacca, and J. Rayner (2004). Spextool: A Spectral Extraction Package for SpeX, a 0.8–5.5 Micron Cross-Dispersed Spectrograph. *Publications of the Astronomical Society of the Pacific*, **116**(818), pp. 362–376. ISSN 0004-6280. doi:10.1086/382907.

Cushing, M. C., J. D. Kirkpatrick, C. R. Gelino, R. L. Griffith, M. F. Skrutskie, A. Mainzer, K. A. Marsh, C. A. Beichman, A. J. Burgasser, L. A. Prato, R. A. Simcoe, M. S. Marley, D. Saumon, R. S. Freedman, P. R. Eisenhardt, and E. L. Wright (2011). The discovery of y dwarfs using data from the wide-field infrared survey explorer (WISE). *Astrophysical Journal*, **743**(1). ISSN 15384357. doi: 10.1088/0004-637X/743/1/50.

Cushing, M. C., M. S. Marley, D. Saumon, B. C. Kelly, W. D. Vacca, J. T. Rayner, R. S. Freedman, K. Lodders, and T. L. Roellig (2008). Atmospheric Parameters of Field L and T Dwarfs1. *The Astrophysical Journal*, **678**(2), pp. 1372–1395. ISSN 0004-637X. doi:10.1086/526489.

Cushing, M. C., T. L. Roellig, M. S. Marley, D. Saumon, S. K. Leggett, J. D. Kirkpatrick, J. C. Wilson, G. C. Sloan, A. K. Mainzer, J. E. Van Cleve, and J. R. Houck (2006). A Spitzer Infrared Spectrograph Spectral Sequence of M, L, and T Dwarfs. *The Astrophysical Journal*, **648**(1), pp. 614–628. ISSN 0004-637X. doi:10.1086/505637.

Cushing, M. C., D. Saumon, and M. S. Marley (2010). SDSS J141624.08+134826.7: Blue L dwarfs and non-equilibrium chemistry. *Astronomical Journal*, **140**(5), pp. 1428–1432. ISSN 00046256. doi:10.1088/0004-6256/140/5/1428.

Cutri, R. M., M. F. Skrutskie, S. van Dyk, C. A. Beichman, J. M. Carpenter, T. Chester, L. Cambresy, T. Evans, J. Fowler, J. Gizis, E. Howard, J. Huchra, T. Jarrett, E. L. Kopan, J. D. Kirkpatrick, R. M. Light, K. A. Marsh, H. McCallon,

S. Schneider, R. Stiening, M. Sykes, M. Weinberg, W. Wheaton, S. Wheelock, and N. Zacarias (2003). 2MASS All Sky Catalog of point sources. Technical report, The IRSA 2MASS All-Sky Point Source Catalog, NASA/IPAC Infrared Science Archive.

Delaughter, J. E. and S. Stein (1998). Preconceptions about earth science among students in an introductory course. *Voices*, **79**(36), pp. 429–432.

Delgado, C. (2013). Navigating deep time: Landmarks for time from the big bang to the present. *Journal of Geoscience Education*, **61**(1), pp. 103–112. ISSN 10899995. doi:10.5408/12-300.1.

Díaz, R. F., J. Rey, O. Demangeon, G. Hébrard, I. Boisse, L. Arnold, N. Astudillo-Defru, J.-L. Beuzit, X. Bonfils, S. Borgniet, F. Bouchy, V. Bourrier, B. Courcol, M. Deleuil, X. Delfosse, D. Ehrenreich, T. Forveille, A.-M. Lagrange, M. Mayor, C. Moutou, F. Pepe, D. Queloz, A. Santerne, N. C. Santos, J. Sahlmann, D. Ségransan, S. Udry, and P. A. Wilson (2016). The SOPHIE search for northern extrasolar planets. *Astronomy Astrophysics*, **591**, p. A146. ISSN 0004-6361. doi:10.1051/0004-6361/201628331.

Dieterich, S. B., A. J. Weinberger, A. P. Boss, T. J. Henry, W.-C. Jao, J. Gagné, T. L. Astraatmadja, M. A. Thompson, and G. Anglada-Escudé (2018). Dynamical Masses of ϵ Indi B and C: Two Massive Brown Dwarfs at the Edge of the Stellar–substellar Boundary. *The Astrophysical Journal*, **865**(1), p. 28. ISSN 1538-4357. doi:10.3847/1538-4357/aadadc.

Diolaiti, E., O. Bendinelli, D. Bonaccini, L. Close, D. Currie, and G. Parmeggiani (2000). Analysis of isoplanatic high resolution stellar fields by the StarFinder code. *Astronomy and Astrophysics Supplement Series*, **147**(2), pp. 335–346. ISSN 03650138. doi:10.1051/aas:2000305.

DiSessa, A. A. (1988). *Knowledge in pieces*. Erlbaum, Hillsdale, NJ.

Dodick, J. (2007). Understanding evolutionary change within the framework of geological time. *Journal of Education*, **42**(2), pp. 245–264.

Dodick, J. and N. Orion (2003a). Cognitive factors affecting student understanding of geologic time. *Journal of Research in Science Teaching*, **40**(4), pp. 415–442. ISSN 00224308. doi:10.1002/tea.10083.

Dodick, J. and N. Orion (2003b). Measuring Student Understanding of Geological Time. *Science Education*, **87**(5), pp. 708–731. ISSN 00368326. doi:10.1002/sce.1057.

Dodick, J. and N. Orion (2006). Building an understanding of geological time: A cognitive synthesis of the "macro" and "micro" scales of time. *GSA Special Papers*, **413**, p. 77. ISSN 00721077. doi:10.1130/2006.2413(06).

Dodick, J. and N. I. R. Orion (2003c). Geology as an Historical Science: Its Perception within Science and the Education System. *Science Education*, **12**(2), pp. 197–211.

Dorman, B., L. A. Nelson, and W. Y. Chau (1989). Theoretical Models of Low-Mass Stars and Brown Dwarfs. I. The Lower Main Sequence. *The Astrophysical Journal*, **342**, pp. 1003–1018.

Dupuy, T. J. and A. L. Kraus (2013). Distances, Luminosities, and Temperatures of the Coldest Known Substellar Objects. *Science*, **341**(6153), pp. 1492–1495.

Dupuy, T. J. and M. C. Liu (2012). The Hawaii infrared parallax program. I. Ultracool binaries and the L/T transition. *Astrophysical Journal, Supplement Series*, **201**(2). ISSN 00670049. doi:10.1088/0067-0049/201/2/19.

Dupuy, T. J. and M. C. Liu (2017). Individual Dynamical Masses of Ultracool Dwarfs. *The Astrophysical Journal Supplement Series*, **231**(2), p. 15. ISSN 0067-0049. doi:10.3847/1538-4365/aa5e4c.

Dupuy, T. J., M. C. Liu, W. M. J. Best, A. W. Mann, M. A. Tucker, Z. Zhang, I. Baraffe, G. Chabrier, T. Forveille, S. A. Metchev, P. Tremblin, A. Do, A. V. Payne, B. J. Shappee, C. Z. Bond, S. Cetre, M. Chun, J.-R. Delorme, N. Jovanovic, S. Lilley, D. Mawet, S. Ragland, E. Wetherell, and P. Wizinowich (2019). WISE J072003.20-084651.2B is a Massive T Dwarf. *The Astronomical Journal*, **158**(5), p. 174. ISSN 1538-3881. doi:10.3847/1538-3881/ab3cd1.

Dupuy, T. J., M. C. Liu, and B. P. Bowler (2009a). Dynamical mass of the M8+M8 binary 2mass J22062280 - 2047058AB. *Astrophysical Journal*, **706**(1), pp. 328–342. ISSN 15384357. doi:10.1088/0004-637X/706/1/328.

Dupuy, T. J., M. C. Liu, and M. J. Ireland (2009b). Dynamical mass of the substellar benchmark binary HD 130948BC. *Astrophysical Journal*, **692**(1), pp. 729–752. ISSN 15384357. doi:10.1088/0004-637X/692/1/729.

Dupuy, T. J., M. C. Liu, and M. J. Ireland (2014). New evidence for a substellar luminosity problem: Dynamical mass for the brown dwarf binary gl 417BC. *Astrophysical Journal*, **790**(2). ISSN 15384357. doi:10.1088/0004-637X/790/2/133.

Dupuy, T. J., M. C. Liu, S. K. Leggett, M. J. Ireland, K. Chiu, and D. A. Golimowski (2015). The mass-luminosity relation in the L/T transition: Individual dynamical masses for the new J-band flux reversal binary SDSS J105213.51+442255.7AB.

Astrophysical Journal, **805**(1), pp. 1–13. ISSN 15384357. doi:10.1088/0004-637X/805/1/56.

Epchtein, N., B. De Batz, L. Capoani, L. Chevallier, E. Copet, P. Fouque, F. Lacombe, T. Le Bertre, S. Pau, D. Rouan, S. Ruphy, G. Simon, D. Tiphene, W. B. Burton, E. Bertin, E. Deul, H. Habing, J. Borsenberger, M. Dennefeld, F. Guglielmo, C. Loup, G. Mamon, Y. Ng, A. Omont, L. Provost, J. C. Renault, F. Tanguy, S. Kimeswenger, C. Kienel, F. Garzon, P. Persi, M. Ferrari-Toniolo, A. Robin, G. Paturel, I. Vauglin, T. Forveille, X. Delfosse, J. Hron, M. Schultheis, I. Appenzeller, S. Wagner, L. Balazs, A. Holl, J. Lepine, P. Boscolo, E. Picazzio, P. A. Duc, and M. O. Mennessier (1997). The Deep Near-Infrared Southern Sky Survey (DENIS). *The Messanger*, **87**, pp. 27–34.

Eriksson, U., C. Linder, J. Airey, and A. Redfors (2014). Who Needs 3D When the Universe Is Flat? *Science Education*, **98**(3), pp. 412–442. ISSN 1098237X. doi:10.1002/sce.21109.

Faherty, J. K., A. J. Burgasser, F. M. Walter, N. Van Der Bliek, M. M. Shara, K. L. Cruz, A. A. West, F. J. Vrba, and G. Anglada-Escudé (2012). The Brown Dwarf Kinematics Project (BDKP). III. Parallaxes for 70 ultracool dwarfs. *Astrophysical Journal*, **752**(1). ISSN 15384357. doi:10.1088/0004-637X/752/1/56.

Faherty, J. K., A. R. Riedel, K. L. Cruz, J. Gagne, J. C. Filippazzo, E. Lambrides, H. Fica, A. Weinberger, J. R. Thorstensen, C. G. Tinney, V. Baldassare, E. Lemonier, and E. L. Rice (2016). Population Properties of Brown Dwarf Analogs To Exoplanets. *The Astrophysical Journal Supplement Series*, **225**(1), p. 10. ISSN 0067-0049. doi:10.3847/0067-0049/225/1/10.

Fegley Jr., B. and K. Lodders (1996). Atmospheric Chemistry of the Brown Dwarf Gliese 229B: Thermochemical Equilibrium Predictions. *The Astrophysical Journal*, **472**(1), pp. L37–L39.

Ferguson, J. W., D. R. Alexander, F. Allard, T. Barman, J. G. Bodnarik, P. H. Hauschildt, A. Heffner-Wong, and A. Tamanai (2005). Low-Temperature Opacities. *The Astrophysical Journal*, **623**(1), pp. 585–596. ISSN 0004-637X. doi:10.1086/428642.

Fergusson, J., C. Oliver, and M. R. Walter (2012). Astrobiology outreach and the nature of science: the role of creativity. *Astrobiology*, **12**(12), pp. 1143–53. ISSN 1557-8070. doi:10.1089/ast.2012.0873.

Filippazzo, J. C., E. L. Rice, J. Faherty, K. L. Cruz, M. M. Van Gordon, and D. L. Looper (2015). FUNDAMENTAL PARAMETERS and SPECTRAL ENERGY

DISTRIBUTIONS of YOUNG and FIELD AGE OBJECTS with MASSES SPANNING the STELLAR to PLANETARY REGIME. *Astrophysical Journal*, **810**(2). ISSN 15384357. doi:10.1088/0004-637X/810/2/158.

Fontenla, J. M., P. C. Stancil, and E. Landi (2015). SOLAR SPECTRAL IRRADIANCE, SOLAR ACTIVITY, and the NEAR-ULTRA-VIOLET. *Astrophysical Journal*, **809**(2), p. 157. ISSN 15384357. doi:10.1088/0004-637X/809/2/157.

Freedman, R. S., M. S. Marley, and K. Lodders (2008). Line and Mean Opacities for Ultracool Dwarfs and Extrasolar Planets. *The Astrophysical Journal Supplement Series*, **174**(2), pp. 504–513. ISSN 0067-0049. doi:10.1086/521793.

Freytag, B., F. Allard, H. G. Ludwig, D. Homeier, and M. Steffen (2010). The role of convection, overshoot, and gravity waves for the transport of dust in M dwarf and brown dwarf atmospheres. *Astronomy and Astrophysics*, **513**(4), pp. 1–14. ISSN 14320746. doi:10.1051/0004-6361/200913354.

Friedman, W. (1989). The representation of temporal structure in children, adolescents, and adults. In Levin, I. and D. Zakay (eds.) *Time and human cognition: A life span perspective*, pp. 259–304. Holland, Amsterdam.

Gaidos, E. J. (1998). Nearby Young Solar Analogs. I. Catalog and Stellar Characteristics. *Publications of the Astronomical Society of the Pacific*, **110**(753), pp. 1259–1276. ISSN 0004-6280. doi:10.1086/316251.

Gao, P., M. S. Marley, and A. S. Ackerman (2018). Sedimentation Efficiency of Condensation Clouds in Substellar Atmospheres. *The Astrophysical Journal*, **855**(2), p. 86. ISSN 1538-4357. doi:10.3847/1538-4357/aab0a1.

Gao, P., D. P. Thorngren, G. K. Lee, J. J. Fortney, C. V. Morley, H. R. Wakeford, D. K. Powell, K. B. Stevenson, and X. Zhang (2020). Aerosol composition of hot giant exoplanets dominated by silicates and hydrocarbon hazes. *Nature Astronomy*, **4**(10), pp. 951–956. ISSN 23973366. doi:10.1038/s41550-020-1114-3.

Gao, P., H. R. Wakeford, S. E. Moran, and V. Parmentier (2021). Aerosols in Exoplanet Atmospheres. *Journal of Geophysical Research: Planets*, **126**(4), pp. 1–46. ISSN 21699100. doi:10.1029/2020JE006655.

Gelino, C. R., R. L. Smart, F. Marocco, J. D. Kirkpatrick, M. C. Cushing, G. Mace, R. A. Mendez, C. G. Tinney, and H. R. Jones (2014). WISEP J061135.13-041024.0 AB: A J-band flux reversal binary at the L/T transition. *Astronomical Journal*, **148**(1), pp. 4–13. ISSN 00046256. doi:10.1088/0004-6256/148/1/6.

Gennaro, M., S. Baggett, and V. Bajaj (2019). A characterization of persistence at short times in the WFC3/IR detector. II. Technical report, STsCI.

Gentner, D. (2001). Spatial metaphors in temporal reasoning. In *Spatial Schemas in Abstract Thought*, pp. 203–222. ISBN 0262072130.

Gentner, D. and A. L. Stevens (eds.) (1983). *Mental Models*. Erlbaum, Hillsdale, NJ.

Gizis, J. E., J. K. Faherty, M. C. Liu, P. J. Castro, J. D. Shaw, F. J. Vrba, H. C. Harris, K. M. Aller, and N. R. Deacon (2012). Discovery of an unusually red L-type brown dwarf. *Astronomical Journal*, **144**(4), pp. 1–7. ISSN 00046256. doi:10.1088/0004-6256/144/4/94.

Glaser, B. and A. Strauss (1967). *The Discovery of Grounded Theory: Strategies for Qualitative Research*. Aldine Transaction, Piscataway.

Golimowski, D. A., S. K. Leggett, M. S. Marley, X. Fan, T. R. Geballe, G. R. Knapp, F. J. Vrba, A. A. Henden, C. B. Luginbuhl, H. H. Guetter, J. A. Munn, B. Canzian, W. Zheng, Z. I. Tsvetanov, K. Chiu, K. Glazebrook, E. A. Hoversten, D. P. Schneider, and J. Brinkmann (2004). L and M Photometry of Ultracool Dwarfs . *The Astronomical Journal*, **127**(6), pp. 3516–3536. ISSN 0004-6256. doi:10.1086/420709.

Goto, M., N. Kobayashi, H. Terada, W. Gaessler, T. Kanzawa, H. Takami, N. Takato, Y. Hayano, Y. Kamata, M. Iye, D. J. Saint-Jacques, A. T. Tokunaga, D. Potter, and M. Cushing (2002). Near-Infrared Adaptive Optics Spectroscopy of Binary Brown Dwarfs HD 130948B and HD 130948C. *The Astrophysical Journal*, **567**(1), pp. L59–L62. ISSN 0004-637X. doi:10.1086/339800.

Grieves, N., F. Bouchy, M. Lendl, T. Carmichael, I. Mireles, A. Shporer, K. K. McLeod, K. A. Collins, R. Brahm, K. G. Stassun, S. Gill, L. G. Bouma, T. Guillot, M. Cointepas, L. A. Dos Santos, S. L. Casewell, J. M. Jenkins, T. Henning, L. D. Nielsen, A. Psaridi, S. Udry, D. Ségransan, J. D. Eastman, G. Zhou, L. Abe, A. Agabi, G. Bakos, D. Charbonneau, K. I. Collins, K. D. Colon, N. Crouzet, G. Dransfield, P. Evans, R. F. Goeke, R. Hart, J. M. Irwin, E. L. Jensen, A. Jordán, J. F. Kielkopf, D. W. Latham, W. Marie-Sainte, D. Mékarnia, P. Nelson, S. N. Quinn, D. J. Radford, D. R. Rodriguez, P. Rowden, F. X. Schmider, R. P. Schwarz, J. C. Smith, C. Stockdale, O. Suarez, T. G. Tan, A. H. Triaud, W. Waalkes, and G. Wingham (2021). Populating the brown dwarf and stellar boundary: Five stars with transiting companions near the hydrogen-burning mass limit. *Astronomy and Astrophysics*, **652**. ISSN 14320746. doi: 10.1051/0004-6361/202141145.

Grondin, S. (2010). Timing and Time Perception: A review of recent behavioral neuroscience findings and theoretical directions. *Attention, Perception, and Psychophysics*, **72**(561). doi:10.3758/APP.

Hammer, D. (1996). Misconceptions or P-Prims: How May Alternative Perspectives of Cognitive Structure Influence Instructional Perceptions and Intentions? *Journal of the Learning Sciences*, **5**(2), pp. 97–127. ISSN 10508406. doi:10.1207/s15327809jls0502_1.

Hammer, D., A. Elby, R. E. Scherr, E. F. Redish, D. Hammer, A. Elby, R. E. Scherr, and E. F. Redish (2004). Resources , framing , and transfer Resources , framing , and transfer. In Mestre, J. P. (ed.) *Transfer of Learning from a Modern Multidisciplinary Perspective*, Rec 0087519, pp. 1–26. Information Age Publishing, Greenwich, CT.

Hannust, T. and E. Kikas (2010). Young children's acquisition of knowledge about the Earth: A longitudinal study. *Journal of Experimental Child Psychology*, **107**(2), pp. 164–180. ISSN 00220965. doi:10.1016/j.jecp.2010.04.002.

Hauschildt, P. H., F. Allard, and E. Baron (1998). The NextGen Model Atmosphere grid for 300010000. *The Astrophysical Journal*, **512**(1), p. 377. ISSN 0004-637X. doi:10.1086/306745.

Hauschildt, P. H., F. Allard, and E. Baron (1999). The NextGen Model Atmosphere Grid for aastex amsbsy amsfonts amssymb bm mathrsfs pifont stmaryrd textcomp portland,xspace. *The Astrophysical Journal*, **512**(1), pp. 377–385. ISSN 0004-637X. doi:10.1086/306745.

Hauschildt, P. H., S. N. Shore, G. J. Schwarz, E. Baron, S. Starrfield, and F. Allard (1997). Detailed Non-LTE Model Atmospheres for Novae during Outburst. I. New Theoretical Results. *The Astrophysical Journal*, **490**(2), pp. 803–818. ISSN 0004-637X. doi:10.1086/304904.

Hauschildt, P. H. and S. Starrfield (1995). The Physics of Early Nova Spectra. *The Astrophysical Journal*, **447**(1), pp. 829–847.

Hegarty, M. and D. Waller (2004). A dissociation between mental rotation and perspective-taking spatial abilities. *Intelligence*, **32**(2), pp. 175–191. ISSN 01602896. doi:10.1016/j.intell.2003.12.001.

Helling, C., A. Ackerman, F. Allard, M. Dehn, P. Hauschildt, D. Homeier, K. Lodders, M. Marley, F. Rietmeijer, T. Tsuji, and P. Woitke (2008a). A comparison of chemistry and dust cloud formation in ultracool dwarf model atmospheres. *Monthly Notices of the Royal Astronomical Society*, **391**(4), pp. 1854–1873. ISSN 00358711. doi:10.1111/j.1365-2966.2008.13991.x.

Helling, C. and S. Casewell (2014). Atmospheres of brown dwarfs. *Astronomy and Astrophysics Review*, **22**(1), pp. 1–45. ISSN 09354956. doi:10.1007/s00159-014-0080-0.

Helling, C., M. Dehn, P. Woitke, and P. H. Hauschildt (2008b). Consistent Simulations of Substellar Atmospheres and Nonequilibrium Dust Cloud Formation. *The Astrophysical Journal*, **675**(2), pp. L105–L108. ISSN 0004-637X. doi: 10.1086/533462.

Helling, C. and P. Woitke (2006). Dust in brown dwarfs V. Growth and evaporation of dirty dust grains. *Astronomy and Astrophysics*, **455**(1), pp. 325–338. ISSN 00046361. doi:10.1051/0004-6361:20054598.

Helling, C., P. Woitke, and W. F. Thi (2008c). Dust in brown dwarfs and extrasolar planets: I. Chemical composition and spectral appearance of quasi-static cloud layers. *Astronomy and Astrophysics*, **485**(2), pp. 547–560. ISSN 00046361. doi:10.1051/0004-6361:20078220.

Hennebelle, P. and G. Chabrier (2008). Analytical Theory for the Initial Mass Function: CO Clumps and Prestellar Cores. *The Astrophysical Journal*, **684**(1), pp. 395–410. ISSN 0004-637X. doi:10.1086/589916.

Heyer, I., S. J. Slater, and T. F. Slater (2013). Establishing the emprical relationship between non-science majoring undergraduate learners' spatial thinking skills and their conceptual astronomy knowledge. *Revista Latino-Americana de Educação em Astronomia - RELEA*, (16), pp. 45–61. ISSN 0419-4209.

Hinkel, N. R., F. X. Timmes, P. A. Young, M. D. Pagano, and M. C. Turnbull (2014). Stellar abundances in the solar neighborhood: The hypatia catalog. *Astronomical Journal*, **148**(3). ISSN 00046256. doi:10.1088/0004-6256/148/3/54.

Hiranaka, K., K. L. Cruz, S. T. Douglas, M. S. Marley, and V. F. Baldassare (2016). Exploring the Role of Sub-Micron-Sized Dust Grains in the Atmospheres of Red L0–L6 Dwarfs. *The Astrophysical Journal*, **830**(2), p. 96. ISSN 1538-4357. doi: 10.3847/0004-637x/830/2/96.

Jelinek, J. A. (2021). Children's astronomy. Development of the shape of the earth concept in polish children between 5 and 10 years of age. *Education Sciences*, **11**(2), pp. 1–21. ISSN 22277102. doi:10.3390/educsci11020075.

Johnson-Laird, P. N. (ed.) (1983). *Mental Models*. Harvard University Press, Cambridge, MA.

Jones, H. R. A. and T. Tsuji (1997). Spectral Evidence for Dust in Late-Type M Dwarfs. *The Astrophysical Journal*, **480**(1), pp. L39–L41. ISSN 0004637X. doi:10.1086/310619.

Kaplan, L. D. (1959). No Title. *Journal of the Optical Society of America (1917-1983)*, **49**, p. 1004.

Kasper, M., A. Burrows, and W. Brandner (2009). Testing the models: NIR imaging and spectroscopy of the benchmark T-dwarf binary Eps Indi B. *Astrophysical Journal*, **695**(1), pp. 788–792. ISSN 15384357. doi:10.1088/0004-637X/695/1/788.

Kikas, E. (2006). The effect of verbal and visuo-spatial abilities on the development of knowledge of the Earth. *Research in Science Education*, **36**(3), pp. 269–283. ISSN 0157244X. doi:10.1007/s11165-005-9010-5.

King, R. R., M. J. McCaughrean, D. Homeier, F. Allard, R. D. Scholz, and N. Lodieu (2010). ϵ Indi Ba, Bb: A detailed study of the nearest known brown dwarfs. *Astronomy and Astrophysics*, **510**(1). ISSN 00046361. doi:10.1051/0004-6361/200912981.

Kirkpatrick, J. D. (2005). New Spectral Types L and T. *Annual Review of Astronomy and Astrophysics*, **43**(1), pp. 195–245. ISSN 0066-4146. doi:10.1146/annurev.astro.42.053102.134017.

Kirkpatrick, J. D., K. L. Cruz, T. S. Barman, A. J. Burgasser, D. L. Looper, C. G. Tinney, C. R. Gelino, P. J. Lowrance, J. Liebert, J. M. Carpenter, L. A. Hillenbrand, and J. R. Stauffer (2008). A Sample of Very Young Field L Dwarfs and Implications for the Brown Dwarf "Lithium Test" at Early Ages. *The Astrophysical Journal*, **689**(2), pp. 1295–1326. ISSN 0004-637X. doi:10.1086/592768.

Kirkpatrick, J. D., C. R. Gelino, M. C. Cushing, G. N. MacE, R. L. Griffith, M. F. Skrutskie, K. A. Marsh, E. L. Wright, P. R. Eisenhardt, I. S. McLean, A. K. Mainzer, A. J. Burgasser, C. G. Tinney, S. Parker, and G. Salter (2012). Further defining spectral type "y" and exploring the low-mass end of the field brown dwarf mass function. *Astrophysical Journal*, **753**(2). ISSN 15384357. doi:10.1088/0004-637X/753/2/156.

Kirkpatrick, J. D., C. R. Gelino, J. K. Faherty, A. M. Meisner, D. Caselden, A. C. Schneider, F. Marocco, A. J. Cayago, R. L. Smart, P. R. Eisenhardt, M. J. Kuchner, E. L. Wright, M. C. Cushing, K. N. Allers, D. C. Bardalez Gagliuffi, A. J. Burgasser, J. Gagné, S. E. Logsdon, E. C. Martin, J. G. Ingalls, P. J. Lowrance, E. S. Abrahams, C. Aganze, R. Gerasimov, E. C. Gonzales, C.-C. Hsu, N. Kamraj, R. Kiman, J. Rees, C. Theissen, K. Ammar, N. S. Andersen, P. Beaulieu, G. Colin, C. A. Elachi, S. J. Goodman, L. Gramaize, L. K. Hamlet, J. Hong, A. Jonkeren, M. Khalil, D. W. Martin, W. Pendrill, B. Pumphrey, A. Rothermich, A. Sainio, A. Stenner, C. Tanner, M. Thévenot, N. V. Voloshin, J. Walla, and Z. Wędracki (2021). The Field Substellar Mass Function Based on the Full-sky 20 pc Census of 525 L, T, and Y Dwarfs. *The Astrophysical Journal Supplement Series*, **253**(1), p. 7. ISSN 0067-0049. doi:10.3847/1538-4365/abd107.

Kirkpatrick, J. D., D. L. Looper, A. J. Burgasser, S. D. Schurr, R. M. Cutri, M. C. Cushing, K. L. Cruz, A. C. Sweet, G. R. Knapp, T. S. Barman, J. J. Bochanski, T. L. Roellig, I. S. McLean, M. R. McGovern, and E. L. Rice (2010). Discoveries from a near-infrared proper motion survey using multi-epoch Two Micron All-Sky Survey data. *Astrophysical Journal, Supplement Series*, **190**(1), pp. 100–146. ISSN 00670049. doi:10.1088/0067-0049/190/1/100.

Kirkpatrick, J. D., E. C. Martin, R. L. Smart, A. J. Cayago, C. A. Beichman, F. Marocco, C. R. Gelino, J. K. Faherty, M. C. Cushing, A. C. Schneider, G. N. Mace, C. G. Tinney, E. L. Wright, P. J. Lowrance, J. G. Ingalls, F. J. Vrba, J. A. Munn, S. E. Dahm, and I. S. McLean (2019). Preliminary Trigonometric Parallaxes of 184 Late-T and Y Dwarfs and an Analysis of the Field Substellar Mass Function into the "Planetary" Mass Regime. *The Astrophysical Journal Supplement Series*, **240**(2), p. 19. ISSN 0067-0049. doi:10.3847/1538-4365/aaf6af.

Kirkpatrick, J. D., I. N. Reid, J. Liebert, R. M. Cutri, B. Nelson, C. A. Beichman, C. C. Dahn, D. G. Monet, J. E. Gizis, and M. F. Skrutskie (1999). Dwarfs Cooler than "M": The Definition of Spectral Type "L" Using Discoveries from the 2 Micron All-Sky Survey (2MASS). *The Astrophysical Journal*, **519**(2), pp. 802–833. ISSN 0004-637X. doi:10.1086/307414.

Knapp, G. R., S. K. Leggett, X. Fan, M. S. Marley, T. R. Geballe, D. A. Golimowski, F. D., J. E. Gunn, J. Hennawi, Z. Ivezic, R. H. Lupton, D. J. Schlegel, M. A. Strauss, Z. I. Tsvetanova, K. Chiu, E. A. Hoversten, K. Glazebrook, W. Zheng, M. Hendrickson, C. C. Williams, A. Uomoto, F. J. Vrba, A. A. Henden, C. B. Luginbuhl, H. H. Guetter, J. A. Munn, B. Canzian, D. P. Schneider, and J. Brinkmann (2004). Near-infrared photometry and spectroscopy of L and T dwarfs: The effects of clouds, gravity, and effective temperature. *The Astrophysical Journal*, (127), pp. 3553–3578. ISSN 03796566.

Konopacky, Q. M., A. M. Ghez, T. S. Barman, E. L. Rice, J. I. Bailey, R. J. White, I. S. McLean, and G. Duchne (2010). High-precision dynamical masses of very low mass binaries. *Astrophysical Journal*, **711**(2), pp. 1087–1122. ISSN 15384357. doi:10.1088/0004-637X/711/2/1087.

Konopacky, Q. M., A. M. Ghez, D. C. Fabrycky, B. A. MacIntosh, R. J. White, T. S. Barman, E. L. Rice, G. Hallinan, and G. Duchêne (2012). Rotational velocities of individual components in very low mass binaries. *Astrophysical Journal*, **750**(1). ISSN 15384357. doi:10.1088/0004-637X/750/1/79.

Krabbe, A., T. Gasaway, I. Song, C. Iserlohe, J. Weiss, J. E. Larkin, M. Barczys, and D. Lafreniere (2004). Data reduction pipeline for OSIRIS, the new NIR diffraction-limited imaging field spectrograph for the Keck adaptive optics system. In *Ground-based Instrumentation for Astronomy*, p. Volume 5492.

Kumar, S. S. (1963). The Structure of Stars of Very Low Mass. *The Astrophysical Journal*, **137**(1), p. 1121.

Kurby, C. A. and J. M. Zacks (2011). Age differences in the perception of hierarchical structure in events. *Memory and Cognition*, **39**(1), pp. 75–91. ISSN 0090502X. doi:10.3758/s13421-010-0027-2.

Landy, D., N. Silbert, and A. Goldin (2013). Estimating large numbers. *Cognitive Science*, **37**(5), pp. 775–799. ISSN 03640213. doi:10.1111/cogs.12028.

Lane, B. F., M. R. Z. Osorio, M. C. Britton, E. L. Martin, and S. R. Kulkarni (2002). The Orbit of the Brown Dwarf Binary Gliese 569B. *The Astrophysical Journal*, **560**(1), pp. 390–399. ISSN 0004-637X. doi:10.1086/322506.

Larkin, J., M. Barczys, A. Krabbe, S. Adkins, T. Aliado, P. Amico, G. Brims, R. Campbell, J. Canfield, T. Gasaway, A. Honey, C. Iserlohe, C. Johnson, E. Kress, D. LaFreniere, K. Magnone, N. Magnone, M. McElwain, J. Moon, A. Quirrenbach, G. Skulason, I. Song, M. Spencer, J. Weiss, and S. Wright (2006). OSIRIS: A diffraction limited integral field spectrograph for Keck. *New Astronomy Reviews*, **50**(4-5), pp. 362–364. ISSN 13876473. doi:10.1016/j.newar.2006.02.005.

Lee, H. S., O. L. Liu, C. A. Price, and A. L. Kendall (2011). College students' temporal-magnitude recognition ability associated with durations of scientific changes. *Journal of Research in Science Teaching*, **48**(3), pp. 317–335. ISSN 00224308. doi:10.1002/tea.20401.

Leggett, S. K., T. R. Geballe, X. Fan, D. P. Schneider, J. E. Gunn, R. H. Lupton, G. R. Knapp, M. A. Strauss, A. McDaniel, D. A. Golimowski, T. J. Henry, E. Peng, Z. I. Tsvetanov, A. Uomoto, W. Zheng, G. J. Hill, L. W. Ramsey, S. F. Anderson, J. A. Annis, N. A. Bahcall, J. Brinkmann, B. Chen, I. Csabai, M. Fukugita, G. S. Hennessy, R. B. Hindsley, Ž. Ivezić, D. Q. Lamb, J. A. Munn, J. R. Pier, D. J. Schlegel, J. A. Smith, C. Stoughton, A. R. Thakar, and D. G. York (2000). The Missing Link: Early Methane ("T") Dwarfs in the Sloan Digital Sky Survey. *The Astrophysical Journal*, **536**(1), pp. L35–L38. ISSN 0004637X. doi:10.1086/312728.

Leggett, S. K., D. A. Golimowski, X. Fan, T. R. Geballe, G. R. Knapp, J. Brinkmann, I. Csabai, J. E. Gunn, S. L. Hawley, T. J. Henry, R. Hindsley, Ž. Ivezić, R. H. Lupton, J. R. Pier, D. P. Schneider, J. A. Smith, M. A. Strauss, A. Uomoto, and D. G. York (2002). Infrared Photometry of Late-M, L, and T Dwarfs. *The Astrophysical Journal*, **564**(1), pp. 452–465. ISSN 0004-637X. doi:10.1086/324037.

Leggett, S. K., D. Saumon, L. Albert, M. C. Cushing, M. C. Liu, K. L. Luhman, M. S. Marley, J. D. Kirkpatrick, T. L. Roellig, and K. N. Allers (2008). HN Peg

B: A Test of Models of the L to T Dwarf Transition. *The Astrophysical Journal*, **682**(2), pp. 1256–1263. ISSN 0004-637X. doi:10.1086/589146.

Lelliott, A. and M. Rollnick (2010). Big Ideas: A review of astronomy education research 1974–2008. *International Journal of Science Education*, **32**(13), pp. 1771–1799. ISSN 0950-0693. doi:10.1080/09500690903214546.

Levin, I. (1992). The Development of the Concept of Time in Children: An Integrative Model. In Macar, F., V. Pouthas, and W. J. Friedman (eds.) *Time, Action and Cognition: Towards Bridging the Gap*, pp. 13–32. Springer Netherlands, Dordrecht. ISBN 978-94-017-3536-0. doi:10.1007/978-94-017-3536-0_3.

Lew, B. W. P., D. Apai, M. Marley, D. Saumon, G. Schneider, Y. Zhou, N. B. Cowan, T. Karalidi, E. Manjavacas, L. R. Bedin, and P. A. Miles-Páez (2020). Cloud Atlas: Unraveling the vertical cloud structure with the time-series spectrophotometry of an unusually red brown dwarf. *The Astrophysical Journal*, **903**(1). ISSN 23318422. doi:10.3847/1538-4357/abb81d.

Lew, B. W. P., D. Apai, Y. Zhou, G. Schneider, A. J. Burgasser, T. Karalidi, H. Yang, M. S. Marley, N. B. Cowan, L. R. Bedin, S. A. Metchev, J. Radigan, and P. J. Lowrance (2016). Cloud Atlas: Discovery of Patchy Clouds and High-amplitude Rotational Modulations In a Young, Extremely Red L-type Brown Dwarf. *The Astrophysical Journal Letters*, **829**(2), pp. 1–7. ISSN 2041-8213. doi:10.3847/2041-8205/829/2/L32.

Libarkin, J. C. and S. W. Anderson (2005). Assessment of Learning in Entry-Level Geoscience Courses : Results from the Geoscience Concept Inventory. *Journal of Geoscience Education*, **53**(4), pp. 394–401. ISSN 10899995.

Libarkin, J. C., S. W. Anderson, J. Dahl, M. Beilfuss, and W. Boone (2005). Qualitative Analysis of College Students' Ideas About the Earth: Interviews and Open-Ended Questionnaires. *Journal of Geoscience Education*, **53**(1), pp. 17–26. ISSN 10899995.

Libarkin, J. C., J. P. Kurdziel, and S. W. Anderson (2007). College Student Conceptions of Geological Time and the Disconnect Between Ordering and Scale. *Journal of Geoscience Education*, **55**(5), pp. 413–422. ISSN 10899995.

Liben, L. S. and R. M. Downs (1993). Understanding person-space-map relations: Cartographic and developmental perspectives. *Developmental Psychology*, **29**(73).

Line, M. R., M. S. Marley, M. C. Liu, B. Burningham, C. V. Morley, N. R. Hinkel, J. Teske, J. J. Fortney, R. Freedman, and R. Lupu (2017). Uniform Atmospheric Retrieval Analysis of Ultracool Dwarfs. II. Properties of 11 T dwarfs. *The Astrophysical Journal*, **848**(2), p. 83. ISSN 0004-637X. doi:10.3847/1538-4357/aa7ff0.

Liu, M. C., T. J. Dupuy, and K. N. Allers (2016). The Hawaii Infrared Parallax Program. II. Young Ultracool Field Dwarfs. *The Astrophysical Journal*, **833**(1), pp. 1–65. ISSN 1538-4357. doi:10.3847/1538-4357/833/1/96.

Liu, M. C., T. J. Dupuy, and M. J. Ireland (2008). Keck Laser Guide Star Adaptive Optics Monitoring of 2MASS J153449842952274AB: First Dynamical Mass Determination of a Binary T Dwarf. *The Astrophysical Journal*, **689**(1), pp. 436–460. ISSN 0004-637X. doi:10.1086/591837.

Lockhart, K. E., T. Do, J. E. Larkin, A. Boehle, R. D. Campbell, S. Chappell, D. Chu, A. Ciurlo, M. Cosens, M. P. Fitzgerald, A. Ghez, J. R. Lu, J. E. Lyke, E. Mieda, A. R. Rudy, A. Vayner, G. Walth, and S. A. Wright (2019). Characterizing and Improving the Data Reduction Pipeline for the Keck OSIRIS Integral Field Spectrograph. *The Astronomical Journal*, **157**(2), p. 75. ISSN 0004-6256. doi:10.3847/1538-3881/aaf64e.

Lodders, K. and B. Fegley (2002). Atmospheric chemistry in giant planets, brown dwarfs, and low-mass dwarf stars. I. Carbon, nitrogen, and oxygen. *Icarus*, **155**(2), pp. 393–424. ISSN 00191035. doi:10.1006/icar.2001.6740.

Looper, D. L., J. D. Kirkpatrick, and A. J. Burgasser (2008a). Discovery of 11 New T Dwarfs in the Two Micron All Sky Survey, Including a Possible L/T Transition Binary. *The Astronomical Journal*, **134**(3), pp. 1162–1182. ISSN 0004-6256. doi:10.1086/520645.

Looper, D. L., J. D. Kirkpatrick, R. M. Cutri, T. Barman, A. J. Burgasser, M. C. Cushing, T. Roellig, M. R. McGovern, I. S. McLean, E. Rice, B. J. Swift, and S. D. Schurr (2008b). Discovery of Two Nearby Peculiar L Dwarfs from the 2MASS Proper-Motion Survey: Young or Metal-Rich? *The Astrophysical Journal*, **686**(1), pp. 528–541. ISSN 0004-637X. doi:10.1086/591025.

Luhman, K. L., E. E. Mamajek, P. R. Allen, and K. L. Cruz (2009). An infrared/x-ray survey for new members of the taurus star-forming region. *Astrophysical Journal*, **703**(1), pp. 399–419. ISSN 15384357. doi:10.1088/0004-637X/703/1/399.

Luna, J. L. and C. V. Morley (2021). Empirically Determining Substellar Cloud Compositions in the era of JWST. pp. 1–24.

Lunine, J. I., W. B. Hubbard, and M. S. Marley (1986). Evolution and Infrared Spectra of Brown Dwarfs. *The Astrophysical Journal*, **310**, pp. 238–260.

Ma, B. and J. Ge (2014). Statistical properties of brown dwarf companions: Implications for different formation mechanisms. *Monthly Notices of the Royal Astronomical Society*, **439**(3), pp. 2781–2789. ISSN 13652966. doi:10.1093/mnras/stu134.

Madhusudhan, N., O. Mousis, T. V. Johnson, and J. I. Lunine (2011). Carbon-rich giant planets: Atmospheric chemistry, thermal inversions, spectra, and formation conditions. *Astrophysical Journal*, **743**(2). ISSN 15384357. doi: 10.1088/0004-637X/743/2/191.

Maldonado, J. and E. Villaver (2017). Searching for chemical signatures of brown dwarf formation. *Astronomy and Astrophysics*, **602**. ISSN 14320746. doi:10.1051/0004-6361/201630120.

Mamajek, E. E. and L. A. Hillenbrand (2008). Improved Age Estimation for Solar-Type Dwarfs Using Activity-Rotation Diagnostics. *The Astrophysical Journal*, **687**(2), pp. 1264–1293. ISSN 0004-637X. doi:10.1086/591785.

Manjavacas, E., D. Apai, B. W. P. Lew, Y. Zhou, G. Schneider, A. J. Burgasser, T. Karalidi, P. A. Miles-Páez, P. J. Lowrance, N. Cowan, L. R. Bedin, M. S. Marley, S. Metchev, and J. Radigan (2019). Cloud Atlas: Rotational Spectral Modulations and Potential Sulfide Clouds in the Planetary-mass, Late T-type Companion Ross 458C. *The Astrophysical Journal*, **875**(2), p. L15. ISSN 2041-8213. doi:10.3847/2041-8213/ab13b9.

Manjavacas, E., D. Apai, Y. Zhou, T. Karalidi, B. W. P. Lew, G. Schneider, N. Cowan, S. Metchev, P. A. Miles-Páez, A. J. Burgasser, J. Radigan, L. R. Bedin, P. J. Lowrance, and M. S. Marley (2017). Cloud Atlas: Discovery of Rotational Spectral Modulations in a Low-mass, L-type Brown Dwarf Companion to a Star. *The Astronomical Journal*, **155**(1), p. 11. ISSN 1538-3881. doi: 10.3847/1538-3881/aa984f.

Marley, M. S., C. Gelino, D. Stephens, J. I. Lunine, and R. Freedman (1999). Reflected Spectra and Albedos of Extrasolar Giant Planets. I. Clear and Cloudy Atmospheres. *The Astrophysical Journal*, **513**(2), pp. 879–893. ISSN 0004-637X. doi:10.1086/306881.

Marley, M. S. and T. D. Robinson (2015). On the cool side: Modeling the atmospheres of brown dwarfs and giant planets. *Annual Review of Astronomy and Astrophysics*, **53**(1), pp. 279–323. ISSN 00664146. doi:10.1146/annurev-astro-082214-122522.

Marley, M. S., D. Saumon, and C. Goldblatt (2010). A patchy cloud model for the L to T dwarf transition. *Astrophysical Journal Letters*, **723**(1 PART 2), pp. 117–121. ISSN 20418213. doi:10.1088/2041-8205/723/1/L117.

Marley, M. S., D. Saumon, C. Visscher, R. Lupu, R. Freedman, C. Morley, J. J. Fortney, C. Seay, A. J. R. W. Smith, D. J. Teal, and R. Wang (2021). The Sonora Brown Dwarf Atmosphere and Evolution Models I. Model Description and Application to Cloudless Atmospheres in Rainout Chemical Equilibrium. *arXiv*.

Marley, M. S., S. Seager, D. Saumon, K. Lodders, A. S. Ackerman, R. S. Freedman, and X. Fan (2002). Clouds and Chemistry: Ultracool Dwarf Atmospheric Properties from Optical and Infrared Colors. *The Astrophysical Journal*, **568**(1), pp. 335–342. ISSN 0004-637X. doi:10.1086/338800.

Marocco, F., A. C. Day-jones, P. W. Lucas, H. R. Jones, R. L. Smart, Z. H. Zhang, J. I. Gomes, B. Burningham, D. J. Pinfield, R. Raddi, and L. Smith (2014). The extremely red L dwarf ULAS J222711-004547-dominated by dust. *Monthly Notices of the Royal Astronomical Society*, **439**(1), pp. 372–386. ISSN 00358711. doi:10.1093/mnras/stt2463.

Marois, C., B. Zuckerman, Q. M. Konopacky, B. Macintosh, and T. Barman (2010). Images of a fourth planet orbiting HR 8799. *Nature*, **468**(7327), pp. 1080–1083. ISSN 00280836. doi:10.1038/nature09684.

Marques, L. and D. Thompson (1997). Portuguese students' understanding at ages 10-11 and 14-15 of the origin and nature of the Earth and the development of life. *Research in Science Technological Education*, **15**(1), pp. 29–51. ISSN 0263-5143. doi:10.1080/0263514970150103.

Martín, E. L., G. Basri, and M. R. Z. Osorio (1999). The Lithium Test in Young Brown Dwarf Candidates. *The Astronomical Journal*, **118**(2), pp. 1005–1014. ISSN 00046256. doi:10.1086/300983.

Matlock, T., M. Ramscar, and L. Boroditsky (2005). On the experiential link between spatial and temporal language. *Cognitive Science*, **29**(4), pp. 655–664. ISSN 0364-0213. doi:10.1207/s15516709cog0000_17.

McLean, I. S., M. R. McGovern, A. J. Burgasser, J. D. Kirkpatrick, L. Prato, and S. S. Kim (2003). The NIRSPEC Brown Dwarf Spectroscopic Survey. I. Low-Resolution Near-Infrared Spectra. *The Astrophysical Journal*, **596**(1), pp. 561–586. ISSN 0004-637X. doi:10.1086/377636.

Mclean, I. S., L. Prato, M. R. Mcgovern, A. J. Burgasser, J. D. Kirkpatrick, E. L. Rice, and S. S. Kim (2007). THE NIRSPEC BROWN DWARF SPECTROSCOPIC SURVEY . II . HIGH-RESOLUTION Online material : color figures ONLINE MATERIALCOLOR FIGURES. *The Astrophysical Journal*, **658**, pp. 1217–1235.

Mclean, I. S., M. K. Wilcox, E. E. Becklin, D. F. Figer, A. M. Gilbert, J. R. Graham, J. E. Larkin, N. A. Levenson, H. I. Teplitz, and J. D. Kirkpatrick (2000). J-band Infrared Spectroscopy of a Sample of Brown Dwarfs using NIRSPEC on Keck II. *The Astrophysical Journal*, **533**, pp. 45–48.

Metchev, S. A., A. Heinze, D. Apai, D. Flateau, J. Radigan, A. Burgasser, M. S. Marley, É. Artigau, P. Plavchan, and B. Goldman (2015). Weather on other worlds. II. Survey results: Spots are ubiquitous on L and T dwarfs. *Astrophysical Journal*, **799**(2). ISSN 15384357. doi:10.1088/0004-637X/799/2/154.

Metchev, S. A. and L. A. Hillenbrand (2006). HD 203030B: An Unusually Cool Young Substellar Companion near the L/T Transition. *The Astrophysical Journal*, **651**(2), pp. 1166–1176. ISSN 0004-637X. doi:10.1086/507836.

Miles, B. E., A. J. I. Skemer, C. V. Morley, M. S. Marley, J. J. Fortney, K. N. Allers, J. K. Faherty, T. R. Geballe, A. C. Schneider, R. Lupu, R. S. Freedman, and G. L. Bjoraker (2020). Observations of Disequilibrium CO Chemistry in the Coldest Brown Dwarfs. *The Astronomical Journal*, **160**(2), p. 63. ISSN 1538-3881. doi:10.3847/1538-3881/ab9114.

Montangero, J. (1985). The Development of Temporal Inferences and Meanings in 5- to 8-Year Old Children. In *Time, Mind, and Behavior*, pp. 279–287. Springer Berlin Heidelberg, Berlin, Heidelberg. doi:10.1007/978-3-642-70491-8_19.

Morley, C. V., J. J. Fortney, M. S. Marley, C. Visscher, D. Saumon, and S. K. Leggett (2012). Neglected clouds in T and y dwarf atmospheres. *Astrophysical Journal*, **756**(2). ISSN 15384357. doi:10.1088/0004-637X/756/2/172.

Mould, J. R. (1975). A Study of M Dwarfs. I. Preliminary Model Atmospheres. *AA*, **38**, pp. 283–288.

Mould, J. R. (1976). A Study of M Dwarfs. II. A Grid of Model Atmospheres. *AA*, **48**, pp. 443–459.

Mullan, D. J. and J. MacDonald (2010). Magnetic models of the brown dwarfs HD 130948B and HD 130948C. *Astrophysical Journal*, **713**(2), pp. 1249–1255. ISSN 15384357. doi:10.1088/0004-637X/713/2/1249.

Nakajima, T., B. R. Oppenheimer, S. R. Kulkarni, D. A. Golimowski, K. Matthews, and S. T. Durrance (1995). Discovery of a cool brown dwarf. *Nature*, **378**(6556), pp. 463–465. ISSN 00280836. doi:10.1038/378463a0.

Nakajima, T., T. Tsuji, and K. Yanagisawa (2004). Spectral Classification and Effective Temperatures of L and T Dwarfs Based on Near-Infrared Spectra. *The Astrophysical Journal*, **607**(1), pp. 499–510. ISSN 0004-637X. doi:10.1086/383299.

Nussbaum, J. (1979). Children's conceptions of the earth as a cosmic body: A cross age study. *Science Education*, **63**, pp. 83–93.

Nussbaum, J. and J. D. Novak (1976). An assessment of children's concepts of the earth utilizing structured interviews. *Science Education*, **60**(4), pp. 535–550.

Oliver, C. A. and J. Fergusson (2007). Astrobiology: A pathway to adult science literacy? *Acta Astronautica*, **61**(7-8), pp. 716–723. ISSN 00945765. doi:10.1016/j.actaastro.2006.12.010.

Oppenheimer, B. R., S. R. Kulkarni, and K. Matthews (1998). The spectrum of the brown dwarf gliese 229b. *The Astrophysical Journal*, **1**, pp. 932–943.

Oppenheimer, B. R., S. R. Kulkarni, K. Matthews, and T. Nakajima (1995). Infrared Spectrum of the Cool Brown Dwarf Gl 229B. *Science*, **270**(5241), pp. 1478–1479.

Özdemir, G. and D. B. Clark (2007). An overview of conceptual change. *Eurasia Journal of Mathematics Science Technology Education*, **3**(4), pp. 351–361. ISSN 1305-8223. doi:10.1016/j.mseb.2009.10.004.

Piaget, J. (1929). *The child's perception of the world*. Kegan Paul, London, England.

Piaget, J. (1969). *The child's conception of time*. Ballantine Books, New York.

Piaget, J. and M. Gabain (1930). *The child's conception of physical causality*. Kegan Paul, London, England. ISBN 076580641X. doi:10.2307/1415393.

Plummer, J. (2011). Correction to: "Children Learning to Explain Daily Celestial Motion: Understanding astronomy across moving frames of reference". *International Journal of Science Education*, **33**(15), pp. 2181–2181. ISSN 0950-0693. doi:10.1080/09500693.2011.618256.

Plummer, J. D. (2009). A Cross-age Study of Children's Knowledge of Apparent Celestial Motion. *International Journal of Science Education*, **31**(12), pp. 1571–1605. ISSN 0950-0693. doi:10.1080/09500690802126635.

Plummer, J. D. (2014). Spatial thinking as the dimension of progress in an astronomy learning progression. *Studies in Science Education*, **50**(1), pp. 1–45.

Plummer, J. D., C. A. Bower, and L. S. Liben (2016). The role of perspective taking in how children connect reference frames when explaining astronomical phenomena. *International Journal of Science Education*, **38**(3), pp. 345–365. ISSN 0950-0693. doi:10.1080/09500693.2016.1140921.

Plummer, J. D., C. Palma, A. Flarend, K. Rubin, Y. S. Ong, B. Botzer, S. McDonald, and T. Furman (2015). Development of a learning progression for the formation of the solar system. *International Journal of Science Education*, **37**(9), pp. 1381–1401. ISSN 0950-0693. doi:10.1080/09500693.2015.1036386.

Pollack, J. B., O. Hubickyj, P. Bodenheimer, J. J. Lissauer, M. Podolak, and Y. Greenzweig (1996). Formation of the Giant Planets by Concurrent Accretion of Solids and Gas. *Icarus*, **124**(1), pp. 62–85.

Potter, D., E. L. Martín, M. C. Cushing, P. Baudoz, W. Brandner, O. Guyon, and R. Neuhäuser (2002). Hokupa'a-Gemini Discovery of Two Ultracool Companions to the Young Star HD 130948. *The Astrophysical Journal*, **567**(2), pp. L133–L136. ISSN 0004-637X. doi:10.1086/339999.

Prather, E. E., T. F. Slater, and E. G. Offerdahl (2002). Hints of a Fundamental Misconception in Cosmology. *Astronomy Education Review*, **1**(2), p. 28. doi:10.3847/AER2002003.

Radigan, J. (2014). An independent analysis of the Brown dwarf Atmosphere Monitoring (BAM) data: Large-amplitude variability is rare outside the L/T transition. *Astrophysical Journal*, **797**(2). ISSN 15384357. doi:10.1088/0004-637X/797/2/120.

Radvansky, G. A. and J. M. Zacks (2011). Event perception. *Wiley Interdisciplinary Reviews: Cognitive Science*, **2**(6), pp. 608–620. ISSN 19395078. doi:10.1002/wcs.133.

Reid, I. N., E. Lewitus, A. J. Burgasser, and K. L. Cruz (2006). 2MASS J225210731730134: A Resolved L/T Binary at 14 Parsecs. *The Astrophysical Journal*, **639**(2), pp. 1114–1119. ISSN 0004-637X. doi:10.1086/499484.

Rice, E. L., T. Barman, I. S. McLean, L. Prato, and J. D. Kirkpatrick (2010). Physical properties of young brown dwarfs and very low mass stars inferred from high-resolution model spectra. *Astrophysical Journal, Supplement Series*, **186**(1), pp. 63–84. ISSN 00670049. doi:10.1088/0067-0049/186/1/63.

Rossow, W. B. (1978). Cloud microphysics: Analysis of the clouds of Earth, Venus, Mars and Jupiter. *Icarus*, **36**(1), pp. 1–50. ISSN 10902643. doi:10.1016/0019-1035(78)90072-6.

Sahlmann, J., D. Ségransan, D. Queloz, S. Udry, N. C. Santos, M. Marmier, M. Mayor, D. Naef, F. Pepe, and S. Zucker (2011). Search for brown-dwarf companions of stars. *Astronomy and Astrophysics*, **525**(12), pp. 1–24. ISSN 00046361.

Saumon, D., P. Bergeron, J. I. Lunine, W. B. Hubbard, and A. Burrows (2012). Cool Zero-Metallicity Stellar Atmospheres. *The Astrophysical Journal*, **424**, pp. 333–344.

Saumon, D. and M. S. Marley (2008). The Evolution of L and T Dwarfs in Color-Magnitude Diagrams. *The Astrophysical Journal*, **689**(2), pp. 1327–1344. ISSN 0004-637X. doi:10.1086/592734.

Saumon, D., M. S. Marley, M. C. Cushing, S. K. Leggett, T. L. Roellig, K. Lodders, and R. S. Freedman (2006). Ammonia as a Tracer of Chemical Equilibrium in the T7.5 Dwarf Gliese 570D. *The Astrophysical Journal*, **647**(1), pp. 552–557. ISSN 0004-637X. doi:10.1086/505419.

Schmidt, S. J., A. A. West, A. J. Burgasser, J. J. Bochanski, and S. L. Hawley (2010). Discovery of an unusually blue l dwarf within 10 pc of the sun. *Astronomical Journal*, **139**(3), pp. 1045–1050. ISSN 00046256. doi:10.1088/0004-6256/139/3/1045.

Schneps, M. H., J. Ruel, G. Sonnert, M. Dussault, M. Griffin, and P. M. Sadler (2014). Conceptualizing astronomical scale: Virtual simulations on handheld tablet computers reverse misconceptions. *Computers and Education*, **70**, pp. 269–280. ISSN 03601315. doi:10.1016/j.compedu.2013.09.001.

Schoon, K. J. (1992). Students' Alternative Conceptions of Earth and Space. *Journal of Geological Education*, **40**(3), pp. 209–214. ISSN 00221368.

Schweingruber, H. A., R. A. Duschl, and A. W. Shouse (2007). *Taking Science to School:: Learning and Teaching Science in Grades K-8*. National Academies Press, Washington, DC. ISBN 0309102057. doi:10.1002/tea.20316.

Sharp, C. M. and A. Burrows (2007). Atomic and Molecular Opacities for Brown Dwarf and Giant Planet Atmospheres. *The Astrophysical Journal Supplement Series*, **168**(1), pp. 140–166. ISSN 0067-0049. doi:10.1086/508708.

Showman, A. P. and Y. Kaspi (2013). Atmospheric dynamics of brown dwarfs and directly imaged giant planets. *Astrophysical Journal*, **776**(2). ISSN 15384357. doi:10.1088/0004-637X/776/2/85.

Showman, A. P., X. Tan, and X. Zhang (2018). Atmospheric circulation of brown dwarfs and Jupiter and Saturn-like planets: Zonal jets, long-term variability, and QBO-type oscillations. *The Astronomical Journal*, **883**(1), p. 4. ISSN 0004-637X. doi:10.3847/1538-4357/ab384a.

Simon, M., S. Buxner, and C. Impey (2018). A survey and analysis of college students' understanding of planet formation before instruction. *Astrobiology*, **18**(12), pp. 1594–1610.

Skrutskie, M. F., R. M. Cutri, R. Stiening, M. D. Weinberg, S. Schneider, J. M. Carpenter, C. Beichman, R. Capps, T. Chester, J. Elias, J. Huchra, J. Liebert, C. Lonsdale, D. G. Monet, S. Price, P. Seitzer, T. Jarrett, J. D. Kirkpatrick, J. E. Gizis, E. Howard, T. Evans, J. Fowler, L. Fullmer, R. Hurt, R. Light, E. L. Kopan, K. A. Marsh, H. L. McCallon, R. Tam, S. Van Dyk, and S. Wheelock (2006). The

Two Micron All Sky Survey (2MASS). *The Astronomical Journal*, **131**(2), pp. 1163–1183. ISSN 0004-6256. doi:10.1086/498708.

Slater, S. J. (2015). The Development And Validation Of The Test Of Astronomy STandards (TOAST). *Journal of Astronomy Earth Sciences Education (JAESE)*, **1**(1), p. 1. ISSN 2374-6246. doi:10.19030/jaese.v1i1.9102.

Slater, T. F., J. P. Adams, and G. Brissenden (2001). What topics are taught in introductory astronomy courses? *The Physics Teacher*, **39**(52).

Smart, R. L., F. Marocco, J. A. Caballero, H. R. Jones, D. Barrado, J. C. Beamín, D. J. Pinfield, and L. M. Sarro (2017). The Gaia ultracool dwarf sample - I. Known L and T dwarfs and the first Gaia data release. *Monthly Notices of the Royal Astronomical Society: Letters*, **469**(1), pp. 401–415. ISSN 17453933. doi: 10.1093/mnras/stx800.

Staley, J. T. (2003). Astrobiology, the transcendent science: The promise of astrobiology as an integrative approach for science and engineering education and research. *Current Opinion in Biotechnology*, **14**(3), pp. 347–354. ISSN 09581669. doi:10.1016/S0958-1669(03)00073-9.

States, N. L. (2013). *Next Generation Science Standards: For States, By States*, volume 1-2. National Academies Press, Washington, DC. ISBN 0309272270. doi:10.17226/18290.

Stephens, D. C., S. K. Leggett, M. C. Cushing, M. S. Marley, D. Saumon, T. R. Geballe, D. A. Golimowski, X. Fan, and K. S. Noll (2009). The 0.8-14.5 μm Spectra of mid-L to mid-T dwarfs: Diagnostics of effective temperature, grain sedimentation, gas transport, and surface gravity. *Astrophysical Journal*, **702**(1), pp. 154–170. ISSN 15384357. doi:10.1088/0004-637X/702/1/154.

Stone, J. M., T. Barman, A. J. Skemer, Z. W. Briesemeister, L. S. Brock, P. M. Hinz, J. M. Leisenring, C. E. Woodward, M. F. Skrutskie, and E. Spalding (2020). High contrast thermal infrared spectroscopy with ALES: The 3-4µm spectrum of κ andromedae b. *arXiv*, **160**(6), p. 262. ISSN 23318422. doi:10.3847/1538-3881/abbef3.

Stone, J. M., J. Eisner, A. Skemer, K. M. Morzinski, L. Close, J. Males, T. J. Rodigas, P. Hinz, and A. Puglisi (2016). L-BAND SPECTROSCOPY WITH MAGELLAN-AO/Clio2: FIRST RESULTS ON YOUNG LOW-MASS COMPANIONS. *The Astrophysical Journal*, **829**(1), p. 39. ISSN 1538-4357. doi: 10.3847/0004-637x/829/1/39.

Straatemeier, M., H. L. J. van der Maas, and B. R. J. Jansen (2008). Children's knowledge of the earth: A new methodological and statistical approach. *Journal*

of Experimental Child Psychology, **100**(4), pp. 276–296. ISSN 00220965. doi: 10.1016/j.jecp.2008.03.004.

Tan, X. and A. P. Showman (2019). Atmospheric Variability Driven by Radiative Cloud Feedback in Brown Dwarfs and Directly Imaged Extrasolar Giant Planets. *The Astrophysical Journal*, **874**(2), p. 111. ISSN 0004-637X. doi: 10.3847/1538-4357/ab0c07.

Tan, X. and A. P. Showman (2021). Atmospheric circulation of brown dwarfs and directly imaged exoplanets driven by cloud radiative feedback: effects of rotation. *Monthly Notices of the Royal Astronomical Society*, **502**(1), pp. 678–699. ISSN 23318422. doi:10.1093/mnras/stab060.

Tennyson, J. and S. N. Yurchenko (2012). ExoMol: Molecular line lists for exoplanet and other atmospheres. *Monthly Notices of the Royal Astronomical Society*, **425**(1), pp. 21–33. ISSN 00358711. doi:10.1111/j.1365-2966.2012.21440.x.

Tinney, C. G. (1993). The Faintest Stars: The Luminosity and Mass Functions at the Bottom of the Main Sequence. *The Astrophysical Journal*, **414**, pp. 279–301.

Tremblin, P., D. S. Amundsen, G. Chabrier, I. Baraffe, B. Drummond, S. Hinkley, P. Mourier, and O. Venot (2016). Cloudless Atmospheres for L/T Dwarfs and Extrasolar Giant Planets. *The Astrophysical Journal*, **817**(2), p. L19. ISSN 2041-8213. doi:10.3847/2041-8205/817/2/l19.

Trend, R. (1998). An investigation into understanding of geological time among 10- and 11-year-old children. *International Journal of Science Education*, **20**(8), pp. 973–988. ISSN 0950-0693. doi:10.1080/0950069980200805.

Trend, R. (2001a). An Investigation into the Understanding of Geological Time among 17-year-old Students, with Implications for the Subject Matter Knowledge of Future Teachers. *International Research in Geographical and Environmental Education*, **10**(3), pp. 298–321. ISSN 1038-2046. doi:10.1080/10382040108667447.

Trend, R. (2001b). Deep time framework: A preliminary study of U.K. primary teachers' conceptions of geological time and perceptions of geoscience. *Journal of Research in Science Teaching*, **38**(191-221), pp. 191–221.

Tretter, T. R., M. G. Jones, and J. Minogue (2006). Accuracy of scale conceptions in science: Mental maneuverings across many orders of spatial magnitude. *Journal of Research in Science Teaching*, **43**(10), pp. 1061–1085. ISSN 00224308. doi: 10.1002/tea.20155.

Tsuji, T. (2005). Dust in the Photospheric Environment. III. A Fundamental Element in the Characterization of Ultracool Dwarfs. *The Astrophysical Journal*, **621**(2), pp. 1033–1048. ISSN 0004-637X. doi:10.1086/427747.

Tsuji, T. and T. Nakajima (2003). TRANSITION FROM L TO T DWARFS ON THE COLOR-MAGNITUDE DIAGRAM. *The Astrophysical Journal*, (585), pp. 151–154.

Tsuji, T., K. Ohnaka, W. Aoki, and T. Nakajima (1996). Evolution of dusy photospheres through red to brown dwarfs: how dust forms in very low mass objects. *Astronomy & Astrophysics*, **308**(1), pp. L29–L32. ISSN 14712458.

Uttal, D. H., N. G. Meadow, E. Tipton, L. L. Hand, A. R. Alden, C. Warren, and N. S. Newcombe (2012). The Malleability of Spatial Skills: A Meta-Analysis of Training Studies. *Psychological Bulletin*, **139**(2), pp. 352–402. ISSN 0033-2909. doi:10.1037/a0028446.

Valenti, J. A. and D. A. Fischer (2005). Spectroscopic Properties of Cool Stars (SPOCS). I. 1040 F, G, and K Dwarfs from Keck, Lick, and AAT Planet Search Programs. *The Astrophysical Journal Supplement Series*, **159**(1), pp. 141–166. ISSN 0067-0049. doi:10.1086/430500.

Van Leeuwen, F. (2007). Validation of the new Hipparcos reduction. *Astronomy and Astrophysics*, **474**(2), pp. 653–664. ISSN 00046361. doi:10.1051/0004-6361:20078357.

VandenBerg, D. A., F. D. A. Hartwick, and P. Dawson (1983). Studies of Late-Type Dwarfs. V. Theoretical Models for Lower Main-Sequence Stars. *The Astrophysical Journal*, **266**, pp. 747–754.

Visscher, C., K. Lodders, and B. Fegley (2010). Atmospheric chemistry in giant planets, brown dwarfs, and low-mass dwarf stars. III. Iron, magnesium, and silicon. *Astrophysical Journal*, **716**(2), pp. 1060–1075. ISSN 15384357. doi:10.1088/0004-637X/716/2/1060.

Vos, J. M., B. A. Biller, K. N. Allers, J. K. Faherty, M. C. Liu, S. Metchev, S. Eriksson, E. Manjavacas, T. J. Dupuy, M. Janson, J. Radigan-Hoffman, I. Crossfield, M. Bonnefoy, W. M. J. Best, D. Homeier, J. E. Schlieder, W. Brandner, T. Henning, M. Bonavita, and E. Buenzli (2020). Spitzer Variability Properties of Low-gravity L Dwarfs. *The Astronomical Journal*, **160**(1), p. 38. ISSN 1538-3881. doi:10.3847/1538-3881/ab9642.

Vosniadou, S. and W. F. Brewer (1992). Mental Models of the Earth : A Study of Conceptual Change in Childhood. *Cognitive Psychology*, **24**, pp. 535–585. ISSN 0010-0285. doi:10.1016/0010-0285(92)90018-W.

Vosniadou, S. and W. F. Brewer (1994). Mental models of the day/night cycle. *Cognitive Science*, **18**(1), pp. 123–183. ISSN 03640213. doi:10.1016/0364-0213(94)90022-1.

Wallace, C. S., E. E. Prather, and D. K. Duncan (2012). A Study of General Education Astronomy Students' Understandings of Cosmology. Part IV. *Astronomy Education Review*, **11**(010104). doi:10.3847/AER2011029.

Wilcomb, K. K., Q. M. Konopacky, T. S. Barman, C. A. Theissen, J.-B. Ruffio, L. Brock, B. Macintosh, and C. Marois (2020). Moderate-resolution K -band Spectroscopy of Substellar Companion κ Andromedae b. *The Astronomical Journal*, **160**(5), p. 207. ISSN 1538-3881. doi:10.3847/1538-3881/abb9b1.

Wilhelm, J. (2003). Gender Differences in Lunar-related Scientific and Mathematical Understandings. *International Journal of Science Education*, **31**(10), pp. 2105–2122. ISSN 0960-9822. doi:10.1037/A0016127.

Wood, C. M., T. Boyajian, K. von Braun, J. M. Brewer, J. R. Crepp, G. Schaefer, A. Adams, and T. R. White (2019). Benchmarking substellar evolutionary models using new age estimates for HD 4747 B and HD 19467 B. *The Astrophysical Journal*, **873**(1), p. 83. ISSN 23318422. doi:10.3847/1538-4357/aafe01.

Wright, E. L., P. R. Eisenhardt, A. K. Mainzer, M. E. Ressler, R. M. Cutri, T. Jarrett, J. D. Kirkpatrick, D. Padgett, R. S. McMillan, M. Skrutskie, S. A. Stanford, M. Cohen, R. G. Walker, J. C. Mather, D. Leisawitz, T. N. Gautier, I. McLean, D. Benford, C. J. Lonsdale, A. Blain, B. Mendez, W. R. Irace, V. Duval, F. Liu, D. Royer, I. Heinrichsen, J. Howard, M. Shannon, M. Kendall, A. L. Walsh, M. Larsen, J. G. Cardon, S. Schick, M. Schwalm, M. Abid, B. Fabinsky, L. Naes, and C. W. Tsai (2010). The Wide-field Infrared Survey Explorer (wise): Mission description and initial on-orbit performance. *Astronomical Journal*, **140**(6), pp. 1868–1881. ISSN 00046256. doi:10.1088/0004-6256/140/6/1868.

York, D. G., J. Adelman, J. E. Anderson, S. F. Anderson, J. Annis, N. A. Bahcall, J. A. Bakken, R. Barkhouser, S. Bastian, E. Berman, W. N. Boroski, S. Bracker, C. Briegel, J. W. Briggs, J. Brinkmann, R. Brunner, S. Burles, L. Carey, M. A. Carr, F. J. Castander, B. Chen, P. L. Colestock, A. J. Connolly, N. Csabai, P. C. Czarapata, J. E. Davis, M. Doi, T. O. M. Dombeck, D. Eisenstein, N. Ellman, B. R. Elms, M. L. Evans, X. Fan, G. R. Federwitz, L. Fiscelli, S. Friedman, J. A. Frieman, M. Fukugita, B. Gillespie, J. E. Gunn, V. K. Gurbani, E. D. E. Haas, M. Haldeman, F. H. Harris, J. Hayes, T. M. Heckman, G. S. Hennessy, R. B. Hindsley, S. Holm, D. J. Holmgren, C.-h. Huang, C. Hull, D. O. N. Husby, S.-i. Ichikawa, T. Ichikawa, E. Ivezic, S. Kent, R. S. J. Kim, E. Kinney, M. Klaene, A. N. Kleinman, S. Kleinman, G. R. Knapp, J. Korienek, R. G. Kron, P. Z. Kunszt, D. Q. Lamb, B. Lee, R. F. Leger, S. Limmongkol, C. Lindenmeyer, D. C. Long, C. Loomis, J. O. N. Loveday, R. Lucinio, R. H. Lupton, B. Mackinnon, E. J. Mannery, P. M. Mantsch, B. Margon, P. Mcgehee, T. A. Mckay, A. Meiksin, A. Merelli, D. G. Monet, J. A. Munn, V. K. Narayanan, T. Nash, E. Neilsen,

R. Neswold, H. J. O. Newberg, R. C. Nichol, T. O. M. Nicinski, M. Nonino, N. Okada, S. Okamura, J. P. Ostriker, R. Owen, A. G. Pauls, J. Peoples, R. L. Peterson, D. Petravick, J. R. Pier, A. Pope, R. Pordes, A. Prosapio, R. O. N. Rechenmacher, T. R. Quinn, G. T. Richards, M. W. Richmond, C. H. Rivetta, C. M. Rockosi, K. Ruthmansdorfer, D. Sandford, D. J. Schlegel, D. P. Schneider, M. Sekiguchi, G. Sergey, K. Shimasaku, W. A. Siegmund, S. Smee, J. A. Smith, S. Snedden, R. Stone, C. Stoughton, M. A. Strauss, C. Stubbs, M. Subbarao, A. S. Szalay, I. Szapudi, G. P. Szokoly, A. R. Thakar, C. Tremonti, D. L. Tucker, A. Uomoto, D. A. N. V. Berk, M. S. Vogeley, P. Waddell, S.-i. Wang, M. Watanabe, D. H. Weinberg, B. Yanny, and N. Yasuda (2000). The Sloan Digital Sky Survey: Technical Summary. *The Astronomical Journal*, **120**, pp. 1579–1587.

Zahnle, K. J. and M. S. Marley (2014). Methane, carbon monoxide, and ammonia in brown dwarfs and self-luminous giant planets. *Astrophysical Journal*, **797**(1). ISSN 15384357. doi:10.1088/0004-637X/797/1/41.

Zalesky, J. A., M. R. Line, A. C. Schneider, and J. Patience (2019). A Uniform Retrieval Analysis of Ultra-cool Dwarfs. III. Properties of Y Dwarfs. *The Astrophysical Journal*, **877**(1), p. 24. ISSN 1538-4357. doi:10.3847/1538-4357/ab16db.

Zhang, X. and A. P. Showman (2014). Atmospheric circulation of brown dwarfs: Jets, vortices, and time variability. *Astrophysical Journal Letters*, **788**(1), pp. 2–7. ISSN 20418213. doi:10.1088/2041-8205/788/1/L6.

Zhang, Z., M. C. Liu, M. S. Marley, M. R. Line, and W. M. Best (2020). Uniform forward-modeling analysis of ultracool dwarfs. I. methodology and benchmarking. *arXiv*, pp. 1–46. ISSN 23318422.

Zhou, Y., D. Apai, S. Metchev, B. W. P. Lew, G. Schneider, M. S. Marley, T. Karalidi, E. Manjavacas, L. R. Bedin, N. B. Cowan, P. A. Miles-Páez, P. J. Lowrance, J. Radigan, and A. J. Burgasser (2018). Cloud Atlas: Rotational Modulations in the L/T Transition Brown Dwarf Companion HN Peg B. *The Astronomical Journal*, **155**(3), p. 132. ISSN 1538-3881. doi:10.3847/1538-3881/aaabbd.